Nucleophilic substitution reactions of α-haloketones: A computational study

by

Carl Johan van der Westhuizen

Supervisor: Prof Ignacy Cukrowski

Co-supervisor: Dr Darren Riley

Submitted in partial fulfilment of the requirements for the degree

Master of Science

in the Faculty of Natural & Agricultural Sciences

University of Pretoria

Pretoria

January, 2017

Declaration

I, Carl Johan van der Westhuizen, declare that the dissertation, which I hereby submit for the degree Masters of Science (Chemistry) at the University of Pretoria, is my own work and has not previously been submitted by me for a degree at this or any other tertiary institution.

Signature:…………………….

Date:………………………….

Summary

This dissertation describes the computational modelling of reactions between α-haloketones and various nucleophiles. Nucleophilic substitution reactions of α-haloketones (also known as α-halocarbonyls in literature) are utilised in synthetic laboratories to obtain 1,2-disconnections; which are typically difficult to obtain otherwise. To gain insight into these reactions, DFT modelling was carried out in this project, with further understanding into these reactions being obtained using Quantum Fragment Along Reaction Pathway (QFARP) which is an extension of Interacting Quantum Atoms (IQA).

The nucleophilic substitution reaction was modelled between α-bromoacetophenone (**α-BrAcPh**), to represent α-haloketones, and the common nucleophiles phenolate (**PhO⁻**) and acetate (**AcO⁻**). QFARP provided insight into the reactions which could not have been obtained with other computational approaches. It was shown that the reaction with **AcO⁻** results in greater destabilisation for the α-group of **α-BrAcPh** as compared to the reaction of **PhO⁻**, explaining the difference in activation energies for the reactions. Diatomic- and fragment-interactions provided awareness into the driving force of the reactions and showed how the hydrogens for the α-group of **α-BrAcPh** provide significant attractive interactions with the nucleophiles during the initial stages of the nucleophilic substitution reaction.

Furthermore, reactions modelled between **α-BrAcPh** and **MeO⁻** was done, as experimental literature has reported the presence of two competing reactions: nucleophilic substitution and epoxidation. Modelling showed the two reactions have low activation energies which are comparable with another. Interestingly, the rate determining step for the epoxidation reaction is not the formation of the transition state structure but rather the rotational barrier which is required to allow the leaving group, bromine, to be *trans* to the carbonyl-*O* of **α-BrAcPh**.

Previous reports indicated that the presence of an electron donating/withdrawing group on the phenyl ring of **α-BrAcPh** had a significant influence on the reaction rate and selectivity between the two reactions. These experimental observations correlated well with the modelling results when comparing the potential energy surfaces (PES) of the reactions. Analysis using QFARP was also applied to these reactions to gain a more fundamental understanding of the reactions and how they differ. While QFARP was not able to explain the selectivity with different substituents present, insight into the dominating interactions that are involved in the reactions was recovered.

Acknowledgements

I would like to first thank my Heavenly Father, for the good health and well-being necessary to complete this project.

To my supervisor, Prof Ignacy Cukrowski, for the patience and guidance that you have provided. Your mentoring has opened my mind to the complexities of chemistry. Thank you for challenging my work, even when I did not want it challenged.

To my co-supervisor, Dr Darren Riley, for all the kind support and contributions offered during the project.

To the research group, for the intellectual discussions and inspiration which has allowed me to learn from not just this project.

To my parents, while words will never be enough, thank you for all the support which you have given throughout this project and the years before. I am very blessed for the education which you have financed for me.

And finally, to Danielle, for all the coffees (and chemistry) we shared. Your endless support has reinforced my curiosity for the world.

Table of Content

List of Figures

List of Tables

List of Abbreviations

B3LYP   Becke, 3-parameter, Lee-Yang-Parr

BCP   Bond Critical Point

BO   Born-Oppenheimer

CA   Carbonyl Addition

CP   Critical Point

DFT   Density Functional Theory

EDG   Electron Donating Groups

EWG   Electron Withdrawing Groups

FMO   Frontier Molecular Orbitals

HF   Hartee Fock

HOMO   Highest Occupied Molecular Orbital

HSAB   Hard Soft Acid Base

IEF   Integral Equation Formalism

IQA   Interacting Quantum Atoms

IQF   Interacting Quantum Fragments

IRC   Intrinsic Reaction Coordinate

LG   Leaving Group

LUMO   Lowest Unoccupied Molecular Orbital

MD   Molecular Dynamics

MO   Molecular Orbitals

P   Product

PC   Product Complex

PCM   Polarizable Continuum Model

PES   Potential Energy Surface

QFARP   Quantum Fragment Along Reaction Pathway

QTAIM   Quantum Theory of Atoms In Molecules

R   Reactants

RC   Reactant Complex

SCD   State Correlation Diagram

S_N1 Unimolecular Nucleophilic Substitution

S_N2 Bimolecular Nucleophilic Substitution

TS   Transition State

VBCM   Valence Bond Configuration Mixing Model

Chapter 1

Introduction

Computational chemistry is a rapidly growing field that is contributing to the understanding of chemistry in ways which are not possible through experimental chemistry alone. With the rapid development in the processing powers of computers, it is becoming possible to study larger molecular systems with greater accuracy. While computational chemistry has come a long way, there is still a critical need for the development of more sophisticated models, computational protocols and interpretation of data. Ideally, computational chemistry should provide insight into a particular issue such as the prediction of chemical reactivity and how variation in the substrate and reaction conditions may influence the reaction. In doing so synthetic chemists would then be able to better predict and optimise the outcome of reactions before they even set foot into a "wet" lab.

While numerous reactions have been studied extensively using computational chemistry basic synthetically reactions such as nucleophilic substitution are still not comprehensively understood. In this project, computational studies focusing on the reactivity of nucleophilic substitution reactions of α-haloketone compounds with various nucleophiles are reported.

1.1 Review of nucleophilic substitution reactions from experimental and theoretical viewpoints

Nucleophilic substitution is one of the most extensively studied reactions.[3] The reaction rates are strongly influenced by substrate structure[4] and the environment[5] around the species of interest. Nucleophilic substitution reactions occur when two atoms, of different electronegativity, are covalently bonded. The atom or functional group which has higher electronegativity withdraws electron density from the other atom, typically carbon, resulting in it being electrophilic. The electronegative atom or functional group is also known as the "leaving group". If a nucleophile is present, it will react with the electrophilic atom via nucleophilic attack. A covalent bond is formed between the nucleophile and the electrophile, and the initial polarised bond of the electrophilic atom to the leaving group is broken. The reaction is called bimolecular nucleophilic substitution (S_N2) when simultaneous bond formation and breaking occurs (**Scheme 1.1**), characterised by the nucleophile attacking from the back-side resulting in the inversion of stereochemistry. Unimolecular nucleophilic substitution (S_N1) occurs when the leaving group departs before the new bond with the nucleophile is established (**Scheme 1.2**). If the leaving group is bonded to a carbon, removal of the leaving group results in the formation of a carbocation. The carbocation is then subsequently attacked by a nucleophile from the front- or back-side resulting in a racemic mixture. S_N1 reactions tend to dominate over the S_N2 reaction when the central atom is surrounded by substituents which are bulky or are able to stabilise the carbocation (i.e. electron donating groups). The rate determining

2

step of the S$_N$1 reaction is determined by the rate of the carbocation formation, not the strength of the nucleophile which has significant influence in the S$_N$2 reaction mechanism.

Scheme 1.1: Typical S$_N$2 reaction mechanism.

Scheme 1.2: Typical S$_N$1 reaction mechanism.

1.1.1 Theoretical and experimental studies of S$_N$2 reactions

Nucleophilic bimolecular substitution (S$_N$2) reactions are widely used and have been studied both computationally and experimentally for decades. Computational studies on these reactions have covered topics such as orbitals (molecular orbitals,[1,2] natural bond orbitals[6] and intrinsic bond orbitals[7]), valence bonds,[3] molecular dynamics (MD),[8–10] solvent effects,[9–15] substituents effects on entropy and enthalpy[16–19] and Bader's Quantum Theory of Atoms in Molecules (QTAIM).[20] Unfortunately, the majority of the computational studies that have been done have been restricted to very simple systems such as halogenated methane and ethane molecules.[1,6,8,11–15]

From reaction data, Olmstead and Brauman[21] were the first to deduce the basic energy profile of the S$_N$2 reaction, which resembles a double well when plotted along reaction coordinates - **Figure 1.1**. This potential energy surface[22] (PES) shows the two reactants (R) coming together to form a reactant-complex (RC) which is lower in energy than the separated molecules. The RC molecules then react to form the transition state (TS) which is larger in energy, to finally produce the product-complex (PC). Typically for exothermic reactions the energy of the PC and separate products (P) will be lower than the energies of RC as well as R.

3

Figure 1.1: Potential energy surface of S_N2 reaction.

The rate of reaction can be calculated by looking at the energy difference ΔE_{ovr} ($\Delta E_{ovr} = E_{TS} - E_R$) and not ΔE_{cent} ($\Delta E_{cent} = E_{TS} - E_{RC}$). The ΔE_{ovr} is negative suggesting that the reaction is barrierless and thus spontaneous, however 100% yield is not obtained. This is because the TS is more highly ordered, thus there is a higher density of states for the reactants compared to the TS. This means there is an additional entropic barrier.[21]

When entropy is taken into account, by considering the Gibbs free energy, then the free energy profiles for a reaction shows the TS is in fact higher in energy than the separate reactants - **Figure 1.2**. In **Figure 1.2** the nucleophile and leaving group are identical, thus the reactants and products have the same energies. This provides a positive activation energy barrier accounting for the less than 100% efficiency.

Note that the Gibbs free energy gives a clearer indication of the rate of a reaction as entropy is taken into account and is dependent of the temperature of the system. Whereas, the electronic energy provides information on the energy barrier hence the activation for the reaction, from reactants to products can be estimated.

Figure 1.2: Potential energy surface of Gibbs free energy and enthalpy for an S_N2 reaction.

4

Fernández *et al*[23,24] have shown that for more sterically hindered systems, the increase in the S_N2 activation energy results from a weakening of electrostatic attraction and the loss of attractive orbital interaction, not steric repulsion which was previously thought to be the case in classical organic chemistry.

Uggerud[25] showed that S_N2 activation energy decreases going left to right on the periodic table due to the increase in ionization energy, substrates with stronger electrostatic character result in lower activation energies due to decreased electron repulsion in the TS. Recently Grabowski[26] showed that in some cases σ-hole bonding occurs in the preliminary stages of S_N2 reactions.

Dewar and Dougherty[27] have discussed the effect of the solvent on the PES of the S_N2 reaction in relation to the gas phase PES, which is supported by other studies.[1,28,29] As shown in **Figure 1.3**, the additional solvation stabilisation obtained for the reactants, $\Delta H_{sol}(X^-) + \Delta H_{sol}(RY)$, is greater than that of the TS, $\Delta H_{sol}(X\text{-}R\text{-}Y^{\ddagger-})$. This leads to an increase in the activation energy of reaction in solution. The energy difference between R and RC in solution is also much less significant than those of gas phase calculations.
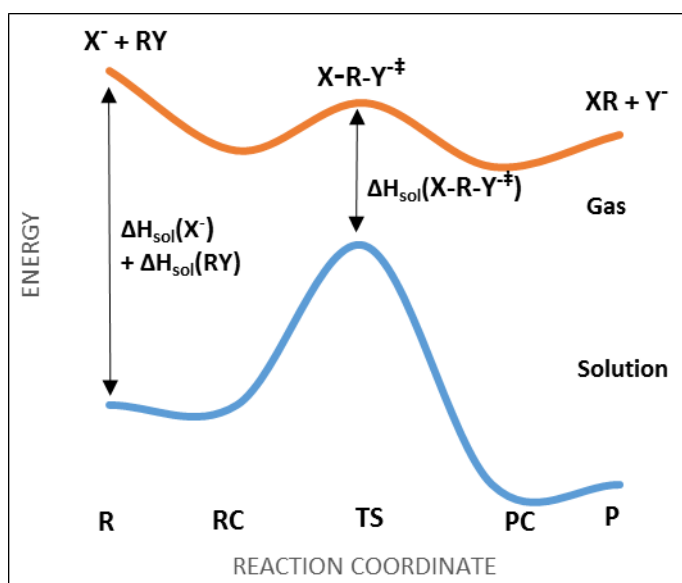
Figure 1.3: Relative potential energy surface of an S_N2 reaction in gas-phase (orange) and solution-phase (blue).

The leaving group which is displaced during the S_N2 reaction plays an important role. Synthetically, halogens such as bromine and chlorine are utilised, along with organic leaving groups such as sulfonic acids. Computational studies mostly use halogens in S_N2 reaction modelling. Using the activation strain model, Bento and Bickelhaupt[30] have shown that the leaving-group ability is derived directly from the bond strength of carbon-leaving group. Hence fluorine which forms a

5

much stronger bond to carbon is a weaker leaving group than bromine which has a weaker bond to carbon.

Similarly, the nucleophile also has significant influence on the reactivity of the reaction. Bento and Bickelhaupt[30] showed that the nucleophilicity is determined by the electron-donor capability of the nucleophile. In summary, the S_N2 reaction is largely affected by changes in the leaving group, environment (i.e. solvent) and strength of the nucleophile.

Several theories have been developed to explain and predict the reactivity of nucleophilic substitution reactions. The three most prominent being the Hard-Soft Acid-Base (HSAB) theory,[31] the Frontier molecular orbital (FMO)[32,33] theory and the valence bond configuration mixing model (VBCM).[3]

The Hard-Soft Acid Base (HSAB) theory developed in 1963 by Pearson,[31] states that the more similar the nucleophile (Lewis base) and substrate (Lewis acid) are in terms of "hardness" and "softness" the greater their reactivity with each other. Hard acids and bases are smaller in size, have low polarizability and a lower tendency to form covalent bonds; while soft acids have the opposite characteristics.

Frontier molecular orbital (FMO) theory has also been used to explain reactivity,[32,33] which considers the energy difference of the highest occupied molecular orbital (HOMO) and lowest unoccupied molecular orbital (LUMO). Dewar[34] has however shown the theory to be inadequate to explain some aspects of S_N2 reactions and other reactions such as electrophilic aromatic substitution. He concluded that FMO theory does not have a good basis in quantum mechanics and does not provide a satisfactory account of chemical reactions and chemical reactivity.

Another theory which is similar to FMO is the valence bond configuration mixing model (VBCM) which was developed by Shaik and Pross. For a detailed understanding of VBCM the reader is directed to Shaik, Schlegel and Wolfe's book titled "*Theoretical aspects of physical organic chemistry: the S_N2 mechanism*",[3] where the theory is explained in detail and findings published in literature are covered. The model is rooted in a central statement of Bell-Evans-Polyani (BEP) principle that the reaction profile is the crossing of the reactant and product like energy curves. The theory considers the S_N2 reaction as a transfer of a <u>single</u> electron and the activation energy barrier is a function of the distortion in the structure to achieve the transition state. This principle is shown in the State Correlation Diagram (SCD) – **Figure 1.4**.

6
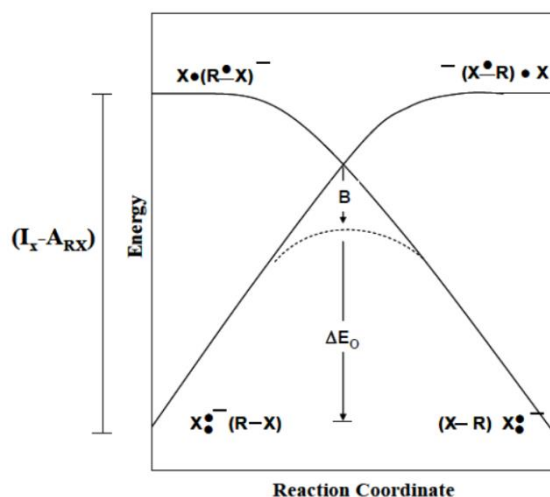
Figure 1.4: State Correlation Diagram for VBCM.

The SCD comprises of the energy for the equilibrium ground state structures at the bottom of the figure and the energy for the charge transfer state structures at the top of the figure. As the reaction proceeds the structures undergo distortions which increase the energy, ΔE_o, and brings them to a point of equivalent energy. Interactions between X^- and RX that are favourable will further reduce the activation energy by the amount of the avoided crossing over, B. Another major concept of VBCM is that the reactivity is related to the "looseness" or "tightness" of the transition state.[35]

1.2 S_N2 reactions with α-haloketones

Compounds which have two heteroatoms between two carbon atoms on an organic scaffold are known as "1,2-relationships". Synthesis of such structures are often difficult as there are limited synthetic approaches to them. One approach is the use of nucleophilic attack on an epoxide which generates an alcohol with a 1,2-relationship. Another approach which is used extensively for systems containing a carbonyl as part of the 1,2-relationship is the use of α-haloketones (also referred to as α-halocarbonyls in literature) with nucleophiles to obtain the desired scaffold via an S_N2 reaction. Synthesis of these α-haloketones is trivial as there are several methods available.[36,37] The simplest approach involves the bromination of aliphatic ketones with bromine liquid in a solvent (**Scheme 1.3**).
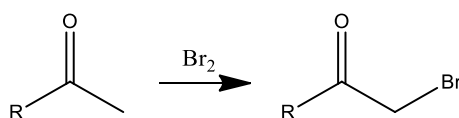
Scheme 1.3: Bromination of an aliphatic ketone to afford an α-haloketone.

7

Several reviews[37,38] highlight the use of these compounds in S_N2 reactions to access a wide range of organic scaffolds. α-Haloketone compounds have been extensively used in the synthesis of 5 and 6 membered rings with between 1 and 3 heteroatoms. An example of this is shown in **Scheme 1.4** where α-haloketones react with *o*-mercaptonitriles **1**, to form 3-aminothiophenes **2**.[39]
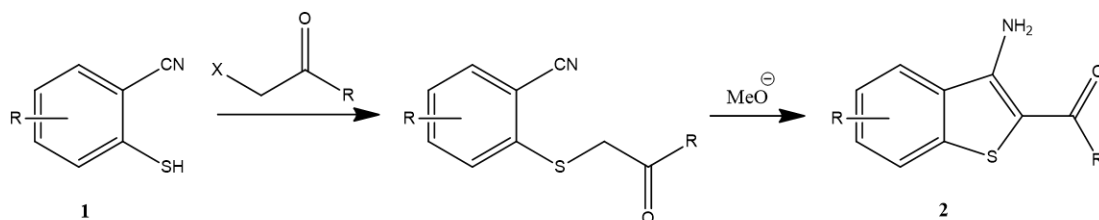
Scheme 1.4: Synthesis of 3-aminothiophenes with α-haloketones and *o*-mercaptonitriles.

α-Haloketones are also less readily utilised in other organic reactions such as Favorskii rearrangement reactions[40,41] whereby a ring contraction is observed – see **Scheme 1.5**.
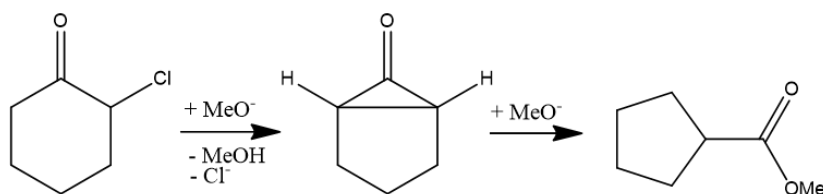
Scheme 1.5: Favorskii rearrangement of α-haloketones.

1.3 Enhanced reactivity of α-haloketone compounds for S_N2 reactions

1.3.1 Kinetic and computational studies

Kinetic studies[4,42–47] on the reactivity of α-haloketones have been performed and it is generally accepted that halogens alpha to carbonyl groups are more reactive to nucleophilic substitution than simple halo-alkane compounds.[48] In 1949[49] and 1950,[50] two independent research groups isolated relatively stable epoxides from the reactions of α-haloketones with sodium methoxide. This result indicated the existence of alternative reaction pathways indicating an increased level of complexity when compared to the displacement of simple haloalkanes. Initial explanations though not well supported for the observed enhancement in reactivity include ideas such as (i) the electrostatics enhancing the reaction rate as described by Pearson[51] and (ii) the presence of a complex mechanism[52] with an intermediate epoxide that is formed - **Scheme 1.6**.

8
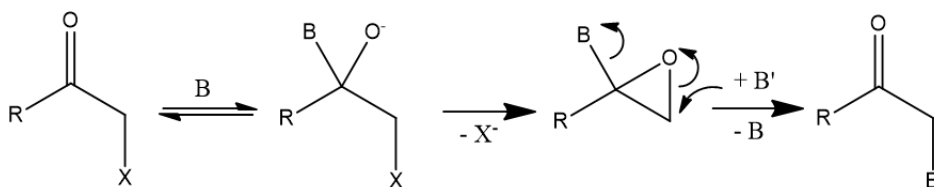
Scheme 1.6: Proposed mechanism of intermediate epoxide formation and a second nucleophile attacking the epoxide to for the S_N2 product.

An alternative and potentially more attractive explanation that has been proposed is that the nucleophile first attacks the carbonyl group before moving to the α-carbon to produce the S_N2 product.[53] A kinetic study[46] suggested that pyridines underwent this process where carbonyl addition (CA) occurs initially, followed by transfer to the α-carbon, but a computational study[54] of α-haloketones reacting with pyridine as the nucleophile showed that while there is some interaction between the carbonyl group and nucleophile, CA does not occur as an intermediate step in the S_N2 reaction. Early MO studies[2,33,55] concluded that the low lying "allylic" bond orbitals of α-haloketones result in the stabilisation of the transition state which thus enhances the reactivity. These studies only considered the TS of the S_N2 reaction and MO studies of the nucleophile undergoing CA have to date not been undertaken.

Yamataka and co-workers have observed CA when a strong nucleophile such as hydroxide or methoxide is used. Their computational studies[56] initially suggested the possibility of a bifurcation mechanism. Bifurcation reaction mechanisms[57] have a single TS which leads to the formation of two different products. (Readers interested in bifurcation mechanisms that have been found are referred to a review titled "*Bifurcations on Potential Energy Surfaces of Organic Reactions*" by Ess *et al*.[57]) Yamataka's molecular dynamic (MD) studies[56] showed that if an electron donating group (EDG) is present on the aromatic ring of α-bromoacetophenone, the hydroxide nucleophile would undergo the typical S_N2 attack. Whereas if an electron withdrawing group (EWG) is present, the hydroxide nucleophile would undergo CA. Subsequent kinetic studies were undertaken by Yamataka and co-workers[58,59] in which the reaction rates of methoxide reacting with α-bromoacetophenones and α-chloroacetophenones showed that the bifurcation path does in fact not occur. The kinetic studies showed that two possible products can be formed, (i) the expected S_N2 product, an ether and (ii) an alcohol which was produced following epoxide formation.

The kinetic results, when plotted on a Hammett plot (**Figure 1.5**), show a straight line for the reaction rates. These Hammett plots are based on the logarithmic effect of the addition of an EWG/EDG on the reaction rate and are relative to a pre-established σ value associated with the strength of the EWG/EDG. If a straight line was not obtained, then there would be change in the

reaction mechanism (which was observed from the MD studies). They concluded that the reaction does not undergo a bifurcation mechanism, but rather a competition between two different reaction routes takes place (**Scheme 1.7**). For the nucleophilic substation, the nucleophile would attack the α-carbon of α-bromoacetophenone **3** to form the ether product **4**. While for the other reaction route, the nucleophile undergoes CA with **3** for form the intermediate **5**. The carbonyl-*O* of **5** attacks the α-carbon to form the epoxide **6**. Lately, the epoxide ring opens to form the alcohol product **7**.
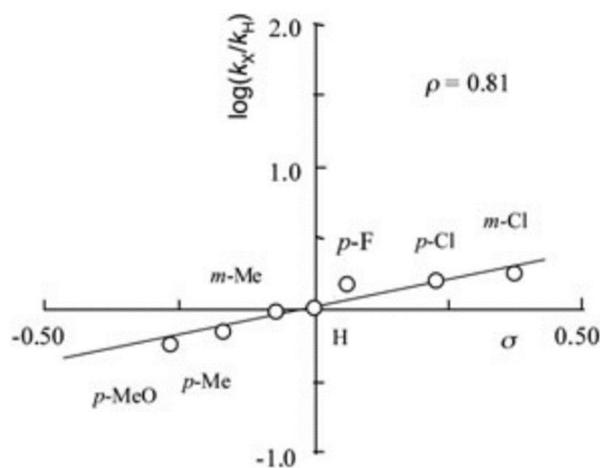
Figure 1.5: Hammett plot for the ether formation pathway of the reaction of $XC_6H_4COCH_2Cl$ and NaOMe in MeOH at 25°C.[58]
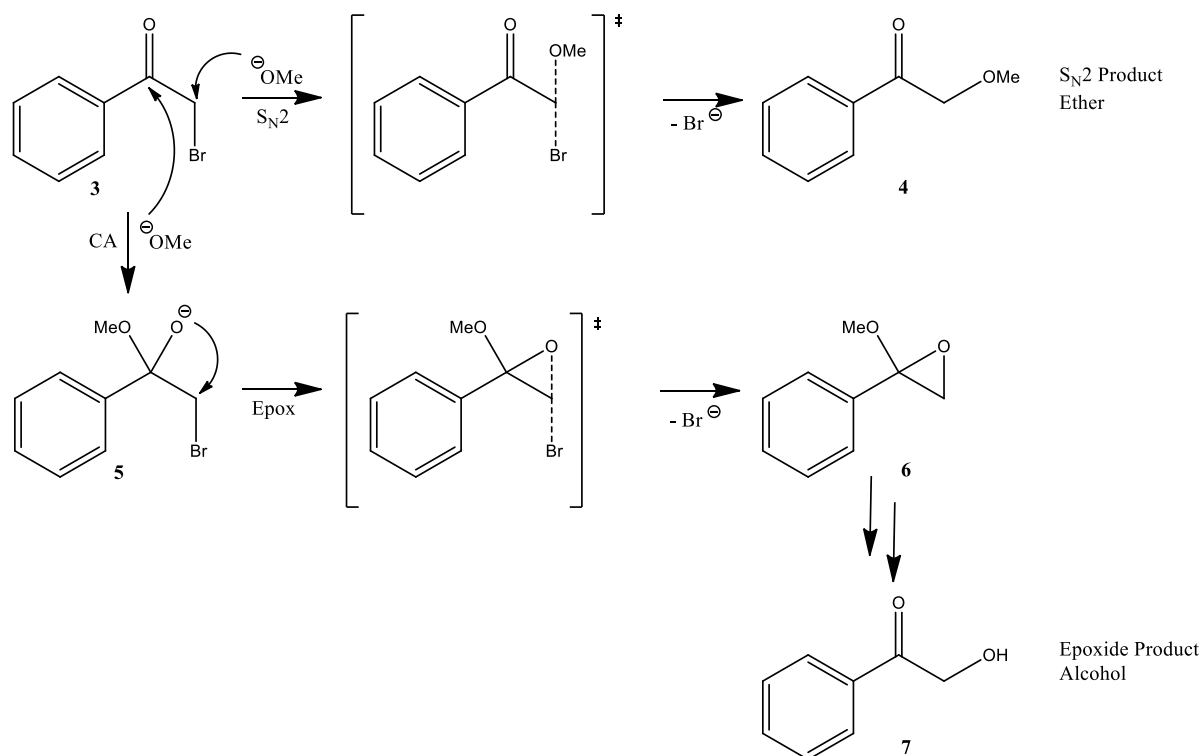
Scheme 1.7: Proposed reaction mechanism for methoxide reacting with α-bromoacetophenone.

One might wonder how the epoxide compound **6** reacts further to form the alcohol **7**. Yamataka and co-workers[58] have proposed that an additional methoxide nucleophile attacks the higher substituted carbon of **6** which opens the cyclic ring. The two methoxy-groups are then removed via hydrolysis with a phosphate buffer to afford the alcohol **7**.

1.3.2   Influence of substituents

Yamataka and co-workers[58,59] have shown experimentally how the yield of the two products, **4** and **7** (**Scheme 1.7**), is greatly affected by the addition of EDG/EWG on the phenyl group of α-haloacetophenone. If an EDG (such as *p*-OMe) is present, there is a clear increase in yield of the S_N2 reaction route yielding ether compound **4**. When no group are present it is shown that the epoxidation reaction route yielding compound **7** is favoured. While if an EDG (such as *p*-NO₂) is present this favourability towards the epoxidation reaction is increased significantly. Several EDGs and EWGs of various strengths were utilised, and excellent correlation in selectivity based on yield is observed. Note also that the reaction rates of both reaction routes decrease or increase with stronger EDG and EWG, respectively.

1.4 Aim

The discussion of previous work shows that there is not a thorough understanding of reaction mechanisms and selectivity of α-haloketones in S_N2 reactions. Thus, the aim of this project is to model these reactions with different nucleophiles to elucidate the competition mechanisms which have been observed in kinetic studies. α-Bromoacetophenone is utilised as the model system of α-haloketones in this modelling project as it has been used in several other kinetic and computational studies. The reactions of α-bromoacetophenone with nucleophiles which have excellent experimental yield are described in chapter 3. While chapter 4 details studies on the reaction with methoxide which has been shown to have poor yields and generate by-products. The studies described in chapter 3 and 4 provide insight into what cause the two reactions to differ from each other. Modelling is also done to explain how EDG/EWG have a profound effect on the reaction rate and the experimental yield on competing reaction routes.

Note that the computational methods described in this chapter have not been used in this project. To explain reactivity in this project the PES of the modelled reactions (in relation to electronic energy and Gibbs free energy) are considered and a new in-house developed method called Quantum Fragment Along Reaction Pathway (QFARP) an extension of Interacting Quantum Atoms (IQA) is utilised extensively. Explanations of these methods can be found in chapter 2.

1.5 References

(1)   Bickelhaupt, F. M. *J. Comput. Chem.* **1999**, *20* (1), 114.

(2)   Bach, R. D.; Coddens, B. A.; Wolber, G. J. *J. Org. Chem.* **1986**, *51* (7), 1030.

(3)   Sason, S.; H. Bernhard, S.; Wolfe, S. *Theoretical aspects of physical organic chemistry: the SN2 mechanism*; Wiley: New York, 1992.

(4)   Kalendra, D. M.; Sickles, B. R. *J. Org. Chem.* **2003**, *68* (4), 1594.

(5)   Kim, Y.; Cramer, C. J.; Truhlar, D. G. *J. Phys. Chem. A* **2009**, *113* (32), 9109.

(6)   Ahmadi, A. A.; Fattahi, A. *Comput. Theor. Chem.* **2015**, *1067*, 71.

(7)   Knizia, G.; Klein, J. E. M. N. *Angew. Chemie Int. Ed.* **2015**, *54* (18), 5518.

(8)   Ensing, B.; Klein, M. L. *Proc. Natl. Acad. Sci. U. S. A.* **2005**, *102* (19), 6755.

(9)   Mo, Y.; Gao, J. *J. Comput. Chem.* **2000**, *21* (16), 1458.

(10)   Sato, M.; Yamataka, H.; Komeiji, Y.; Mochizuki, Y.; Ishikawa, T.; Nakano, T. *J. Am. Chem. Soc.* **2008**, *130* (8), 2396.

(11)   Safi, B.; Choho, K.; Geerlings, P. *J. Phys. Chem. A* **2001**, *105* (3), 591.

(12)   Adamovic, I.; Gordon, M. S. *J. Phys. Chem. A* **2005**, *109* (8), 1629.

(13)   Oh, Y.-H.; Ahn, D.-S.; Chung, S.-Y.; Jeon, J.-H.; Park, S.-W.; Oh, S. J.; Kim, D. W.; Kil, H. S.; Chi, D. Y.; Lee, S. *J. Phys. Chem. A* **2007**, *111* (40), 10152.

(14)   Raugei, S.; Cardini, G.; Schettino, V. *J. Chem. Phys.* **2001**, *114* (9), 4089.

(15)   Truong, T. N.; Stefanovich, E. V. *J. Phys. Chem.* **1995**, *99* (40), 14700.

(16)   Ruff, F.; Farkas, Ö. *J. Org. Chem.* **2006**, *71* (9), 3409.

(17)   Vlasov, V. *J. Appl. Solut. Chem. Model.* **2014**, No. 3, 81.

(18)   Vlasov, V. M. *New J. Chem.* **2010**, *34* (7), 1408.

(19)   Vlasov, V. M. *J. Phys. Org. Chem.* **2012**, *25* (4), 296.

(20)   Bader, R. F. W. *Acc. Chem. Res.* **1985**, *18* (1), 9.

(21)   Olmstead, W. N.; Brauman, J. I. *J. Am. Chem. Soc.* **1977**, *99* (13), 4219.

(22)   Swart, M.; Solà, M.; Bickelhaupt, F. M. *J. Comput. Chem.* **2007**, *28* (9), 1551.

(23)   Fernández, I.; Frenking, G.; Uggerud, E. *Chem. - A Eur. J.* **2009**, *15* (9), 2166.

(24)   Fernández, I.; Frenking, G.; Uggerud, E. *Chem. - A Eur. J.* **2010**, *16* (19), 5542.

(25)   Uggerud, E. *Chem. - A Eur. J.* **2006**, *12* (4), 1127.

(26)   Grabowski, S. J. *Phys. Chem. Chem. Phys.* **2014**, *16* (5), 1824.

(27)   Dewar, M. J. S.; Dougherty, R. C. *The PMO Theory of Organic Chemistry*; Plenum Press: New York, 1975.

(28)   Chandrasekhar, J.; Smith, S. F.; Jorgensen, W. L. *J. Am. Chem. Soc.* **1985**, *107* (1), 154.

(29)   Chen, X.; Regan, C. K.; Craig, S. L.; Krenske, E. H.; Houk, K. N.; Jorgensen, W. L.; Brauman, J. I. *J. Am. Chem. Soc.* **2009**, *131* (44), 16162.

(30)   Bento, A. P.; Bickelhaupt, F. M. *J. Org. Chem.* **2008**, *73* (18), 7290.

(31)   Pearson, R. G. *J. Am. Chem. Soc.* **1963**, *85* (22), 3533.

(32)   Kost, D.; Aviram, K. *Tetrahedron Lett.* **1982**, *23* (40), 4157.

(33)   Bach, R. D.; Wolber, G. J. *J. Am. Chem. Soc.* **1985**, *107* (5), 1352.

(34)   Dewar, M. J. S. *J. Mol. Struct. THEOCHEM* **1989**, *200* (C), 301.

(35)   Shaik, S. S.; Schlegel, H. B.; Wolfe, S. *J. Chem. Soc. Chem. Commun.* **1988**, No. 19, 1322.

(36)   De Kimpe, N.; Verhé, R. *The Chemistry of α-Haloketones, α-Haloaldehydes and α-Haloimines*; Interscience: New York, 1988.

(37)   Erian, A. W.; Sherif, S. M.; Gaber, H. M. *Molecules* **2003**, *8* (11), 793.

(38)   Moiseev, I. K.; Makarova, N. V; Zemtsova, M. N. *Russ. J. Org. Chem.* **2003**, *39* (12), 1759.

(39)   Markert, J.; Hagen, H. *Liebigs Ann. der Chemie* **1980**, *1980* (5), 768.

(40)   Föhlisch, B.; Franz, T.; Kreiselmeier, G. *European J. Org. Chem.* **2005**, *2005* (21), 4687.

(41)   Sakai, T.; Katayama, T.; Takeda, A. *J. Org. Chem.* **1981**, *46* (14), 2924.

(42)   Halvorsen, A.; Songstad, J. *J. Chem. Soc. Chem. Commun.* **1978**, No. 7, 327.

(43)   Lee, I.; Lee, H. W.; Yu, Y. *Bull. Chem. Soc.* **2003**, *24* (7), 993.

(44)   Ross, S. D.; Finkelstein, M.; Petersen, R. C. *J. Am. Chem. Soc.* **1968**, *90* (23), 6411.

(45)   Bordwell, F. G.; Brannen, W. T. *J. Am. Chem. Soc.* **1964**, *86* (21), 4645.

(46)   Koh, H. J.; Han, K. L.; Lee, H. W.; Lee, I. *J. Org. Chem.* **2000**, *65* (15), 4706.

(47)   Lee, I.; Shim, C. S.; Chung, S. Y.; Lee, H. W. *J. Chem. Soc., Perkin Trans. 2* **1988**, No. 6, 975.

(48)   Thorpe, J. W.; Warkentin, J. *Can. J. Chem.* **1973**, *51* (6), 927.

(49)   Temnikova; Kropacheva. *J. Gen. Chem. U.S.S.R.* **1949**, *19* (72), 1917.

(50)   Stevens, C. L.; Malik, W.; Pratt, R. *J. Am. Chem. Soc.* **1950**, *72* (10), 4758.

(51) Pearson, R. G.; Langer, S. H.; Williams, F. V; McGuire, W. J. *J. Am. Chem. Soc.* **1952**, *74* (20), 5130.

(52) Baker, J. W. *J. Chem. Soc.* **1938**, 445.

(53) Bunton, C. A. *Nucleophilic Substitution at a Saturated Carbon Atom*; Elsevier: London, 1963.

(54) Fábián, A.; Ruff, F.; Farkas, Ö. *J. Phys. Org. Chem.* **2008**, *21* (11), 988.

(55) Kost, D.; Aviram, K. *J. Am. Chem. Soc.* **1986**, *108* (8), 2006.

(56) Itoh, S.; Yoshimura, N.; Sato, M.; Yamataka, H. *J. Org. Chem.* **2011**, *76* (20), 8294.

(57) Ess, D. H.; Wheeler, S. E.; Iafe, R. G.; Xu, L.; Çelebi-Ölçüm, N.; Houk, K. N. *Angew. Chemie Int. Ed.* **2008**, *47* (40), 7592.

(58) Katayama, M.; Sasagawa, K.; Yamataka, H. *J. Phys. Org. Chem.* **2012**, *25* (8), 680.

(59) Tagawa, K.; Sasagawa, K.; Wakisaka, K.; Monjiyama, S.; Katayama, M.; Yamataka, H. *Bull. Chem. Soc. Jpn.* **2014**, *87* (1), 119.

Chapter 2

Theoretical Background

Computational chemistry should be able to provide predictive power (and fundamental understanding) of a chemical environment and additional insight which could not have been obtained from experimental studies alone. With many models having been developed, there is a strong correlation between the accuracy of a model and the computational cost (the time required for the calculation), which itself is associated with a given molecular size. Thus, the researcher must decide which model is to be used, and this decision is largely based on (i) the size of the molecular system being studied, (ii) the accuracy that is required for that study and (iii) how much computational power is at the researcher's disposal.

The simplest model utilised is that of molecular mechanics (MM) which is attractive for modelling very large molecular systems. MM has very low costs in terms of computational power and time but is also very inaccurate, as it is based on classical mechanics principles only, such as treating a chemical bond as a spring. MM is based on functional with predetermined potentials. As empirical parameters are fitted, it can result in biased interpretation by altering the parameters to fit proposed interpretation. While MM is useful for determining the structure of compounds at equilibrium, using MM to model reactions, where non-equilibrium structures are involved, are significantly less accurate. Because of its low cost, MM has many useful but very specific applications in computational studies, such as conformational analysis and solvent modelling. On the other end of the modelling spectrum are *ab initio* (Latin for "from the ground up") models that are based on first-principle quantum mechanics. Examples include Hartree Fock (HF) theory as well as post-HF models, such as Coupled Cluster (CC) and Møller-Plesset (MP2, MP4…). These *ab initio* models do not have empirical parameters that may have resulted in biased interpretation. They thus utilise quantum mechanical laws and physical constants. These models are found to be extremely accurate but require very large computational power and as a result only systems containing a limited number of atoms can be reasonably modelled using standard equipment. Density Functional Theory (DFT), though not a true *ab initio* model, has found its way to become extremely popular by theoretical and experimental chemists for studying molecular systems. While DFT is not as accurate as true *ab initio* models, it can handle relatively large systems with good scaling of the system size. One significant drawback of the DFT methods is that the experimental energy of a molecular system is not systematically approached when the level of theory and the basis set are improved. On the other hand, true *ab initio* models approach experimental value as the level of theory and basis set are improved.

This chapter provides a brief theoretical background of the methods that are used in this work. An explanation of quantum chemistry is first provided, and how DFT differs from other commonly

used modelling techniques such as Hartree-Fock (HF) theory. The following section will focus on methods that are used to model reaction mechanisms and difficulties that can be encountered. The last section considers the methods of wavefunction analysis that are used in this work to gain additional insight into the reactions that have been modelled.

Readers interested in an in-depth explanation of quantum mechanics are referred to "*Essentials of Computational Chemistry, Theories and Models*" by C. Cramer[1] and "*Computational Chemistry: Introduction to the Theory and Applications of Molecular and Quantum Mechanics*" by E. Lewars.[2]

2.1 Quantum Chemistry

The aim of computational modelling is to predict the properties of molecular systems which are based on the fundamental laws of quantum mechanics. The wavefunction, Ψ, contains all the information of the system and can be found by solving the (in)famous time-independent Schrödinger equation:

$$\hat{H}\,\Psi(r) = E\Psi(r)\,, \tag{1}$$

where E is the electronic energy of the system and $\hat{H}$ is the Hamiltonian operator:

$$\hat{H} = -\frac{\hbar^2}{2m}\nabla^2 + \hat{V}(r)\,, \tag{2}$$

where $\hbar = h/2\pi$ (Planck's constant divided by 2π), m is the mass of the particle and ∇^2 is the Laplacian operator. The first term in Eq. 2 is the quantum-mechanical kinetic energy operator and $\hat{V}$ is the potential energy operator, giving the potential field which the particle is moving in as its expectation value. Any observable property can be determined from the wavefunction by using the appropriate corresponding operator. The time-independent wavefunction is a function of the position of the electrons and nuclei within a molecule. Therefore, $\hat{V}$ for a molecular system is usually expanded in terms of the interactions between nuclei and electrons, and Eq. 2 can be written as:

$$\hat{H} = -\sum_{i}^{electrons}\frac{\hbar^2}{2m_e}\nabla_e^2 - \sum_{I}^{nuclei}\frac{\hbar^2}{2M_I}\nabla_N^2 - \sum_{I}^{nuclei}\sum_{i}^{electrons}\frac{Z_I e'^2}{r_{Ii}}\nabla_e^2 + \sum_{I<J}^{nuclei}\frac{Z_I Z_J e'^2}{r_{IJ}} + \sum_{i<j}^{electrons}\frac{e'^2}{r_{ij}} \tag{3}$$

or,

17

$$\hat{H} = \hat{T}_e + \hat{T}_N + \hat{V}_{eN} + \hat{V}_N + \hat{V}_e \tag{4}$$

where: $r_{iI} = |r_i - R_I|$, $r_{IJ} = |R_I - R_J|$, $r_{ij} = |r_i - r_j|$, $e' = e/4\pi\varepsilon_0$, e is charge and ε_0 is vacuum permittivity. For the above Eq. 4, the individual terms represent (i) kinetic energy of electrons, (ii) kinetic energy of nuclei, (iii) electron-nuclear attraction, (iv) nuclear repulsion and (v) electron repulsion.

While the exact Schrödinger equation, Eq. 1, can only be solved for the most basic systems, several approximations are used to simplify the solution of the equation. One such approximation is the Born-Oppenheimer (BO) approximation which separates the nuclear and electronic motions. The mass of the nucleus is typically a thousand times greater than that of electrons, thus the nucleus moves much slower than the electrons which orbit it. The electron distribution essentially reacts instantaneously to changes in the position of the nuclei. A new Hamiltonian can be constructed which neglects the kinetic energy of the nuclei, resulting in a Schrödinger equation which describes the motion of electrons with nuclei in a fixed position.

While the BO assumption is justified for most chemical systems, it has profound consequences from a conceptual standpoint in that without the approximation we would lack the concept of a potential energy surface (relating the molecular energy to static nuclear coordinates), which is crucial for the modelling of reactions.

2.1.1   Variational Principle

Since exact solutions to the Schrödinger equation are unavailable for all but the simplest molecules, the variational principle allows a practical method to obtain the best approximate solution to the Schrödinger equation. It states that the use of a trail wavefunction to calculate the energy, E, will always be greater than the true energy, which would be obtained from the exact solution, E^{exact}:

$$E \geq E^{exact} . \tag{5}$$

Because of the variational principle, the electronic energy can be used as a measure of the quality of a trail wavefunction. One can thus minimise the energy with respect to some adjustable parameter within the wavefunction to obtain a solution which is as close as possible to the exact solution. Therefore, a lower energy trail wavefunction will always be closer to the exact solution than a higher energy trail wavefunction.

2.1.2 Molecular Orbital (MO) Theory

While the BO approximation has simplified the Hamiltonian operator, it is still extremely complicated as it represents a many-body, non-linear system of equations when operating on a wavefunction. Thus, a starting point is needed where the solution can be optimised using the variational principle. This is done by breaking up the *N*-electron wavefunction into *N* 1-electron wavefunctions, called molecular orbitals (MO). The simplest way in which MOs can be combined is called a *Hartree product*:

$$\Psi_R^{elec}(r_1, r_2, ..., r_n) = \phi_1(r_1)\phi_2(r_2)...\phi_n(r_n) \tag{6}$$

Note that each individual MO can now be varied separately and through variational calculus one can arrive at a minimised wavefunction. The Hartree product wavefunction in Eq. 6 describes a completely uncorrelated system, with electron-electron repulsions treated in an average manner. In addition, it is not an anti-symmetric wavefunction, a requirement necessitated by the Pauli Exchange Principle, an independent quantum mechanical postulate. The Pauli Exchange Principle can be satisfied, as well as including spin-related electron correlation (*exchange* correlation), by combining MOs as a Slater determinant rather than a Hartree product:

$$\Psi(r_1, r_2, ..., r_n) = \frac{1}{\sqrt{N!}} \begin{vmatrix} \phi_1(r_1) & \phi_2(r_1) & \cdots & \phi_n(r_1) \\ \phi_1(r_2) & \phi_2(r_2) & \cdots & \phi_n(r_2) \\ \vdots & \vdots & & \vdots \\ \phi_1(r_n) & \phi_2(r_n) & \cdots & \phi_n(r_n) \end{vmatrix} \tag{7}$$

For the one-electron wavefunction, another requirement to completely describe the state of an electron is to specify its spin. The spin has two possible states typically denoted α (spin up) or β (spin down).

Thus, the MO is essentially a wavefunction for a single electron, however, it can be occupied by two electrons if the electrons have opposite spin. This is due to the Pauli exclusion principle which states that no two electrons can be characterised with the same set of quantum numbers. Using a Slater determinant satisfies the Pauli Exclusion Principle completely – for instance, placing two electrons of the same spin in the same MO will result in a Slater determinant equal to zero.

2.1.3 Basis set

A wavefunction is usually expressed through a mathematical set of functions, known as a basis set, to provide separately variable components. Specific functions (such as Gaussian functions) are often used to construct the wavefunction. However, it should be emphasised that any mathematical

19

function which follows certain rules can be used to construct a wavefunction. The basis set is a combination of N functions, and each molecular orbital is expanded linearly over the entire basis set:

$$\phi = \sum_{i=1}^{N} a_i \varphi_i .$$

(8)

ϕ is a molecular orbital, N is the number of functions φ_i in the basis set, and a_i are scalar coefficients. In an electronic structure calculation, only the coefficients are varied, with the shape, nature and position of each basis function remaining constant. Basis sets are often pre-optimised or fitted to certain experimental data, which reduces the number of basis functions required.

The use of additional Gaussian primitives allows the systems to be described more accurately. In principle, an infinite number of functions will give a perfect description of the system. However, the use of each additional primitive result in an additional set of equations that need to be solved simultaneously which thus increases computational cost exponentially. These Gaussian primitives are constructed similarly to the one-electron orbitals of the hydrogen atom, the well-known s-, p-, d- and f- type orbitals are used on each of the atoms of the molecular system (although, in principle, any mathematical function can be used). To describe the general trends and show the correct asymptotic behaviour as in the real electron density of a hydrogen atom, several primitives are grouped together (contracted) and scaled linearly.

Basis sets are mathematical descriptions of available orbitals that can be utilised to calculate the electron density. This work utilised 6-311++G(d,p) basis set by Pople and co-workers.[3] This means that there is a split valence basis set of an inner-shell with 6 Gaussian functions contracted into 1 per atomic orbital, while the outer valence orbitals are treated as 5 different functions (with three of them contracted into one). The first and second "+" symbol indicate that a diffuse function was utilised on non-hydrogen and hydrogen atoms respectively, this is to improve the description of regions of little electron density. The last part of the notation results in additional d polarised functions on non-hydrogen atoms and p polarised functions for hydrogen atoms.

2.1.4   Solvation model

The solvent environment can have a profound effect on the molecular system being studied. The interaction between the solute and solvent can alter the energy, reactivity and molecular orientation. Thus, it is critical to take the effect of the solvent into consideration when modelling a system that is in solution. Explicit solvation models include actual individual solvent molecules

which are used extensively in MM studies. A more popular method is the use of implicit solvation models which treat the solvent as a continuum of a uniform dielectric constant. The solute is placed in a cavity within the solvent and different solvation models have distinct methods to define the cavity. The simplest approach is the Onsager Model where the solute occupies a fixed spherical cavity. A molecule with a dipole present will induce a dipole in the solvent field, which thus also interacts with the dipole of the solute. This all leads to a net stabilisation.

A more modern and accurate approach is Tomasi's Polarized Continuum Model[4] (PCM) which defines the cavity as multiple interlocking atomic spheres. The cavity is calculated as a series of overlapping spheres normally defined by the van der Waals radii of the individual atoms. Interested readers are referred to a review article by Tomasi *et al*[5] for a detailed discussion of solvation models. All computations in this work utilised PCM using the integral equation formalism (IEFPCM) as its solvation model.

2.2 Density Functional Theory

2.2.1 Introduction and the Hohenberg-Kohn Theorems

DFT is unique in how it calculates the wavefunction for a system. While other models, such as HF, calculate the wavefunction of the Schrödinger equation directly. DFT first calculates the electron density and then obtains the wavefunction from this density. The electron density, ρ, is directly related to each other with the density being the square of the wavefunction:

$$\rho = |\psi|^2 . \tag{9}$$

The electron density can also be utilised to calculate other properties of the system because the electron density holds the same amount of information as the wavefunction. This is proven in Hohenberg-Hohn's first theorem where all the required information for quantum mechanics is available through analysis of the electron density. However, this theorem only applies to the ground state of a system. The theorem is based on the logical approach of *reductio ad absurdum*, which shows that it is not possible for two wavefunctions, with two distinct Hamiltonians, to obtain the same ground state electron density. Hohenberg-Hohn's second theorem shows that the density with the minimised total energy is the exact ground state density (ρ_0):

$$E[\rho(r)] \geq E_0 = E[\rho_0(r)] . \tag{10}$$

Note that although the Hohenberg-Kohn theorems are powerful, they do not offer any method for computing the ground-state electron density. About one year after Hohenberg and Kohn

developed the above theorems, Kohn and Sham devised a simple method for performing DFT calculations.[6]

2.2.2. The Kohn-Sham Formulation

The difficulty in solving the Schrödinger equation for a system derives from the electron-electron repulsion. For a non-interacting system solving the equation would be a trivial problem. The Hamiltonian would simply be the sum of the one-electron operators. Thus, Kohn and Sham proposed using a system of non-interacting electrons but their overall ground-state density is exactly the same as for the real system of interest. The energy functional can thus be divided into components as follows:

$$E[\rho(r)] = T_{ni}[\rho(r)] + V_{Ne}[\rho(r)] + V_{ee}[\rho(r)] + \Delta T[\rho(r)] + \Delta V[\rho(r)]. \tag{11}$$

The first three terms represent (i) the kinetic energy of the non-interacting electrons, (ii) the nuclear-electron interaction and (iii) the classical electron-electron repulsion. The last two terms $\Delta T[\rho(r)]$ and $\Delta V[\rho(r)]$ represent (i) the correction to the kinetic energy derived from the interacting nature of the electrons and (ii) the non-classical corrections to the electron-electron repulsion energy (or the electron correlation), respectively. Thus, the first three terms obtain the energy for a non-interacting system of electrons while the last two terms provide corrections to the energy. These last two terms are typically summed together to give $E_{XC}[\rho(r)]$, which is referred to as the exchange-correlation energy.

2.2.3. Exchange-Correlation functionals

One of the major fields of DFT development involves the search for exchange-correlation functionals which provide improved accuracy. While many functionals have been developed with a wide range of complexity, some functionals have become extremely popular over the decades. One such group are hybrid-functionals, which combine HF exchange with *exchange* (interactions between electrons with the same spin) and *correlation* (interactions between electrons with *any* spin) functions in a weighted fashion:

$$E_{XC}^{\text{hybrid}} = aE_X^{\text{HF}} + (1-a)E_{XC}^{\text{DFT}}, \tag{12}$$

where *a* is a coefficient which gives weighting to the different components. Both components can be of two distinct types, the first being local functionals which depend on only the electron density, $\rho(r)$. These are known as "Local (spin) density approximations", i.e. L(S)DA. The second type is gradient-corrected functionals which depend on both electron density, $\rho(r)$, and its gradient,

22

$\nabla\rho(r)$. These are known as "Generalised gradient approximations", i.e. GGA. It is emphasised that these functionals are essentially approximated and thus certain interactions such as Van der Waals interactions, which depends on electron correlation, can fall short of the true intrinsic value. Furthermore, dispersion-corrected DFT (DFT-D with empirical corrections) can be used to account for dispersion, which is important for long-range interactions between atoms and molecules.[7]

The work done in this project utilised Becke's three-parameter hybrid functionals combined with Lee-Yang-Parr correlation (B3LYP) which was suggested by Stephens and co-workers in 1994:[8]

$$E_{XC}^{B3LYP} = (1-a)E_X^{LSDA} + aE_X^{HF} + b\Delta E_X^B + (1-c)E_C^{LSDA} + cE_C^{LYP} \tag{13}$$

where the (i) E_X^{LSDA} is the exchange functional using the LSDA, (ii) E_X^{HF} is the exchange energy using the HF scheme, (iii) E_X^B is the exchange from Becke's 1988 exchange functional, (iv) E_C^{LSDA} is correlation functional using the LSDA and finally (v) E_C^{LYP} is the correlation functional using the GGA of Lee, Yang and Parr. The coefficients a, b and c are empirical parameters which were determined by fitting to atomisation energies, ionisation potentials, proton affinities and first-row atomic energies for a set of molecules. Thus, because empirical parameters are used in DFT, it is not a true *ab initio* calculation.

It should be noted that B3LYP has become extremely popular because of its relatively low computational costs and high accuracy. There are more complicated functionals which often do not perform as well as B3LYP, though the lack of success of these functionals cannot be explained. This supports the comment made earlier that DFT methods do not systematically approach the experimental energy when the level of theory and basis set is improved.

2.3. Practical Calculations

Lewars[2] elegantly explains in "*Computational Chemistry*" that: "Chemistry is essentially the study of the stationary points on potential energy surfaces: in studying more or less stable molecules we focus on minima, and in investigating chemical reactions we study the passage of a molecular from a minimum through a transition state to another minimum."

For modelling chemical reactions, there are several tools available in software packages such as Gaussian 09[9] and ADF.[10,11] Reaction mechanisms are studied by determining the PES of a potential reaction. Thus, the structures and energies of the TS, reactant and product are required, along with structures between the TS and reactants/products. A brief explanation of how this is done is discussed.

2.3.1. Geometry optimisations

Locating a stationary point on the PES is called geometry optimisation. A stationary point (also known as a critical point) is either an energy minima structure or a TS, which is discussed separately below. An input structure is provided, which presumably is close to the desired stationary point, and a self-consistent field (SCF) calculation where minimisation of the electronic energy for the wavefunction for fixed nuclear coordinates is done. An algorithm systematically changes the geometry, until it has found a stationary point. With each change in geometry, a new SCF calculation is done. A stationary point is characterised by considering the first and second derivative of the energy with respect to all geometric parameters. The first derivative is required to equal zero along all geometric parameters while the second derivative must be negative for an energy minima structure. For a TS structure on the other hand, the second derivative must be positive along one geometric parameter. The optimisation of TS structures are discussed further in a separate sub-chapter below.

It is important to note that the input structure which is used will find the nearest stationary point. Therefore, the energy minima structure that was obtained from geometry optimisation will not necessarily be the global minimum structure.

2.3.2. Frequency calculations

The second derivative is required (i) for optimisation, (ii) to identify if the stationary point obtained is an energy minimum structure or TS structure, (iii) to calculate the vibrational frequencies for IR (Roman) spectra and (iv) to compute terms such as zero-point vibration energy and determine the thermal energy corrections to the total energy, as well as the entropy and enthalpy of the molecular system.

The second derivatives (of the energy with respect to the geometric parameters) are manipulated into a force constant matrix (also known as the Hessian) which is a rectangular array of numbers. The Hessian is diagonalized to produce a matrix with "direction vectors" and force constants. Mass-weighting the force constants gives the vibrational frequencies that are used to generate the IR spectra. The vibrational frequencies of an energy minima structure would all be real, while a TS has one imaginary (negative) frequency which corresponds to the reaction coordinate.

24

2.3.3. Relaxed Potential Surface Scans

The most robust method to sample the PES of a reaction is by essentially "forcing" the atoms, or molecules, of interest to approach each other by decreasing a distance between selected two atoms. Initially, an energy minimum structure is calculated and then a step is taken; where the scan coordinate such as the distance between two selected atoms is reduced (or increased) by a small distance (e.g. 0.1Å), the new structure is re-optimised while the scan coordinate is fixed. Once the new structure is optimised, the procedure is repeated iteratively until several optimised structures are obtained which represent structures along the PES. It is worth mentioning that using very large incremental steps (e.g. 0.5Å) can result in structures and energies that are not a true reflection of the PES.

2.3.4. Transition state calculations

A TS structure and its energy are critical to obtain if a reaction is to be modelled. The energy of the TS relative to the reactants provides important insight about the feasibility of the reaction and how reactive the reaction might be. The TS is a saddle point on the PES between two energy minima structures and has a single imaginary frequency, which is represented by a single negative vibrational frequency. The vibration of this negative frequency indicates the movement of the atoms and should be visually inspected to confirm the vibrational movement is in line with the expected atom movement leading to a new bond formation.

The software package, Gaussian 09,[9] is able to calculate the TS using (i) Berny optimisation and (ii) QST2/QST3.[12] These TS optimisations are very similar to typical geometry optimisations with the exception that one coordinate is maximised rather than minimised. The term coordinate, in this case, refers to an eigenvector of the force constant matrix (which can be a combination of bond lengths, angles and torsion). A negative eigenvalue is obtained in the matrix which gives rise to the single negative frequency of the TS.

2.3.5. Intrinsic reaction coordinate (IRC)

In theoretical studies of chemical reactions, the reaction pathway is extremely important. While optimisation can be done to obtain the TS and the minima reactant and product structures (on either side of the TS), structures between these critical points are obtained using IRC calculations. IRC calculations are also utilised to confirm that the correct intended TS is obtained. Starting at the TS's first-order saddle point on the PES, the reaction pathway is determined by following the steepest

descent path in either direction to the reactants and products. The differential equation gives the steepest descent pathway:

$$\frac{dx(s)}{ds} = -\frac{g(x)}{|g(x)|}, \tag{14}$$

where x is the vector of the Cartesian coordinates, s is arc length along the path and g is the PES gradient at x. The Hessian (force constant) matrix is utilised for IRC calculations, thus a frequency calculation must be done on the TS structure and thereafter corrections are made to the Hessian matrix for subsequent structures generated. Gaussian09 calculates the IRC of the reaction using the Hessian-based Predictor-Corrector (HPC) method developed by Hratchian and Schlegel.[13,14]

2.4. Electron density analyses

2.4.1. Quantum Theory of Atoms in Molecules (QTAIM)

Bader's Quantum Theory of Atoms in Molecules[15] (QTAIM) is utilised to study atoms within a molecule and each atom is separated from all other atoms based on the electron density (or topology) of the system. The QTAIM atom is hence an open system (Ω) that is bounded by a surface $S(\Omega; r)$ of zero-flux in the gradient vector field of the electron density, $\rho(r)$:

$$\nabla \rho(r) \bullet n(r) = 0, \tag{15}$$

for all r on the surface. The result is an exhaustive and physically sound partitioning of a molecular system into real-space atomic contributions. A graphical representation of this partitioning for two heteroatoms A and B is shown in **Figure 2.1**.
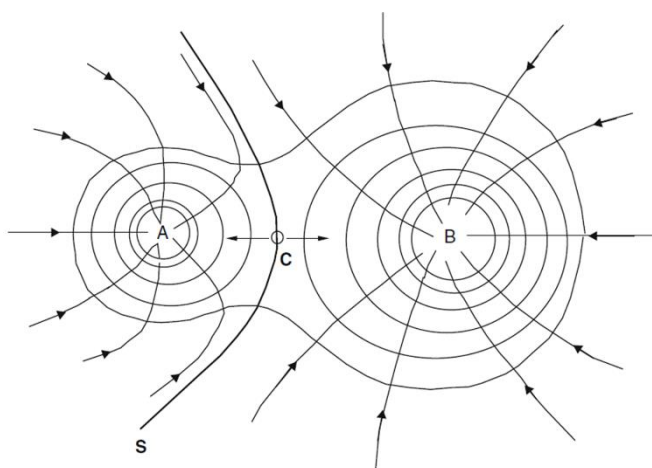
Figure 2.1: Atoms A and B are partitioned in molecule AB. **S** represents a slice through the zero-flux surface the defines the separation between the atoms. The lines with arrows are the trajectories of the gradient vector field. **S** passes through the bond critical point **C** and is not crossed by any trajectories of the gradient vector field. [Reprinted from "*Computational Chemistry: Introduction to the Theory and Applications of Molecular and Quantum Mechanics*" by E. Lewars.[2]]

26

The properties of an atom can be calculated in the same fashion as would have been done for the molecule with the sum of all the atomic properties resulting in the molecular properties. The theory capitalises on the fact that topology can be characterised by critical points (CPs) in the three-dimensions, the place where the density achieves extreme values in all three principal directions. In three-dimensions, there are four kinds of non-degenerate CP: local minima, local maxima and two types of saddle points. QTAIM refers to CPs by (*rank*, *signature*) notation, where the *signature* is the number of positive curvatures minus the number of negative curvatures. An example is the minimum CP which has a positive curvature in all three orthogonal directions, therefore it is called a (3, +3) CP. A maximum is denoted as (3, -3) while saddle points are (3, -1) and (3, +1). Nuclear sites correlate with the topology as having a maximum density, thus they have (3, -3) CPs. [Note that in some cases (3, -3) CPs have been found to not coincide with the position of a nucleus.[16,17]] A (3, +1) CP is found at the centre of ring structures and is known as ring CPs (RCP). A (3, +3) CP is found within cage structures and is known as cage CPs (CCPs).

The last type of CP can be argued as being the most important. A (3, -1) CP is found between two nuclei which have a ridge of maximum density and is thus called a bond CP (BCP). This ridge is represented by the lines of a bond path or atomic interaction line (AIL). The BCP shows several properties associated with the interaction between the two atoms[15,18–20] and integration of specific values related to the surface has been correlated with bond strength.[20]

The last part of this theory that is utilised in this project is the atomic net charge. This is calculated as:

$$q(\Omega) = \int_{\Omega} \rho(r)dr + Z(\Omega) , \qquad\qquad (16)$$

which states the atomic charge is equal to the sum of the integrated electron density of the atomic basin and the nuclear charge. It is worth noting that there are many different definitions of atomic charge such as Mulliken population analysis[21] and Natural Atomic Orbitals.[22] The atomic charge values obtained from all these methods differ significantly and thus there is no golden standard for defining the atomic charge. Although QTAIM charges are considered "exaggerated",[23] Bader and Matta have argued that QTAIM is rooted in quantum mechanics and shows excellent correlation with experimental results.[24]

2.4.2. Interacting Quantum Atoms (IQA)

Interacting Quantum Atoms (IQA) was developed by Pendás, Blanco and Francisco.[25,26] IQA is an energy decomposition scheme which calculates the interaction energy of protons and electrons in an atomic basin defined by QTAIM. IQA splits the terms of the multi-electron Hamiltonian into intra- and interatomic terms which it calculates using the second-order density matrix. Thus, when an electronic structure is calculated the use of levels of theory that have a well-defined 2nd order density matrix is required, hence wavefunctions generated with DFT cannot be used. However, the AIMAll software package makes use of the first order matrix to approximate the second order density matrix through the Müller approximation.[27] A recent paper by Pendás *et al* showed that the new algorithms incorporated into AIMAll (v14.04.17) allowed for the exact B3LYP exchange to be partitioned among atoms, allowing B3LYP level DFT to calculate the atomic exchange energies significantly more accurately.[28]

IQA decomposes the electronic energy of the molecular system, E, by summing the additive energies of all the atoms in the system,

$$E = \sum_X E_{add}^X \ .$$ (17)

If the environment change is large there are several factors which would affect the energy: (i) charge transfer, (ii) a change in the interatomic surface and (iii) electronic reorganisation within a particular atomic basin.[25] The molecular system is represented as a combination of one-body (intra-atomic or "self") contributions and two-body (interatomic or "interactions") contributions. Thus, the additive energy of any atom X, E_{add}^X, is the sum of the self-atomic energy for atom X, E_{self}^X, and half the sum of all the interactions of atom X with all remaining atoms of the system, Y.

$$E_{add}^X = E_{self}^X + \sum_{X \neq Y} 0.5 E_{int}^{X,Y} \ .$$ (18)

Thus, the recovered electronic energy, E, can also be written as

$$E = \sum_X E_{self}^X + 0.5 \sum_X \sum_{Y \neq X} E_{int}^{X,Y} \ .$$ (19)

The one-body "self" energy of a particular atom consists of (i) the atomic kinetic energy, T^X, (ii) the electron-nucleus attraction (within the atomic basin) and (iii) the electron-electron repulsion (within the atomic basin). The sum of these contributions gives the self-atomic energy for atom X:

$$E_{self}^X = T^X + V_{en}^{XX} + V_{ee}^{XX} \ .$$ (20)

When an atom is involved in bonding or an interaction, the atoms self-energy rises as the atomic basin reorganises to allow for the interaction. The energy gained from a favourable interaction will be larger than the loss of the self-energy, resulting in a lowering of the total energy.

The two-body "interaction" energy between 2 atoms, X and Y, is the sum of (i) the nucleus-nucleus repulsion, (ii) attraction between electrons in atomic basin X to nucleus of atom Y, (iii) attraction between nucleus of atom X and electrons in atomic basin Y and finally (iv) the electron-electron repulsion between the atomic basins of X and Y. This gives:

$$E_{\text{int}}^{\text{XY}} = V_{\text{nn}}^{\text{XY}} + V_{\text{en}}^{\text{XY}} + V_{\text{ne}}^{\text{XY}} + V_{\text{ee}}^{\text{XY}} . \tag{21}$$

The electron-electron repulsion, $V_{\text{ee}}^{\text{XY}}$, can be decomposed further into a columbic term and the quantum mechanical exchange-correlation term:

$$V_{\text{ee}}^{\text{XY}} = V_{\text{C}}^{\text{XY}} + V_{\text{XC}}^{\text{XY}} . \tag{22}$$

A new classical term can thus be written as:

$$V_{\text{cl}}^{\text{XY}} = V_{\text{nn}}^{\text{XY}} + V_{\text{en}}^{\text{XY}} + V_{\text{ne}}^{\text{XY}} + V_{\text{C}}^{\text{XY}} . \tag{23}$$

From this the interaction energy, $E_{\text{int}}^{\text{XY}}$, can be re-written so that it is the sum of (i) the classical term (which is electrostatic in nature) and (ii) the exchange-correlation term (which is quantum mechanical in nature):

$$E_{\text{int}}^{\text{XY}} = V_{\text{cl}}^{\text{XY}} + V_{\text{XC}}^{\text{XY}} . \tag{24}$$

The program package AIMAll[29] is utilised in this work to calculated the values of IQA.

2.4.3. Interacting Quantum Fragments (IQF) and Quantum Fragments Along Reaction Pathway (QFARP)

IQA considers the energy terms of individual atoms (and interactions with other atoms). Pendás and co-workers proposed grouping energy terms of atoms so that fragments are considered.[30] This is called Interacting Quantum Fragments (IQF). When the interaction energies of IQA are considered the number of unique interactions in the system grows exponentially with increasing system size. IQF is thus a useful approach to reducing the overwhelming amount of energy terms that must be considered. Our research group developed this concept of using IQF analysis further by considering the IQF energy terms during the course of a reaction. This concept is coined Quantum Fragments Along Reaction Pathway (QFARP). The energy terms of IQF and QFARP are calculated in the same manner and are explained below.

The additive energy of fragment, $\mathcal{M}$, is the sum of the additive energies of the atoms within fragment $\mathcal{M}$:

$$E_{add}^{\mathcal{M}} = \sum_{X \in \mathcal{M}} E_{add}^{X} . \tag{25}$$

Because the additive energy of an atom is the sum of the atoms self-energy and half the interaction-energy, a fragments additive energy can also be written as:

$$E_{add}^{\mathcal{M}} = E_{self}^{\mathcal{M}} + 0.5 \sum_{X \in \mathcal{M}} \sum_{\substack{Y \in \mathcal{M} \\ Y \neq X}} E_{int}^{X,Y} . \tag{26}$$

A fragment is considered as an isolated system. Therefore, the self-energy of a fragment is the sum of the self-energy of atoms within the fragment. Thus, the self-energy of fragment $\mathcal{M}$ can be written as:

$$E_{self}^{\mathcal{M}} = \sum_{X \in \mathcal{M}} E_{self}^{X} . \tag{27}$$

The interaction-energy of fragment $\mathcal{M}$ with atom Y, $E_{int}^{Y,\mathcal{M}}$, can be expressed as:

$$E_{int}^{Y,\mathcal{M}} = \sum_{X \in \mathcal{M}} E_{int}^{X,Y} , \tag{28}$$

or alternatively the interaction energy between two fragments, $\mathcal{M}$ and $\mathcal{N}$, which do not share atoms, can be expressed as:

$$E_{int}^{\mathcal{M},\mathcal{N}} = \sum_{X \in \mathcal{M}} \sum_{Y \in \mathcal{N}} E_{int}^{X,Y} . \tag{29}$$

To be clear, when changes in the energy terms are considered they are determined by calculating the energy difference of the *fin* state and the *ref* state:

$$\Delta E = {}^{fin}E - {}^{ref}E . \tag{30}$$

This approach of calculating changes in the energy can be applied to all energy terms expressed above in order to monitor their significance along the reaction pathway.

2.5. Conclusion

Computational chemistry has advanced significantly to become a vital approach in studying chemical systems on a fundamental level. The molecular systems in this project are modelled using Density Functional Theory. The theory calculates all the classical energetic contributions for a non-interacting system, but the true ground-state electron density is still obtained. The use of exchange-correlation functions which have empirical parameters is used to account for the energy difference of the non-interacting system. Because DFT uses empirical parameters in its functionals, it is not a true *ab initio* model. From the electron density, the wavefunction and other chemical properties can be determined.

A computational chemist has several tools such as IRC calculations to model the PES for a reaction by following the route on either side of the TS which has the steepest descent to the reaction and product minima structures.

This project utilises the techniques of (i) QTAIM, (ii) IQA and (iii) IQF/QFARP to further analyse the molecular systems along the PES. QTAIM gives a mathematically and physically sound description of an atom in a molecule with the use of the electron topology. IQA is an energy decomposition scheme which decomposes the electronic energy into interaction and non-interaction terms. The energy terms of each atom is based on the partitioning scheme of QTAIM. IQF groups the energy terms of IQA into fragments which allow for easier analysis of data. QFARP applies the analysis of IQF for fragments of atoms along a potential energy surface. The work covered in this chapter provides a means to understand the approach and results that were obtained in this project's chapter 3 and 4.

31

2.6. References

(1)   Cramer, C. J. *Essentials of Computational Chemistry: Theories and Models*, Second.; John Wiley & Sons: West-Sussex, 2004.

(2)   Lewars, E. G. *Computational Chemistry: Introduction to the Theory and Applications of Molecular and Quantum Mechanics*, Second.; Springer: Netherlands, 2011.

(3)   Davidson, E. R.; Feller, D. *Chem. Rev.* **1986**, *86* (4), 681.

(4)   Mennucci, B.; Tomasi, J.; Cammi, R.; Cheeseman, J. R.; Frisch, M. J.; Devlin, F. J.; Gabriel, S.; Stephens, P. J. *J. Phys. Chem. A* **2002**, *106* (25), 6102.

(5)   Tomasi, J.; Mennucci, B.; Cammi, R. *Chem. Rev.* **2005**, *105* (8), 2999.

(6)   Kohn, W.; Sham, L. J. *Phys. Rev.* **1965**, *140* (4A), A1133.

(7)   Johnson, E. R.; Mackie, I. D.; Dilabio, G. A. *J. Phys. Org. Chem.* **2009**, *22* (March), 1127.

(8)   Stephens, P. J.; Devlin, F. J.; Chabalowski, C. F.; Frisch, M. J. *J. Phys. Chem.* **1994**, *98* (45), 11623.

(9)   M. J. Frisch, G. W. Trucks, H. B. Schlegel, G. E. Scuseria, M. A. Robb, J. R. Cheeseman, G. Scalmani, V. Barone, B. Mennucci, G. A. Petersson, H. Nakatsuji, M. Caricato, X. Li, H. P. Hratchian, A. F. Izmaylov, J. Bloino, G. Zheng, J. L. Sonnenberg, M. Had, J. C. Gaussian, Inc.: Wallingford, CT 2009,.

(10)   te Velde, G.; Bickelhaupt, F. M.; Baerends, E. J.; Fonseca Guerra, C.; van Gisbergen, S. J. a.; Snijders, J. G.; Ziegler, T. *J. Comput. Chem.* **2001**, *22* (9), 931.

(11)   Fonseca Guerra, C.; Snijders, J. G.; te Velde, G.; Baerends, E. J. *Theor. Chem. Accounts Theory, Comput. Model. (Theoretica Chim. Acta)* **1998**, *99* (6), 391.

(12)   Foresman, J. B.; Frisch, Æ. *Exploring Chemistry with Electronic Structure Methods: A Guide to using Gaussian*; Gaussian, Inc.: Pittsburgh, 1996.

(13)   Hratchian, H. P.; Schlegel, H. B. *J. Chem. Phys.* **2004**, *120* (21), 9918.

(14)   Hratchian, H. P.; Schlegel, H. B. *J. Chem. Theory Comput.* **2005**, *1* (1), 61.

(15)   Bader, R. F. W. *Atoms in Molecules: A Quantum Theory*; Oxford Universisty Press: Oxford, 1990.

(16)   Pendás, A. M.; Blanco, M. A.; Costales, A.; Sánchez, P. M.; Luaña, V. *Phys. Rev. Lett.* **1999**, *83* (10), 1930.

(17)   Jones, T. E.; Eberhart, M. E. *Acta Crystallogr. Sect. A Found. Crystallogr.* **2009**, *65* (2), 141.

(18)   Bader, R. F. W. In *Advances in Quantum Chemistry*; Elsevier B.V., 2009; Vol. 57, pp 285–318.

(19)   Bader, R. F. W.; Fang, D.-C. *J. Chem. Theory Comput.* **2005**, *1* (3), 403.

(20)   Platts, J. A. *Phys. Chem. Chem. Phys.* **2005**, *7* (22), 3805.

(21)   Mulliken, R. S. *J. Chem. Phys.* **1955**, *23* (10), 1833.

(22)   Reed, A. E.; Curtiss, L. a; Weinhold, F. *Chem. Rev.* **1988**, *88* (6), 899.

(23)   Haaland, A.; Helgaker, T. U.; Ruud, K.; Shorokhov, D. J. **2000**, *77* (8), 1076.

(24)   Bader, R. F. W.; Matta, C. F. *J. Phys. Chem. A* **2004**, *108* (40), 8385.

(25)   Blanco, M. A.; Martín Pendás, A.; Francisco, E. *J. Chem. Theory Comput.* **2005**, *1* (6), 1096.

(26)   Francisco, E.; Martín Pendás, A.; Blanco, M. A. *J. Chem. Theory Comput.* **2006**, *2* (1), 90.

(27)   Muller, D. E. *Math. Tables Other Aids to Comput.* **1956**, *10* (56), 208.

(28)   Maxwell, P.; Pendás, Á. M.; Popelier, P. L. A. *Phys. Chem. Chem. Phys.* **2016**, 20986.

(29)   Keith, T. A. TK Grismill Software: Overland Parks KS, USA 2013, aim.tkgristmill.com.

(30)   Martín Pendás, A.; Blanco, M. A.; Francisco, E. *J. Chem. Phys.* **2006**, *125* (18), 184112.

Chapter 3

Energy decomposition of DFT modelled S_N2 reactions of α-bromoacetophenone with phenolate and acetate using QFARP

3.1. Introduction and aim

As previously discussed in Chapter 1, S_N2 reactions have been studied extensively with interest in α-haloketones, due to the enhanced reactivity compared to haloalkanes.[1] These reactions are utilised to obtain 1,2-disconnections which are not easily achieved with other methods.[2] While some computational work has been done to explain the enhanced reactivity a thorough explanation on a fundamental level has not been obtained.

QTAIM has been used to study other S_N2 reactions, however extensions of the theory such as bond bundles[3] and Interacting Quantum Atoms (IQA)[4,5] have rarely been used. While IQA is computationally expensive, it is a very informative tool which decomposes the electronic energy of the molecular system using electron density topology. Unfortunately, as the molecular systems increase in size, the number of interactions increases exponentially. By grouping atoms of the system into fragments, the data analysis becomes more comprehensible and easier to interpret than considering individual interactions between atoms. This approach has been used to consider energy differences for conformers using fragment attributed molecular system energy change (FAMSEC)[6] and considering reaction pathways and selectivity with quantum fragments along reaction pathway (QFARP).

QFARP has successfully been used to explain the specificity for alkylation of adenine at different sites.[7] The technique has been adapted in this work to study the displacement of widely used α-haloketone systems.

Early MO studies[8–10] concluded that the low lying "allylic" bond orbitals of α-haloketones result in the stabilisation of the TS which enhances the reactivity. Most computational studies on S_N2 reactions have used very small molecular systems which are far simpler than the typical size which is encountered in a synthesis laboratory.

In this chapter, α-Bromoacetophenone (**α-BrAcPh**) is used to represent the α-haloketone system as it has been used in experimental[11–15] and computational[16,17] studies extensively and are similar in size to what is encountered in experimental studies.

Experimental literature shows **α-BrAcPh** commonly undergoing S_N2 type reactions with phenolate (**PhO⁻**) and acetate (**AcO⁻**), with Edwards and Pearson[18] showing that **PhO⁻** is somewhat more reactive than **AcO⁻** for these S_N2 reactions. [Note that while several computational studies on the S_N2 reactions of **α-BrAcPh** have been done, the nucleophiles **PhO⁻** and **AcO⁻** have not been used in such studies.]

35

Thousands of analogues of these compounds have also been observed. These reactions are shown in general to be high yielding. In the work reported we have chosen to study these two reactions (**Scheme 3.1**) as they are good representations of the *O*-alkylation of α-haloketones via an S$_N$2 type reaction. In addition, the use **α-BrAcPh** would allow future investigations into the effects of electron withdrawing-/donating-substituents on the aromatic ring system of **α-BrAcPh**.
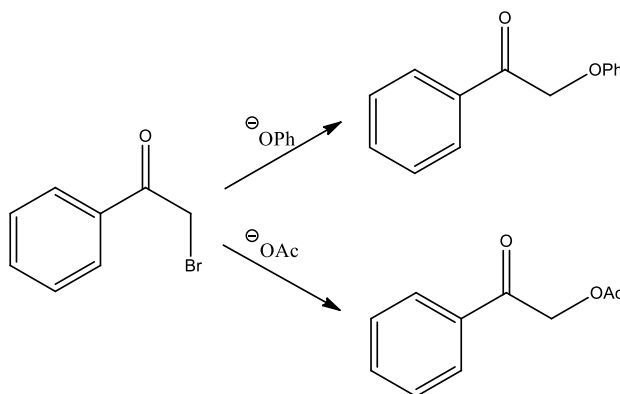
Scheme 3.1: S$_N$2 displacement of α-bromoacetophenone (**α-BrAcPh**) with phenolate (**PhO⁻**) and acetate (**AcO⁻**).

Experimentally, bases such as potassium carbonate,[19] potassium hydroxide[20] and triethylamine[21] are used to deprotonate the nucleophile resulting in the nucleophile have a net charge of -1 *e*. This deprotonation results in a more reactive nucleophile than its neutral counterpart. Therefore, **PhO⁻** and **AcO⁻** were used, rather than phenol and acetic acid.

The aim is to use IQA/QFARP to study S$_N$2 reactions to identify the leading interactions and how they change during the reaction. Studying these interactions would provide a more fundamental understanding of the forces which help progress or hinder the reaction. Comparing the interactions for the reactions of **PhO⁻** and **AcO⁻** are performed to understand how they differ and what causes the difference in reactivity which has been noted experimentally.

3.2 Computational Details

All structure optimisations were done using Gaussian 09, rev. D.01[22] with B3LYP/6-311++G(d,p) level of theory using the Integral Equation Formalism for Polarisable Continuum model (IEFPCM) for simulating acetone and tetrahydrofuran (THF) as the solvent for the **PhO⁻** and **AcO⁻** reactions, respectively. Frequency calculations for structures were done at 80°C and 56°C for the **PhO⁻** and **AcO⁻** reactions, respectively. These conditions follow published experimental procedures for the reactions of **PhO⁻**[19] and **AcO⁻**.[23]

Benchmark studies[24–27] on S_N2 reactions have shown that B3LYP, used in this research, is satisfactory though it does underestimate the activation energy. However, B3LYP is one of the few functionals for which, due to a dedicated protocol implemented in AIMAll,[28] molecular energy is reproduced by the IQA energy terms. Post-HF methods, such as MP2 calculations, were not used due to the extensive computational resources that are required for frequency calculations to obtain the Gibbs free energy and even more so for the IQA calculations.

Transition state (TS) structures were obtained using Berny or QST3 optimisation. The TS conformer with the lowest electronic energy was selected for further studies. Frequency calculations were performed to confirm that a true TS was obtained with a single negative vibrational frequency. Thereafter intrinsic reaction path (IRC) calculations were used to obtain the lowest energy pathway to the reactant- and product-complex. IQA calculations are computationally expensive, and thus only a few selected structures along the IRC were taken. These selected structures were then used to generate their respective formcheck files which were submitted to AIMAll[28] (ver. 15.09.12) to compute topological QTAIM (Quantum theory of atoms in molecules) and IQA defined properties with an increased integration radius of 20 a.u. to account for the molecular system being an anion.

The change in the electronic energy of the molecular systems, E, was consistently underestimated from the IQA additive atomic energies, E(IQA), to within 0.003%. The difference between E and E(IQA) is expected as one must also realise that numerous energy components contribute to the IQA-defined molecular energy and small numerical integration errors (a numerical 'noise') are simply unavoidable. Therefore, it is emphasised that the focus is on relative trends rather than predicting energy terms.

Theoretical Background

The reader is referred to chapter 2 for a discussion on the theoretical background on electron density analyses. To assist in the analysis of IQA data, QFARP is utilised by fragmenting the molecular system based on (i) molecules, (ii) functional groups and (iii) atoms which are show to play an important role. **Table 3.1** shows the molecular graph of the TS of **PhO⁻** and **AcO⁻** reacting with **α-BrAcPh**, along with the fragments that have been used to analyse the system. For nomenclature, note that $\mathcal{H}$ represents a molecular fragment containing "all other atoms".

Table 3.1: Molecular graphs of the TS for **PhO⁻** and **AcO⁻** reacting with **α-BrAcPh**. Fragments which are used in QFARP analysis are represented graphically in dashed lines with each atom having its numbering shown above. [$\mathcal{H}$ = all other atoms]

$\mathcal{B}$ = {C1-H16,Br29}	$\mathcal{A}$ = {C1-H16}
PhO⁻: $\mathcal{N}$ = {O17-H28}	**PhO⁻**: $\mathcal{R}$ = {C18-H28}
$\mathcal{P}$ = {C6-H16}	$\mathcal{K}$ = {C4O5}; $\mathcal{L}$ = {O17C18}
	$\mathcal{M}$ = {C1H2H3}
AcO⁻: $\mathcal{N}$ = {O17-H23}	**AcO⁻**: $\mathcal{R}$ = {C18-H23}

38

3.3   Results and Discussion

3.3.1   Energy change along reaction coordinates (reaction pathways)

The TS for the reactions for **PhO⁻** and **AcO⁻** was determined – **Figure 3.1**. Frequency calculations showed the single negative vibrational frequency. The displacement vectors of the negative vibrational frequency show the α-C (C1) moves towards the attacking-*O* (O17), while there are other smaller movements such as the attacking-*O* moving towards the α-C and the hydrogens on the α-group (C1H2H3) also moving towards to the nucleophile and away from Br. Videos of these vibrations are included on attached CD.
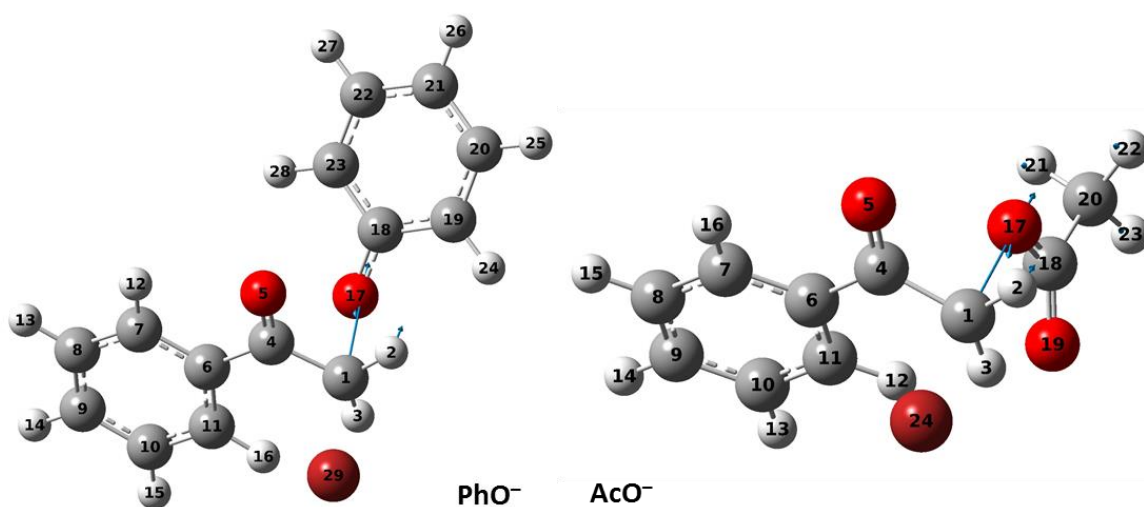
Figure 3.1: S$_N$2 TS structure of **PhO⁻** (left) and **AcO⁻** (right) reacting with **α-BrAcPh**, with blue vectors showing the negative vibrational frequency. Gaussian numbering of the atoms is included for each atom.

The potential energy surface (PES) for the reaction was generated using IRC calculations. The data was represented in relation to a physical measure, namely the distance between C1 and O17 rather than the IRC coordinates. The vertical dashed line shown on all graphs represents the TS structure. The energy profiles with (i) separated reagents and products and (ii) in terms of the IRC coordinate are shown in Appendix A. The energy profile, **Figure 3.2**, shows that the reaction with **PhO⁻** and **AcO⁻** have activation energies of 4.1 and 6.4 kcal/mol, respectively. The difference in energy between the reactant- and product-complex for the **PhO⁻** reaction is larger by 5.5 kcal/mol indicating a more exothermic and favourable change than that of the **AcO⁻** reaction. These two findings, the activation energy and exothermic effect, already suggest that indeed **PhO⁻** is more reactive than **AcO⁻**. This correlates with the reported literature data very well.[18] This can be used to validate the optimised structures used in this studies.

39
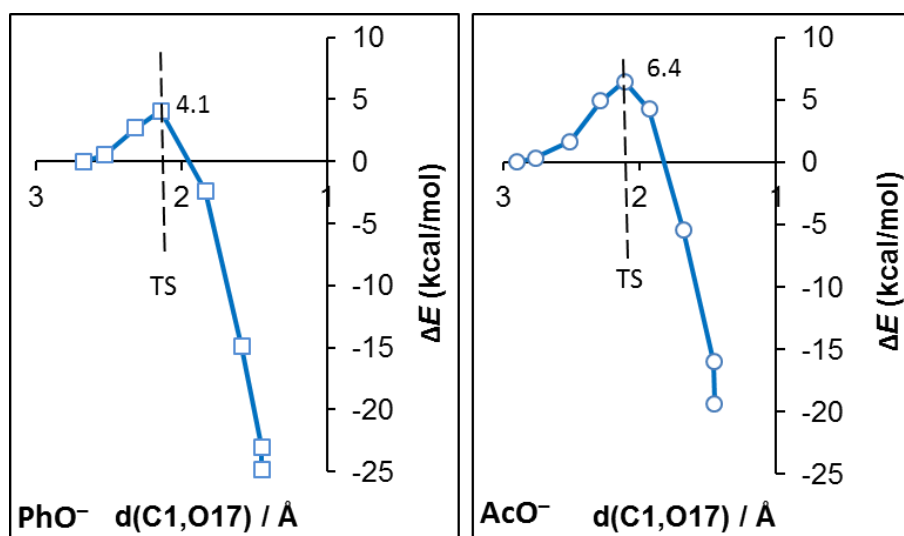
Figure 3.2: PES obtained from IRC calculations showing change in electronic energy, relative to the RC, for S_N2 reactions of **PhO⁻** and **AcO⁻** reacting with **α-BrAcPh**.

A complete PES for the reactions of **PhO⁻** and **AcO⁻** is obtained by optimising the separate reactants (R) and products (P) structures. These additional energies provide a more informative PES of the two reactions, **Figure 3.3**. The electronic energy change, ΔE, shows the favourable formation of the RC, whereas the Gibbs free energy change, ΔG, shows a significant increase in the energy for the RC structure. For the reaction of **PhO⁻**, the electronic energy for the TS structure is shown to be -2.6 kcal/mol lower than the energy of R, suggesting the reaction does not have an energy barrier to overcome. However, as discussed in chapter 1 (**Figure 1.2**), once the Gibbs free energy is considered for a PES, the $\Delta G^{\#}$ of the TS structure is found to be greater than that of R once the thermochemistry is taken into consideration. Furthermore, it is found that the activation energy, $\Delta G^{\#}$, of the **PhO⁻** reaction is -5.4 kcal/mol lower in energy than of the **AcO⁻** reaction, supporting the experimental findings. The final product structures of the **PhO⁻** reaction is also significantly more stabilised than the **AcO⁻** reaction.

40

(a)

(b)
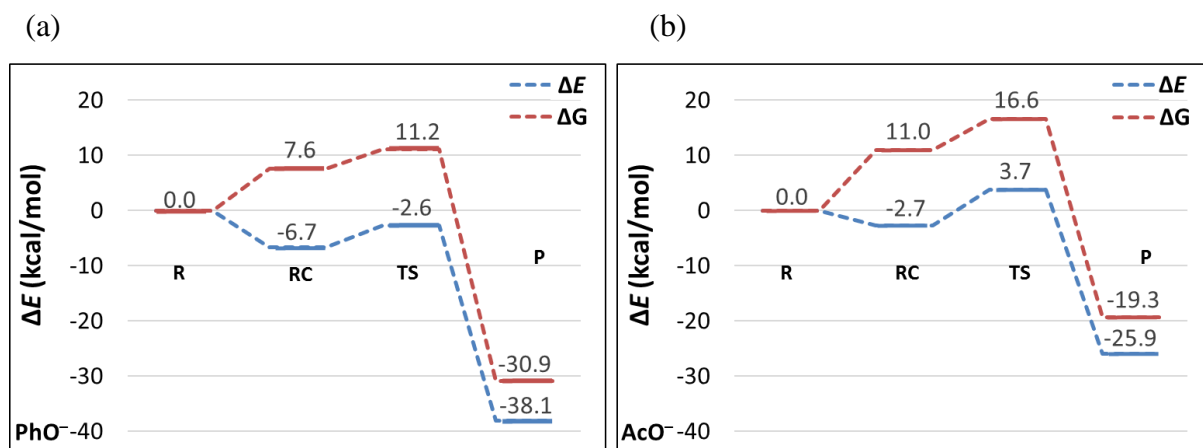
Figure 3.3: PES related to electronic energy (ΔE) and Gibbs free energy (ΔG) generated by the S_N2 reaction of **α-BrAcPh** with (a) **PhO⁻** and (b) **AcO⁻**.

Note that while the two reactions have been modelled in different solvents and at different temperature to follow published procedures,[19,23] the main aim of this study is to analyse the reactions with QFARP to gain a more fundamental understanding of the reactions and how they differ from each other.

Furthermore, a brief literature search of the two reactions showed a clear preference for the **PhO⁻** reaction to be done with acetone as the solvent, while the reaction with **AcO⁻** has been done in various solvents. While it is possible that the solvent has a significant influence on the reaction, further investigation into this noted trend would be required.

3.3.2   Molecular fragment based analysis

In the IQA scheme, the molecular or fragment electronic energy is recovered by summing up atomic energies. This is extremely useful as otherwise one would not be able to monitor changes in electronic energy of a molecular fragment along the reaction pathway.

The change in additive energy of fragments $\mathscr{B}$ and $\mathscr{N}$, which represent the initial 2 molecules - the nucleophile and electrophile, is shown in **Figure 3.4**, along with fragment $\mathscr{A}$ which represents **α-BrAcPh** without the attached leaving group, Br. By decomposing the electronic energy an insight into which fragments contribute to the activation energy and exothermicity of the reaction can be gained.

Firstly, **Figure 3.4** shows that the additive atomic energy of the nucleophile, $\mathscr{N}$, contributes to the activation energy and, after the TS, begins contributing significantly to the exothermicity; this release in energy of the nucleophile is because of it forming a new bond between C1 and O17.

41

Figure 3.4 also shows that the electrophile **α-BrAcPh** without its leaving group, $\mathscr{A}$, contributes to the activation energy the most. However, once the leaving group is also included with fragment of **α-BrAcPh**, $\mathscr{B}$, a large stabilisation effect is noted, showing that the leaving group provides stability which plays an important role in the S_N2 reaction. Importantly, when the additive energies of the fragment for the PC are considered the fragments of **α-BrAcPh**, $\mathscr{A}$ and $\mathscr{B}$, are significantly more destabilised for the reaction of **AcO⁻** than **PhO⁻**. This difference in additive energy of $\mathscr{A}$ and $\mathscr{B}$ results in the differences in the activation energy that is noted. This data is unexpected as it would suggest that it is the electrophile which plays the significant role in determining the energy barrier of a reaction. Note however that the electrophiles for the two reactions are the same. Therefore, it can be concluded that the nucleophiles affect the electrophile in different ways which results in the reactivity difference which is noted experimentally.
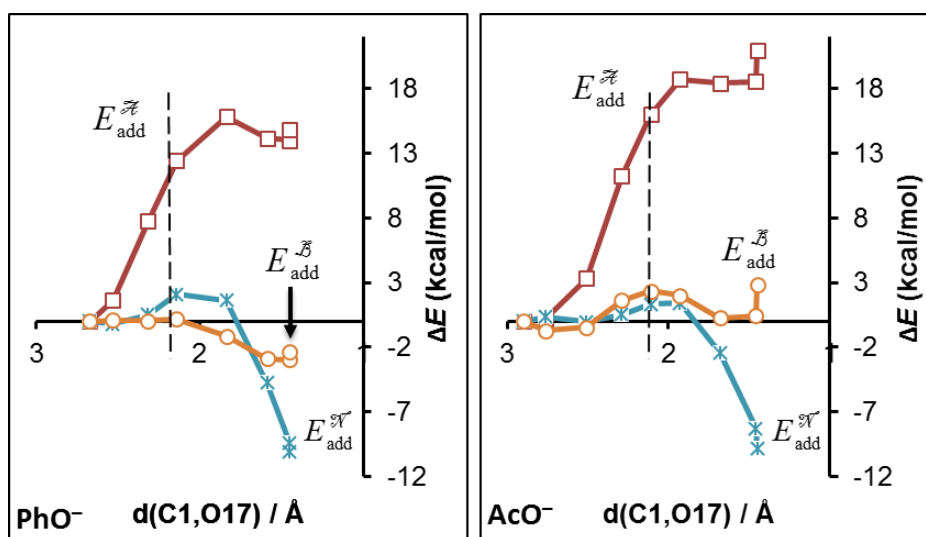
Figure 3.4: Change in additive energy for selected fragments of **α-BrAcPh** (Fragments $\mathscr{A}$ and $\mathscr{B}$ – **Table 3.1**) and nucleophile (Fragment $\mathscr{N}$) for **PhO⁻** and **AcO⁻** undergoing the S_N2 reaction with **α-BrAcPh**.

By splitting the fragment $\mathscr{A}$ and $\mathscr{B}$ into smaller fragments, one can narrow down the fragments which contribute to the trends which have been noted in **Figure 3.4**. The electrophile has been partitioned into the fragments: $\mathscr{M}$, $\mathscr{P}$, $\mathscr{K}$ (as shown in **Table 3.1**) and Br. **Figure 3.5** shows the change in additive energy of the functional groups: $\mathscr{M}$, $\mathscr{N}$ and Br. Fragments $\mathscr{K}$ and $\mathscr{P}$ of **α-BrAcPh** (Appendix A) present little change in their additive energy. This is expected as the atoms further away from the site of reaction the smaller the changes in their additive energy will be.

$\mathscr{M}$ (the CH_2 functional group) experiences a large destabilisation which contributes the most to the activation energy of the reaction, with the reaction of **PhO⁻** experiencing less destabilisation

42

than that of the **AcO⁻** reaction. This destabilisation of fragment $\mathscr{M}$ can be explained by considering the removal of electron density from the fragment, which is noted later.

The leaving-group, Br, plays the most significant role in stabilising the reaction even though its bond to C1 is being broken, with the stabilisation being approximately the same for both reactions resulting in neither reaction being favoured. The stabilisation of Br largely compensates the destabilisation which $\mathscr{M}$ experiences when $E_{\mathrm{add}}^{\mathscr{B}}$ is considered.
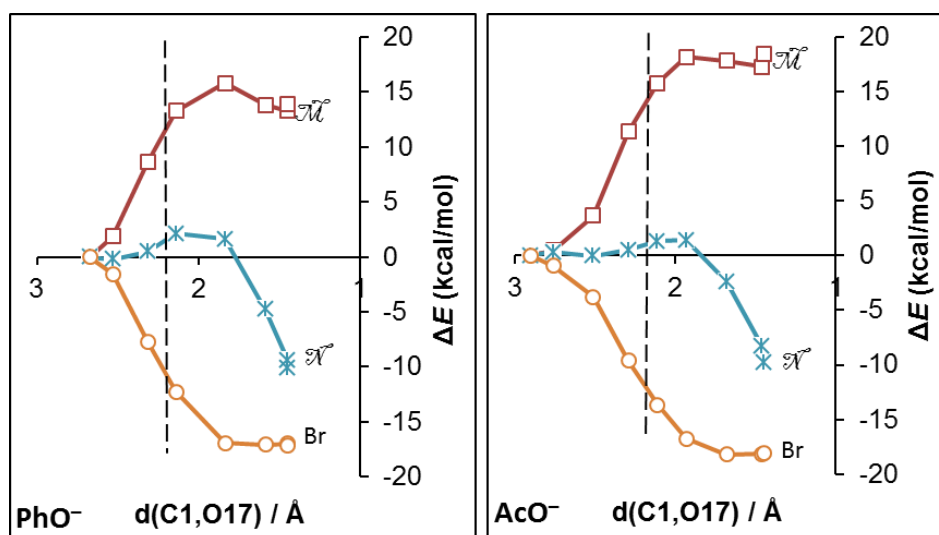
Figure 3.5: Change in additive energy of selected fragments (**Table 3.1**) along S$_N$2 reaction pathway of **α-BrAcPh** with **PhO⁻** or **AcO⁻**.

Consequently, the analysis thus far has shown that the atomic energies of **α-BrAcPh** and not only of the nucleophile, change substantially. While there are some differences in the atomic energies of the nucleophiles, the most significant difference arises from the atomic energies of the electrophiles. This is unexpected as the electrophiles are the same for both reaction. Thus, it is the effect which the nucleophile has upon fragment $\mathscr{M}$ of the electrophiles which result in the differences in reactivity, with little change being noted for the other fragments of the electrophile.

3.3.3 Forces driving the S$_N$2 reaction to completion

Interaction between entire molecules, α-bromoacetophenone ($\mathscr{B}$) and the nucleophile ($\mathscr{N}$)

The approach taken is based on the observation that when a reaction between two molecules is considered then the formation of the final product, or lack thereof, can often be understood using the interaction energy between them, either being attractive or repulsive. Thus, the reactions studied

43

here (α-**BrAcPh** with **PhO⁻** or **AcO⁻**) can be understood by considering the attraction between these molecules from the beginning of the reaction, to the end. For this, much larger fragments are selected (each fragment being a whole molecule, $\mathscr{B}$ and $\mathscr{N}$) and the interaction between the two reactants considered – see **Figure 3.6**. $E_{\text{int}}^{\mathscr{B},\mathscr{N}}$ shows that initially the fragments have highly attractive interactions which increase exponentially as the reaction progresses. This would be the driving force which brings the two molecules together. Importantly, when $E_{\text{int}}^{\mathscr{A},\mathscr{N}}$ is considered, which excludes the interactions of $\mathscr{N}$ with Br, the same trend of $E_{\text{int}}^{\mathscr{B},\mathscr{N}}$ is followed but with a greater attraction being noted. This difference in interaction energy between $E_{\text{int}}^{\mathscr{A},\mathscr{N}}$ and $E_{\text{int}}^{\mathscr{B},\mathscr{N}}$ indicates that there is a repulsive interaction between the leaving group, Br, and the nucleophile, $\mathscr{N}$. This is expected as both fragments are highly negatively charged. With the interaction between Br and $\mathscr{N}$ being repulsive, it would enhance the removal of Br from α-**BrAcPh** as the nucleophile comes closer to the electrophile during the S_N2 reaction.

It is important to note that **AcO⁻** is slightly more attracted to α-**BrAcPh** than the **PhO⁻** reaction. For instance, at the TS, $E_{\text{int}}^{\mathscr{A},\mathscr{N}}$ and $E_{\text{int}}^{\mathscr{B},\mathscr{N}}$ of the **PhO⁻** reaction is 16.1 and 10.5 kcal/mol smaller than of the **AcO⁻** reaction, respectively.
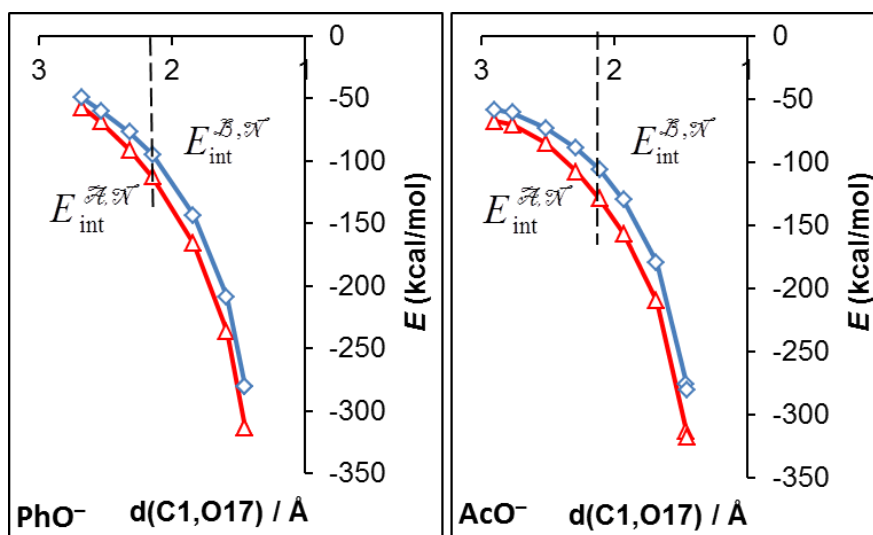
Figure 3.6: Inter-fragment interaction energy between fragments of α-**BrAcPh** ($\mathscr{A}$ and $\mathscr{B}$) and $\mathscr{N}$ (**PhO⁻** and **AcO⁻**) along the S_N2 reaction pathways.

In search of the origin of the relationships shown in **Figure 3.6**. it was necessary to investigate more localised interactions, either diatomic between leading atoms or specific smaller fragments, to understand which interactions drive the reaction forward.

44

Interaction between molecular fragments

Because α-haloketones are more reactive to S_N2 reaction than haloalkane compounds,[1] it suggests that the carbonyl functional group plays a significant role in the reaction by enhancing the reactivity. The interactions of the carbonyl fragment, $\mathcal{K}$, with other fragments were considered to see if it assists in the reaction – **Figure 3.7**.
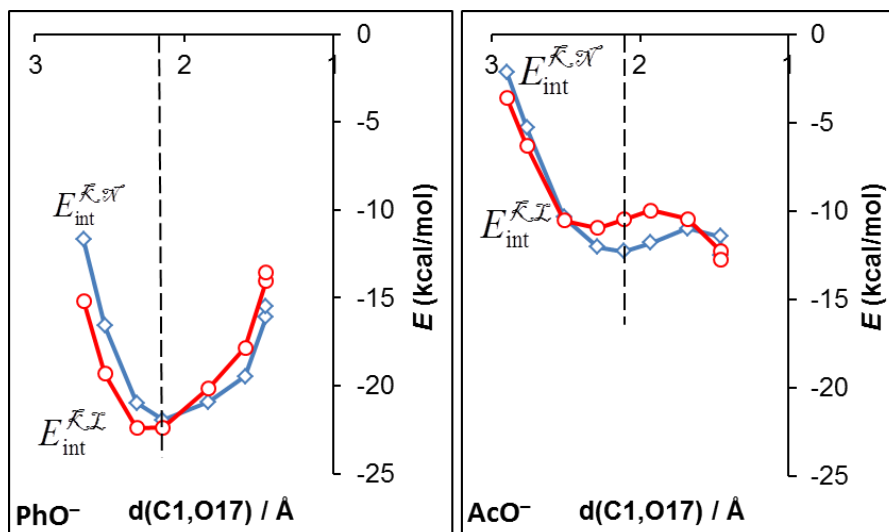
Figure 3.7: Interaction energy of the carbonyl-group, $\mathcal{K}$, with fragment $\mathcal{I}$ (O17C18) and nucleophile, $\mathcal{N}$, along the S_N2 reaction pathway of **α-BrAcPh** with **PhO⁻** or **AcO⁻**.

At the beginning of the reaction, $E_{\text{int}}^{\mathcal{K},\mathcal{N}}$ shows that the nucleophile is experiencing a greater attraction to the carbonyl group for the **PhO⁻** reaction than the **AcO⁻** reaction. As the reaction progresses this attraction between the two fragments increases by approximately -10 kcal/mol. At the TS, $E_{\text{int}}^{\mathcal{K},\mathcal{N}}$ is shown to be -22 and -12 kcal/mol for the reactions with **PhO⁻** and **AcO⁻**, respectively. This additional attraction which is noted for the **PhO⁻** reaction correlates with the greater reactivity which has been noted over the **AcO⁻** reaction. Interestingly, $E_{\text{int}}^{\mathcal{K},\mathcal{N}}$ for the **PhO⁻** reaction is noted to be approximately the same are the beginning and end of the reaction.

Note also that $E_{\text{int}}^{\mathcal{K},\mathcal{I}}$ reproduces the trend which was noted from $E_{\text{int}}^{\mathcal{K},\mathcal{N}}$. This shows that the interactions of $E_{\text{int}}^{\mathcal{K},\mathcal{N}}$ is mostly the result of $\mathcal{I}$ (O17C18), and that the more distant atoms of the nucleophiles play a far smaller role. The trends noted for the two reactions are very different to one another. While fragment $\mathcal{K}$ is common for the reactions, $\mathcal{N}$ and $\mathcal{I}$ are substantially different which thus accounts for the different trends that have been observed.

45

While it is shown that the carbonyl group does provide an attractive force on the nucleophile, which would assist the nucleophilic substitution, QFARP studies on the S_N2 reactions of haloalkanes would be required to further support these findings. Studies with haloalkanes would show if the neighbouring atoms contribute attractive forces that would assist the reaction.

The interactions of the phenyl fragment, $\mathscr{P}$, with other fragments were also considered, however no important trends or values were noted - Appendix A.

3.3.4 Leading diatomic interactions between α-bromoacetophenone ($\mathscr{B}$) and Nucleophile ($\mathscr{N}$)

An examination of the diatomic interactions between atoms of $\mathscr{A}$ and $\mathscr{N}$ was undertaken with the aim of identifying if some of them can be seen as leading interactions which can be used to explain relative placement of the two molecules, hence the approach to form a new bond. There are 406 unique diatomic interactions for the **PhO⁻** molecular system (276 for the **AcO⁻** system) and we examined the molecular system at the RC where d(C1,O17) = 2.67 Å first (2.90 Å for **AcO⁻**). The molecular graphs of these generated reaction pathways are shown in **Table 3.2**.

When the molecular graph of RC for the **PhO⁻** reaction is considered, a bond path is present between C4–O17, d(C4,O17) = 2.64 Å, rather than between C1–O17, d(C1,O17) = 2.67 Å. It is only after the RC, when the distance between C1–O17 decreases, that a bond path between C1–O17 is established. For the reaction of **AcO⁻** on the other hand, a bond path between C1–O17, d(C1,O17) = 2.90 Å, for the RC structure is present. O19 of **AcO⁻** has two additional bond paths with H3 and H12, d(H3,O19) = 2.29 Å and d(H12,O19) = 2.36 Å. O19 continues to have bond paths with H3 and H12 at the TS, while for the PC O19 only has a bond path with H12, d(H12,O19) = 2.63 Å. Furthermore, it is worth noting that at the TS the bond C1–O17 is shorter than C1–Br bond by 0.24 Å and 0.30 Å for the reactions of **PhO⁻** and **AcO⁻**, respectively.

The leaving group should be repelled by the nucleophile in a linear fashion, elongating the C1–Br bond and removing Br from the S_N2 product.[29] The angle of Br–C1–O17 for both reactions stays considerably linear during the course of the reaction with an angle of 175±3° with only significant variation for the RC and PC structures.

For all molecular graphs, a bond path is noted between H3–H16 for **PhO⁻**, and H3–H12 for **AcO⁻**. For **PhO⁻**, $E_{\text{int}}^{\text{H3,H16}}$ is -2.60 kcal/mol at the PC, while **AcO⁻** has $E_{\text{int}}^{\text{H3,H16}}$ of -1.29 kcal/mol. These are weak attractive interactions even though both hydrogen atoms are slightly positively

46

charged. [At the PC, **PhO⁻**: q(H3)=0.05, q(H16)=0.04; **AcO⁻**: q(H3)=0.09, q(H12)=0.05 e.] Further investigation of these hydrogen interactions was not performed.

The most significant attractive and repulsive diatomic interactions between fragment $\mathscr{B}$ and $\mathscr{N}$ were considered – see **Table 3.3** and **Table 3.4**. For the fragment interactions between $\mathscr{B}$ and $\mathscr{N}$, **Table 3.3** shows that the most attractive diatomic interaction, $E_{\text{int}}^{\text{X,Y}}$, for the **PhO⁻** reaction of –151.4 kcal/mol, was found for C4•••O17. This value is directly comparable to $E_{\text{int}}^{\text{X,Y}}$ computed for a covalent bond between C and H in **α-BrAcPh**, $e.g.$, C7–H12 with an $E_{\text{int}}^{\text{C7,H12}}$ of –152.30 kcal/mol. The same is true when considering the attractive interaction between **AcO⁻** and **α-BrAcPh** - see **Table 3.4**, with attractive interactions between C18•••O5 and O17•••C4 of -140.3 and -131.6 kcal/mol respectively.

This is unexpected as one might assume the interaction of C1•••O17 would be greater than that of C4•••O17 as a covalent bond will form between C1-O17 during the reaction.

47

Table 3.2: Molecular graphs of (a) reactant-complex, (b) TS and (c) product-complex generated from IRC-calculations for the S_N2 reaction of **α-BrAcPh** with (i) **PhO⁻** and (ii) **AcO⁻**. The numbering of each atom is shown above.
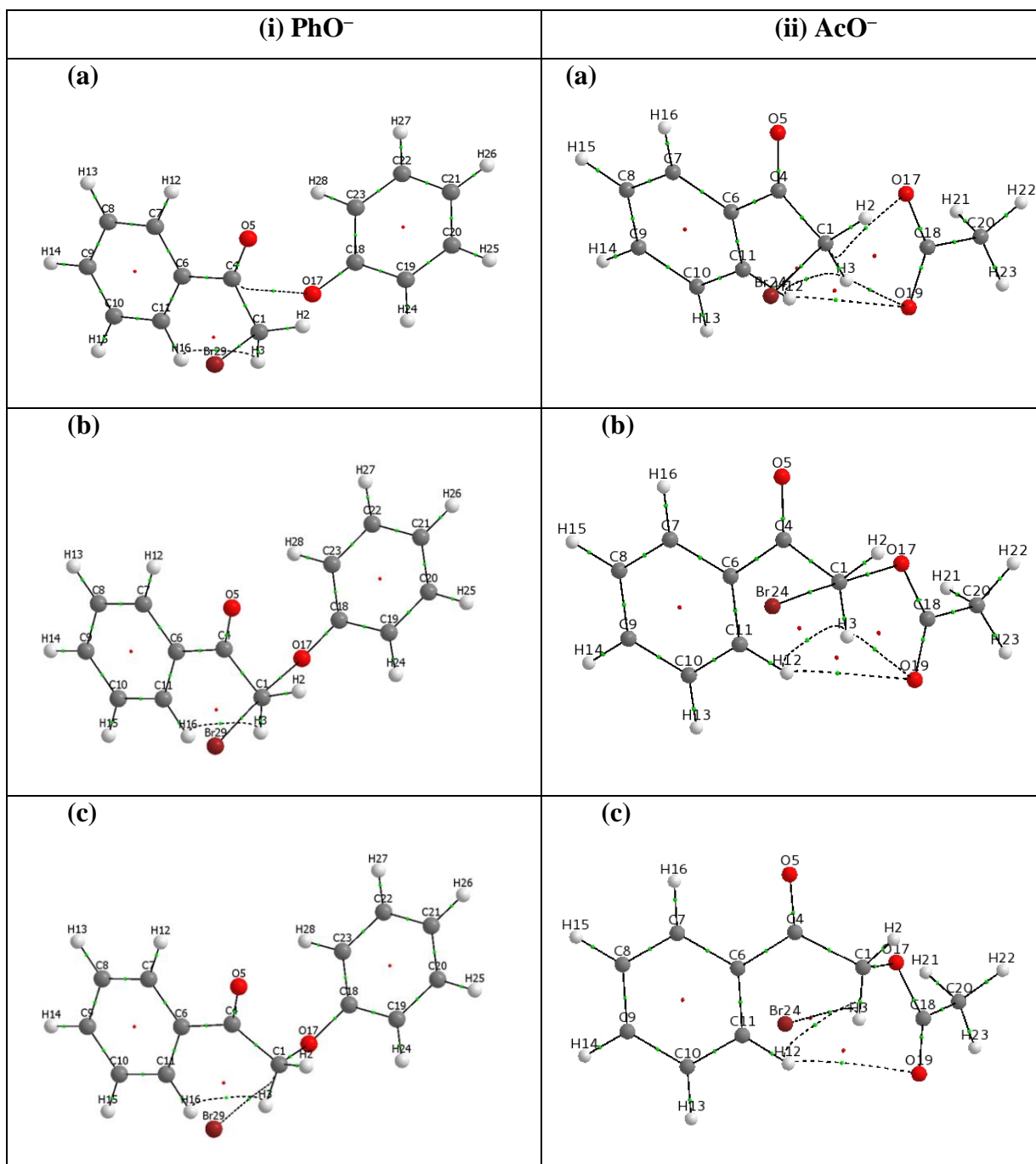
One might immediately assume that because **PhO⁻** and **AcO⁻** have huge attractive interactions with the carbonyl-*C* (C4), the nucleophile will undergo carbonyl addition. However, the total electronic energy of the system, *E*, increased exponentially when the reaction coordinate was set between these two atoms, C4 and O17 to allow for carbonyl addition - Appendix A.

Interestingly, in absolute values, $E_{\text{int}}^{\text{C1,O17}} > E_{\text{int}}^{\text{C4,O17}}$ only well after the TS - see **Figure 3.8**. So why does the nucleophile tend to C1 rather than the carbonyl-*C*, C4, which has greater attraction

initially? This strongly points to the role of repulsive interactions, essentially preventing an attack on C4.
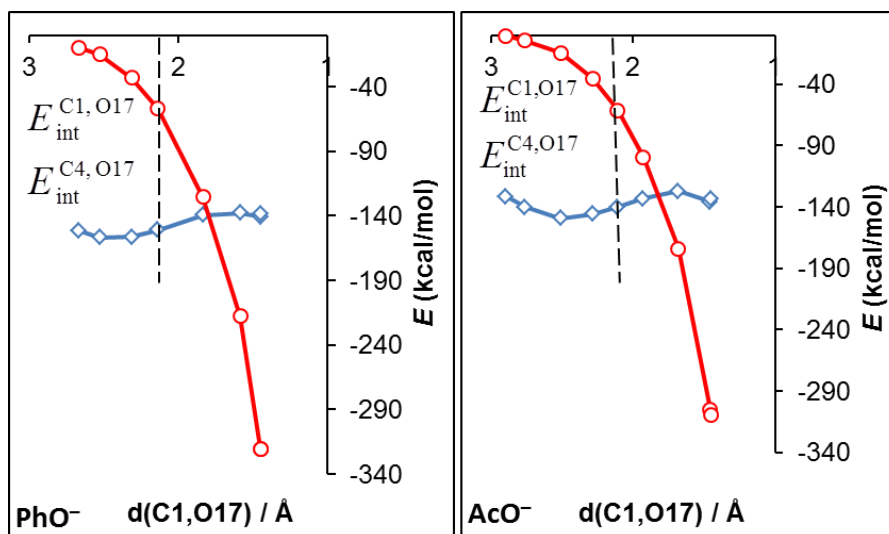
Figure 3.8: Interaction energy of $E_{int}^{C1,O17}$ and $E_{int}^{C4,O17}$, two significant attractive interactions, along the S_N2 reaction pathway for **α-BrAcPh** with **PhO⁻** or **AcO⁻**.

By considering the charges of the atoms, these strong electrostatic interactions can be understood. **Figure 3.9** shows the net atomic charge of selected atoms at the TS, while **Figure 3.10** shows the leading attractive (blue) and repulsive (red) interactions at the TS for the two reactions. When considering the (de)stabilising interactions, it is clear that they correlate with the net charges of the atoms.

The leading attractive interactions of **PhO⁻** and **AcO⁻** with the carbonyl group are opposed by the repulsive interactions between the two groups as well. These repulsive interactions would only grow stronger than the attractive ones if the nucleophile were to undergo carbonyl addition, resulting in the increase in *E*.

49

Table 3.3: The most significant diatomic inter-fragment interaction energies between **PhO⁻** and **α-BrAcPh** found at the initial state of the molecular system, d(C1,O17) = 2.67 Å; values in kcal/mol.

				PhO⁻			
	Attractive			**Repulsive**			
Atom	**Atom**	E_{int}		**Atom**	**Atom**	E_{int}	**Sum**
O17	C4	-151.4		O17	O5	144.9	-6.5
C18	O5	-88.0		C18	C4	79.3	-8.7
O17	H3	-16.2		Br29	O17	12.6	-3.6
O17	H2	-15.5		C23	O5	10.0	-5.5
O17	C1	-9.6		C19	O5	9.6	0.0
C23	C4	-9.1		C18	H2	7.3	-1.8
C19	C4	-8.6		C18	H3	6.8	-1.8
Br29	C18	-8.0		C21	O5	4.5	-3.5
O17	H12	-5.9		C22	O5	4.0	-1.9
Total Sum							**-33.3**

Table 3.4: The most significant diatomic inter-fragment interaction energies between **AcO⁻** and **α-BrAcPh** found at the initial state of the molecular system, d(C1,O17) = 2.90 Å; values in kcal/mol.

				AcO⁻			
	Attractive			**Repulsive**			
Atom	**Atom**	E_{int}		**Atom**	**Atom**	E_{int}	**Sum**
C18	O5	-140.3		C18	C4	135.6	-4.7
O17	C4	-131.6		O17	O5	132.7	1.1
O19	C4	-97.2		O19	O5	98.6	1.4
O19	H3	-31.0		C18	H3	28.2	-2.8
O17	H3	-24.7		C18	H12	16.0	-8.7
O19	H12	-20.7		Br24	O19	13.9	-6.8
Br24	C18	-16.1		C18	H2	13.1	-2.9
O17	H2	-12.6		Br24	O17	11.5	-1.0
O17	H12	-12.3		C18	H16	5.6	-6.7
Total Sum							**-31.3**
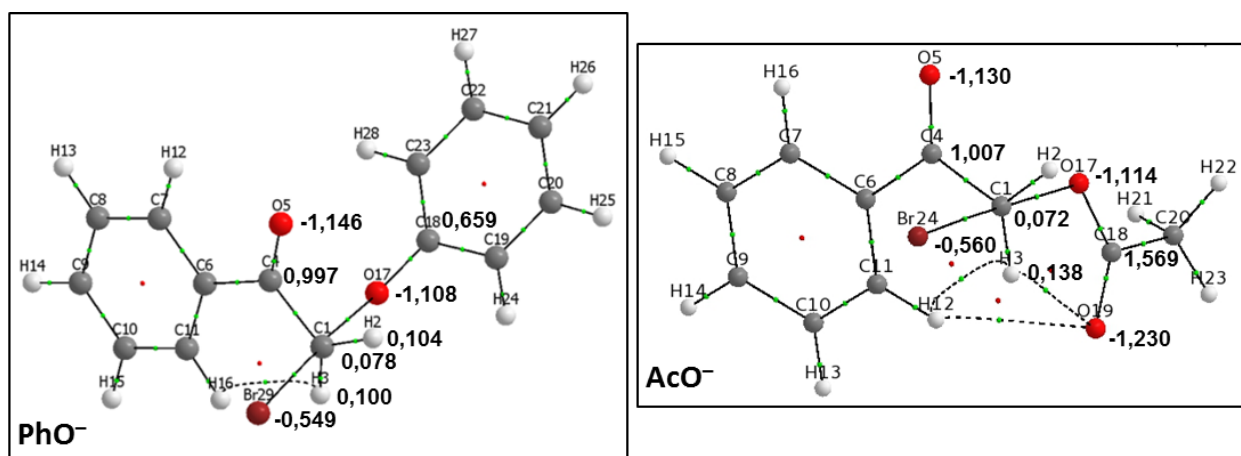
Figure 3.9: Selected net atomic charges (in *e*) on atoms close to reaction centre at the TS for the S$_N$2 reactions pathway for **α-BrAcPh** with **PhO⁻** or **AcO⁻**.
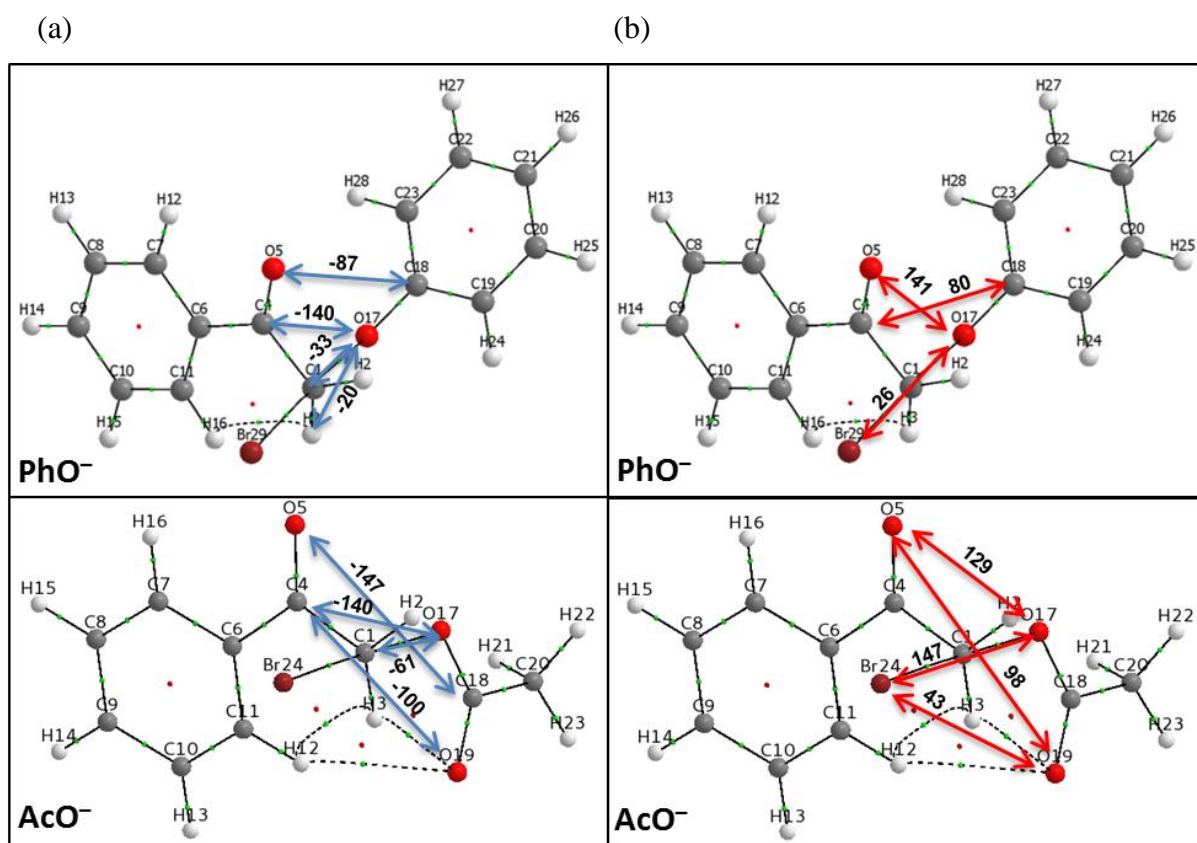
Figure 3.10: Selected (a) attractive and (b) repulsive diatomic interaction energies (in kcal/mol) between atoms of $\mathcal{A}$ and $\mathcal{N}$ at the TS of the S_N2 reaction of **α-BrAcPh** with **PhO⁻** or **AcO⁻**.

Graphical representation of these dominating interactions between the nucleophile and carbonyl group, **Figure 3.11**, shows that during the progression of the reaction these diatomic interactions remain highly (de)stabilising.

Recall from **Figure 3.7,** by summing up all the interactions of the nucleophile with the carbonyl group provides a clearer picture that the carbonyl group only slightly enhances the attraction between the two molecules, $\mathcal{B}$ and $\mathcal{N}$. Thus, this illustrates one of the strengths of using QFARP, by considering the interactions of fragments rather than individual diatomic interactions, it allows one to gain a clearer picture of the general interactions that are being experienced between groups of atoms. Whereas studying diatomic interactions alone can lead to confusion and misinterpretations.

(a)   (b)
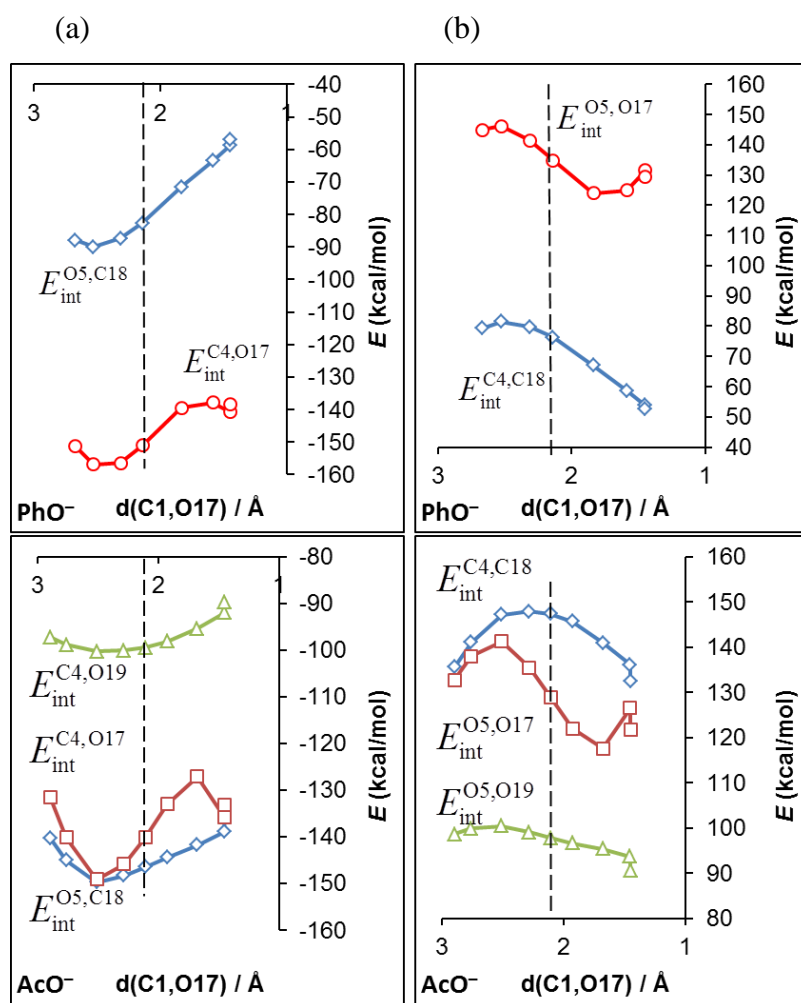
Figure 3.11: Interaction energies of selected leading (a) attractive and (b) repulsive interactions between fragments $\mathscr{A}$ and $\mathscr{N}$ [**PhO⁻** and **AcO⁻**] along the S_N2 reaction pathway for **α-BrAcPh** with **PhO⁻** or **AcO⁻**.

Now the fragment interactions which contribute significantly to the reaction are considered. **Figure 3.12** shows that the attractions of the nucleophile, $\mathscr{N}$, with the carbonyl group, $\mathscr{K}$, and C1 is comparable. However, when the interactions between $\mathscr{N}$ and $\mathscr{M}$ are considered, a drastic increase in attraction is noted. This shows that the hydrogens, H2 and H3, play a significant role in the attraction between **α-BrAcPh** and the nucleophiles, **PhO⁻** and **AcO⁻**. This result shows that the interaction of "less significant" atoms, such as adjacent hydrogens, are also important to consider and that it is not just the atoms directly involved in the reaction which have an influence on the reaction.

It should be emphasised that other computational methods used previously in literature, such as molecular orbitals,[8,10] cannot be used to show how the interactions with less significant atoms, such as Hydrogen, play an important role. Thus, QFARP is a unique approach for the analysis of reactions and provides insight on a fundamental level which cannot be obtained with other methods.

Furthermore, at the beginning of the reaction $E_{\text{int}}^{\mathcal{M},\mathcal{N}}$ for the **AcO⁻** reaction, is shown to be significantly more attracted than for the **PhO⁻** reaction, but have comparatively the same attractive interaction by the final structure of the PC. This additional attraction of $E_{\text{int}}^{\mathcal{M},\mathcal{N}}$ for **AcO⁻** is the result of the additional electronegative oxygen atom of **AcO⁻** (O19) which interacts with the positively charged hydrogen atoms (H2, H3) of fragment $\mathcal{M}$.
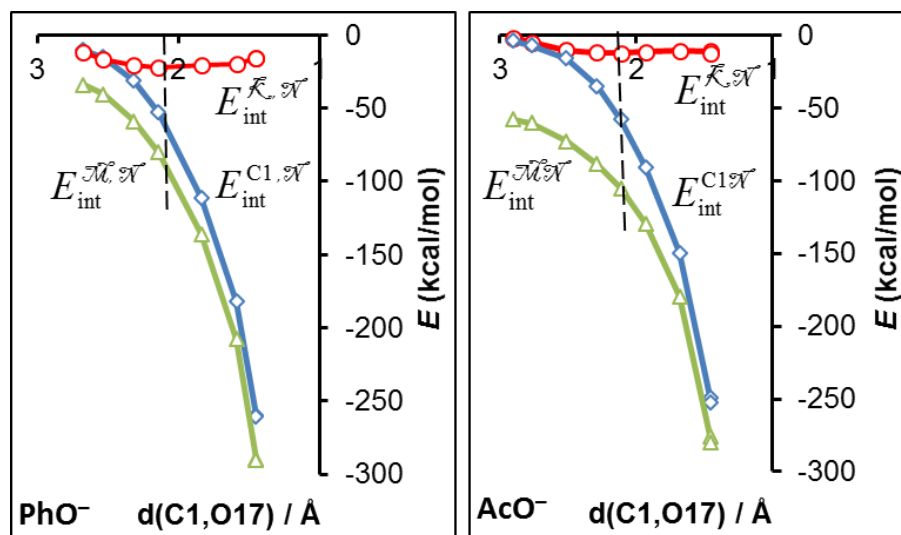
Figure 3.12: Interaction energies of **PhO⁻** or **AcO⁻** ($\mathcal{N}$) with C1 and fragments, $\mathcal{K}$ and $\mathcal{M}$, along the S$_N$2 reaction pathway with **α-BrAcPh**.

3.3.5 The (de)stabilisation of the Nucleophile ($\mathcal{N}$)

As noted from **Figure 3.4**, the change in additive energy of the nucleophile fragment, $\mathcal{N}$, is destabilising at the TS, but also contributes a significant amount of stabilisation to the PC. Thus, why is $\mathcal{N}$ destabilised at the TS but also provides stabilisation at the end of the reaction? Analysis of the interaction energies of O17, see **Figure 3.13**, explains why this is the case. $\Delta E_{\text{int}}^{\text{O17},\mathcal{H}}$ shows that the interaction energy of O17 only becomes significantly stabilising well after the TS, in the same manner as the additive energy of $\mathcal{N}$. The stabilisation is the result of $\Delta E_{\text{int}}^{\text{O17,C1}}$ which increases exponentially as the new covalent bond is formed between O17 and C1. However, at the same time $\Delta E_{\text{int}}^{\text{O17,C18}}$ becomes significantly destabilised as the reaction progresses as the bond weakens between the two atoms. It is only well after the TS that $\Delta E_{\text{int}}^{\text{O17,C1}} > \Delta E_{\text{int}}^{\text{O17,C18}}$, which results in $\mathcal{N}$ contributing a stabilising effect.

In summary, $\mathcal{N}$ is destabilised as the bond between O17 and the adjacent C18 is weakened. Only well after the TS does the stabilisation energy of the newly formed bond between O17 and C1

53

begin to have a significantly more stabilising effect, resulting in $\mathscr{N}$ contributing to the stabilisation of the PC. Furthermore, while the reactions with two different nucleophiles have been studied, the same trends and magnitude have been noted for the reactions showing that nearly identical processes are occurring.
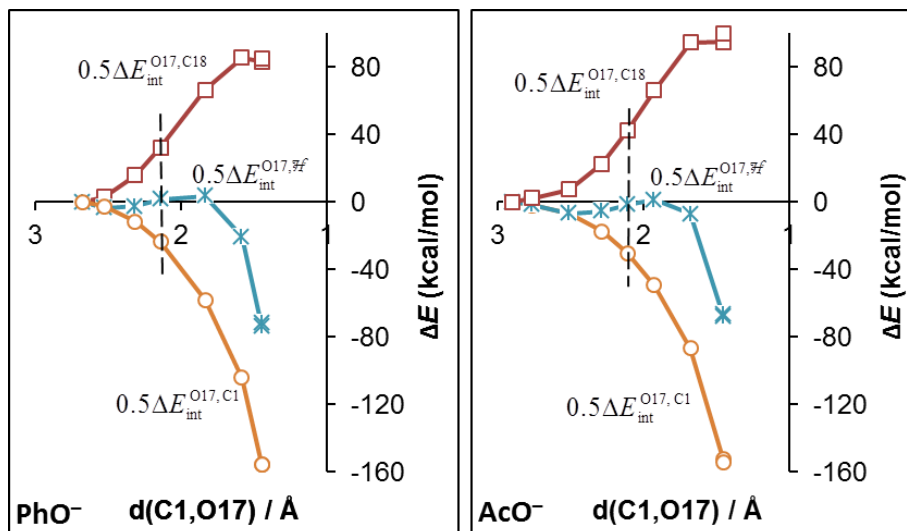
Figure 3.13: Change in interaction energy of O17 with C1, C18 and all atoms ($\mathscr{H}$) along the S_N2 reaction pathway of **α-BrAcPh** with **PhO⁻** or **AcO⁻**.

3.3.6 Role played by the leaving group – Bromine

Using QFARP, the fragments which contribute to the repulsion (and attraction) of Br along the reaction pathway were studied to understand what assists (and hinders) the removal of Br during the reaction. Previous work[7] has shown that the ability of the leaving group to move away after the TS also plays a significant role in selectivity and reactivity of S_N2 reactions.

Figure 3.14 shows the interaction energies which the leaving group, Br, experiences with other fragments. The interaction, $E_{int}^{Br,\mathscr{A}}$, which Br experiences with the rest of **α-BrAcPh**, $\mathscr{A}$, shows that the attraction which Br experiences is weakened significantly as the reaction progressed, with $E_{int}^{Br,\mathscr{M}}$ contributing to the majority of this loss in attraction. This loss in attraction would result in Br being able to move away more easily as the reaction progresses. Additionally, the nucleophile, $\mathscr{N}$, has a repulsive interaction with the leaving group. This repulsion is due to the electrostatic interactions of the two negatively charged fragments, Br and $\mathscr{N}$, which only increases as the nucleophile moves closer to **α-BrAcPh**. By summing the interactions of $E_{int}^{Br,\mathscr{A}}$ and $E_{int}^{Br,\mathscr{N}}$, one obtains all the interactions which Br experiences with the molecular system, i.e. $E_{int}^{Br,\mathscr{H}}$. $E_{int}^{Br,\mathscr{H}}$ is shown to have the same trends as $E_{int}^{Br,\mathscr{A}}$ and $E_{int}^{Br,\mathscr{M}}$, only less attractive after the TS.

54
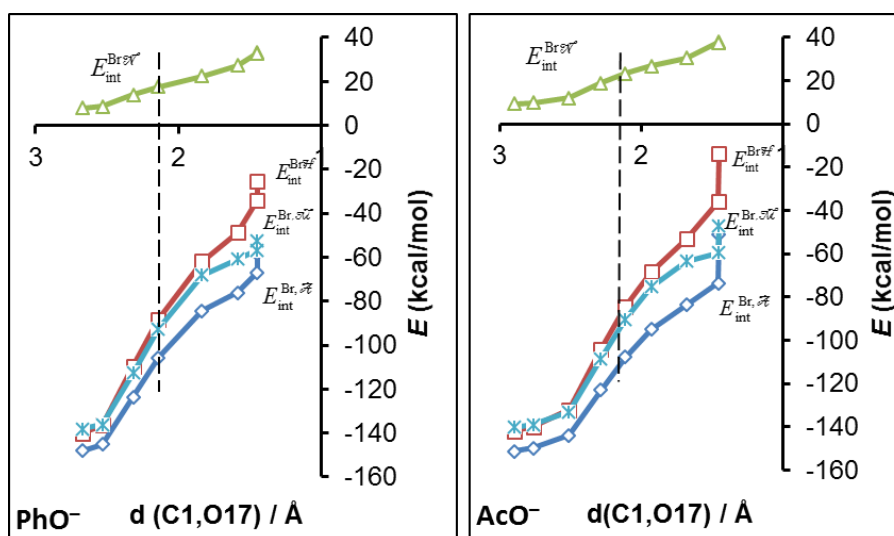
Figure 3.14: Relative change in energy of Br with other fragments along S_N2 pathway for **α-BrAcPh** with **PhO⁻** or **AcO⁻**.

Figure 3.14 shows a significant loss in the interactions energy of Br. However, **Figure 3.5** showed that the additive energy of the leaving group plays an important role in stabilising the reaction as it progresses. Thus, **Figure 3.15** shows how the change in self-energy of Br, $\Delta E_{\text{self}}^{\text{Br}}$, compensates for the energy that is required to weaken the interaction energy of Br with the rest of the system, $0.5\Delta E_{\text{int}}^{\text{Br}\neq f}$. This results in the change of the additive energy for Br, $\Delta E_{\text{add}}^{\text{Br}}$, being stabilising in nature which contributes significantly to the overall stability of the reaction. The additive energy of Br is shown to contribute approximately the same for both reactions. This is expected as there is no difference in the electrophile.
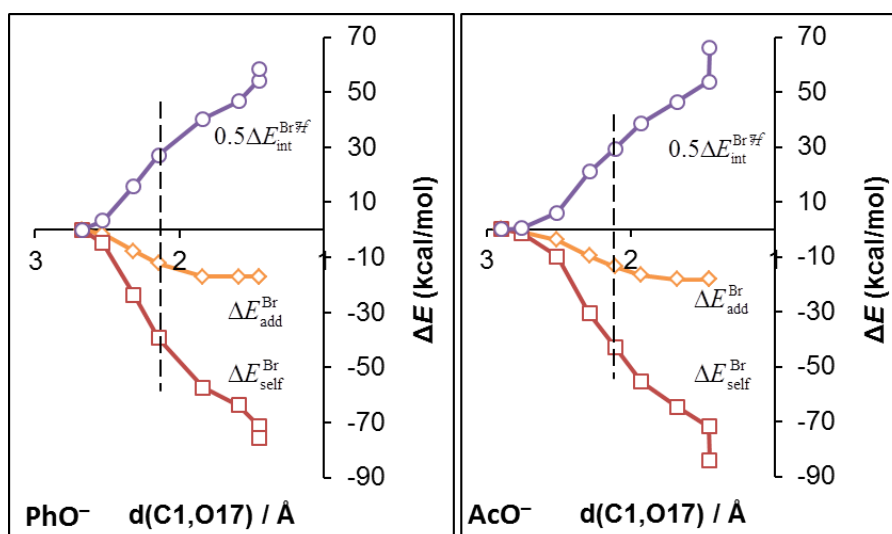
Figure 3.15: The additive-, self- and half interaction-energy of Br along the S_N2 reaction pathway for **α-BrAcPh** with **PhO⁻** or **AcO⁻**.

55

The interaction energies for the bonds formed and broken were considered. While the change in the electronic energy is not the result of changes in interaction energies between bonds broken and formed alone, it is still of value as it provides an indication of their relative strength. **Figure 3.16** shows that the C1–O17 bond that is formed is much stronger than the C1–Br bond which is broken. The interaction energy difference between $E_{\text{int}}^{\text{C1,Br}}$ and $E_{\text{int}}^{\text{C1,O17}}$ is nearly 200 kcal/mol suggesting an exothermic reaction. While when the interactions of $\mathcal{M}$ with atoms C1 and Br are considered, the hydrogens (H2 and H3) also contribute to attractive interactions for both atoms.

What is less obvious however is that the interactions of the hydrogens, contribute more attractive interactions to O17 before the TS than to Br after the TS. This would enhance the attraction between $\mathcal{M}$ and $\mathcal{N}$ but also not hinder the removal of Br after the TS, thus enhancing the reactivity of the S_N2 reaction.
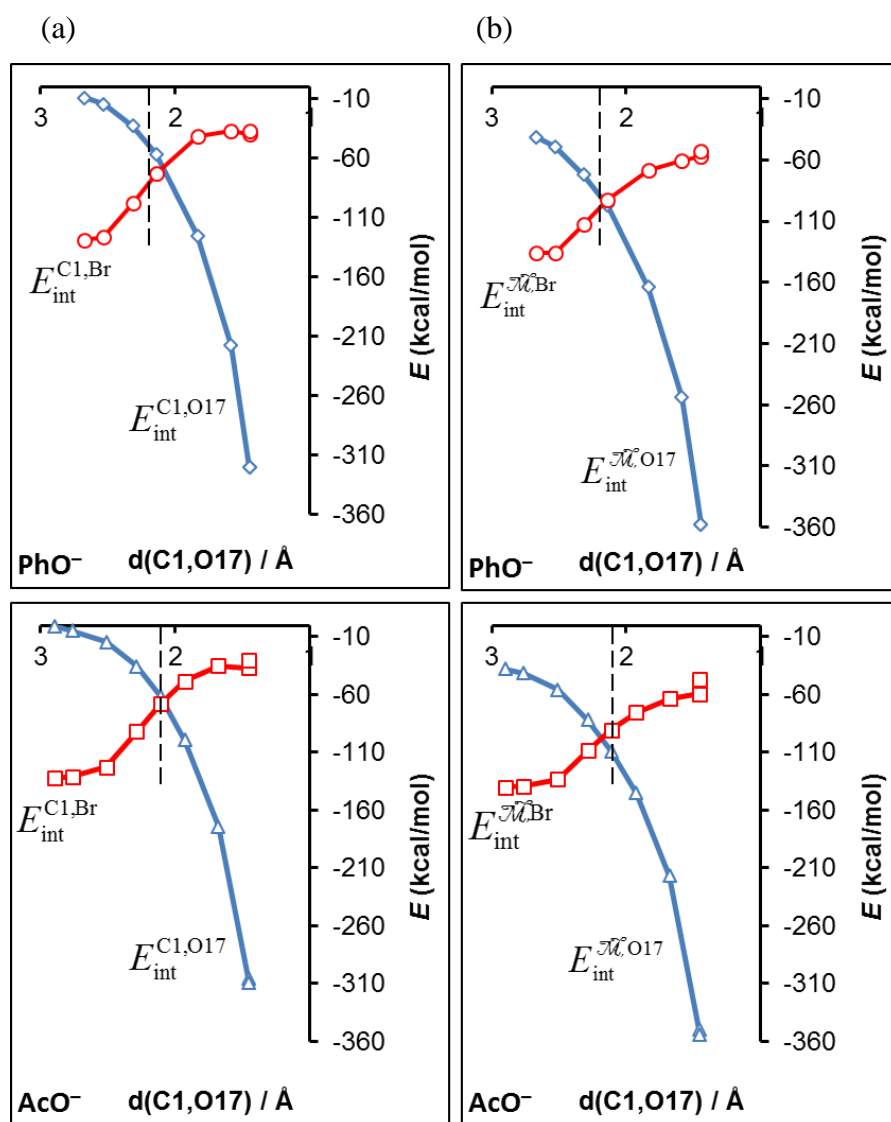
Figure 3.16: Interaction energies for the bonds (a) broken (C1Br) and formed (C1O17), and (b) the interactions of fragments $\mathcal{M}$ with Br and O17, along the S_N2 reaction pathway of **PhO⁻** and **AcO⁻** reacting with **α-BrAcPh**.

3.3.7 Charges of fragments along reaction pathway

Organic theory regularly uses the charges of atoms to understand and explain reaction mechanisms and reactivity, thus it is important to consider the charges of atoms during a reaction. Fortunately, QTAIM uses topology to decompose the electron density of the molecular system into its respective atoms, and thus the net charge of each atom. (The charge of individual atoms is given in Appendix A.) The net charges of atoms can thus be grouped into fragments to gain a further understanding of how electron density changes throughout the system as the reaction occurs - **Figure 3.17**.

Following organic theory, at the beginning of the reaction, **α-BrAcPh** is neutral while the nucleophile (**PhO⁻** and **AcO⁻**) has a net charge of -1 *e*. At the beginning of the reaction the

57

nucleophile, $\mathscr{N}$, has a net charge of approximately -1 e,[32] while if the fragments of **α-BrAcPh** ($\mathscr{M}$, $\mathscr{K}$, $\mathscr{P}$ and Br) are summed up it is found to be neutral.

If the PC is considered, one expects the newly formed product to be neutrally charged and the Br to have a charge of -1 e. **Figure 3.17** shows this is the case, with Br having a charge of -1 and the sum of all other fragments being neutral.

During the reaction, the net charge of the carbonyl-group, $\mathscr{K}$, and phenyl-group, $\mathscr{P}$, remain relatively constant as they are not directly involved in the reaction. On the other hand, the net charges for the other 3 fragments ($\mathscr{M}$, $\mathscr{N}$ and Br) change substantially.

The biggest change in charge is of the leaving group, Br. At the beginning of the reaction the electronegative Br, which has withdrawn electron density from C1, has a net charge of -0.2 e. As the reaction progresses Br gains electron density, gradually becoming more negative, to have a final net charge of approximately -1 e. Even though Br becomes more negative during the reactions it was shown that the additive energy of Br has a significant stabilising effect on the reaction – see **Figure 3.5**. This shows that Br is a stable anion in solution.
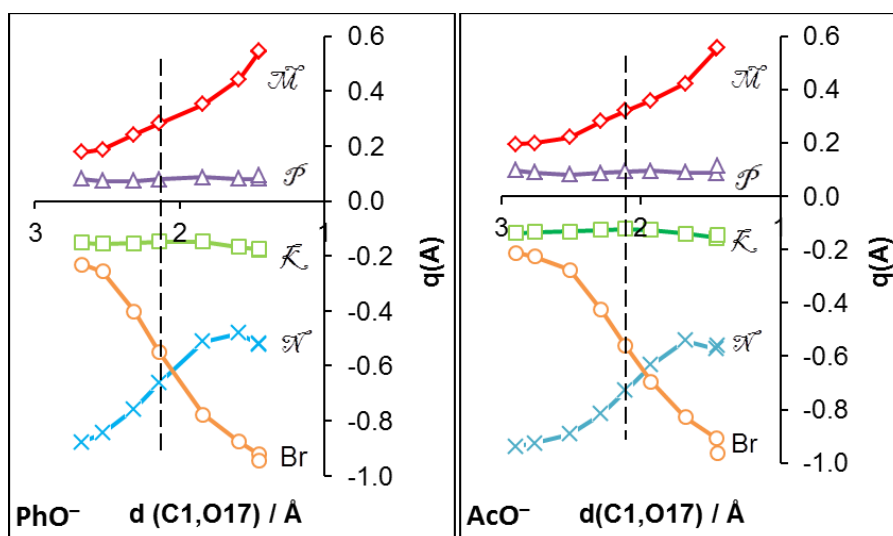
Figure 3.17: Charges of selected fragments (**Table 3.1**) along the S_N2 reaction pathway of **PhO⁻** and **AcO⁻** reacting with **α-BrAcPh**.

The fragment at the centre of the reaction, $\mathscr{M}$, initially has a charge of 0.2 e and becomes more positive as the reaction progresses with a final net charge of 0.55 and 0.56 e for the PC of the **PhO⁻** and **AcO⁻** reactions, respectively. The S_N2 reaction essentially replaces the leaving-group, Br, with the nucleophile. C1 ends up being bonded to an oxygen atom which is more electronegative than Br. This results in more electron density being removed from $\mathscr{M}$, causing it to become more positive

as the reaction progresses. A comparison of ^{1}H NMR spectra in literature for the reagent (**α-BrAcPh**) and products supports this conclusion. A shift downfield of 4.47[30] to 5.28[19] and 5.24[31] ppm is shown for the protons of fragment $\mathcal{M}$ (H2H3), once **PhO⁻** and **AcO⁻** is attached to **α-BrAcPh** respectively. This signifies the removal of electron density from fragment $\mathcal{M}$.

3.4 Conclusion

QFARM is a new tool for the analysis of large amounts of IQA data by grouping atoms of a system into fragments. By studying each fragment and the interactions between them one can gain additional insight on a fundamental level into explaining the reactivity of a system and what drives the reaction forward. S_N2 reactions are often oversimplified and as shown in this work there are many changes that occur during the reaction. The S_N2 reactions of **α-BrAcPh** with nucleophiles, **PhO⁻** and **AcO⁻**, were modelled using IRC calculations to obtain the reaction pathway between the RC and PC. Experimental literature has noted that **PhO⁻** is more reactive than **AcO⁻**, thus the computational work was done to see if the modelling can recover this difference in reactivity and to explain it. IQA/QFARP was thus used to study these modelled reactions to understand them on a more fundamental level.

The modelled reactions have Gibbs free activation energies of 11.2 and 16.6 kcal/mol (relative to the separate reactants) for reactions of **PhO⁻** and **AcO⁻**, respectively, with the **PhO⁻** reaction being 11.6 kcal/mol more exothermic. This supports experimental findings that **PhO⁻** is more reactive than **AcO⁻**.

QFARP analysis showed that the leaving group, Br, and nucleophile, **PhO⁻** and **AcO⁻**, provide large stabilisation in its additive energy for the PC. This correlates with classical organic theory as Br is considered a better leaving group than either nucleophile studied, and Br is a stable anion in solution.

Only fragments $\mathcal{M}$ and $\mathcal{N}$ contribute significant destabilisation to the activation energy of the reaction. $\mathcal{N}$ is destabilised because of the decrease in interaction energy between the attacking-O (O18) and its adjacent Carbon atom (C18), while $\mathcal{M}$ is destabilised the most due to the removal of electron density. The difference in activation energy between **PhO⁻** and **AcO⁻** is the result of additive energy of $\mathcal{M}$ being more destabilised for the reaction of **AcO⁻** than **PhO⁻**. This is unexpected as the electrophile is the same for the two systems. Thus when reactivity is considered, it is important to note what are the effects of having the nucleophile bound to the electrophile. For

59

the cases studied above, it has been shown that the nucleophile **AcO⁻** destabilised the electrophilie, **α-BrAcPh**, more than that of **PhO⁻** which has a significant effect on the PES of the reactions.

The interactions between **α-BrAcPh**, $\mathscr{B}$, and the nucleophile, $\mathscr{N}$, showed significant attractive interactions which increase exponentially as the reaction progresses. However unexpectedly, the interactions of **AcO⁻** with $\mathscr{B}$ was found to be greater than of **PhO⁻**, thus showing that more localised interactions between the molecules must be considered.

When smaller fragments are considered the nucleophiles experiences large attractive and repulsive interactions with the carbonyl group, $\mathscr{K}$, of **α-BrAcPh** which largely cancel one another out. However, it was shown that $\mathscr{N}$ for the **PhO⁻** reaction is -10 kcal/mol more attracted to $\mathscr{K}$ at the TS than that of the **AcO⁻** reaction. It is not clear however if this attractive interaction between $\mathscr{K}$ and $\mathscr{N}$ is what results in enhanced reactivity of α-haloketones which has been noted in literature.

Ultimately, the nucleophile is thus more attracted to the adjacent fragment, $\mathscr{M}$, than to $\mathscr{K}$. This attraction to $\mathscr{M}$ is largely due to the hydrogens of $\mathscr{M}$ during the initial stages of the reaction. The hydrogens of $\mathscr{M}$ provide a greater attraction to **AcO⁻** than **PhO⁻** because of the additional electronegative Oxygen atom (O19) of **AcO⁻**.

The change in the net charge of fragments showed that $\mathscr{P}$ and $\mathscr{K}$ remained constant throughout the reaction, while $\mathscr{N}$ lost its charge of -1 *e* to become -0.5 *e*. Br on the other hand gained the most electron density to have a final charge of -1 *e* from -0.2 *e*. $\mathscr{M}$ progressively becomes more positive because of the initially bonded Br being replaced with a more electronegative Oxygen atom of the nucleophile. The charge of fragments for the two reactions was shown to be nearly identical.

3.5   References

(1)   Thorpe, J. W.; Warkentin, J. *Can. J. Chem.* **1973**, *51* (6), 927.

(2)   Warren, S.; Wyatt, P. *Workbook for Organic Synthesis: The Disconnection Approach*, Second.; John Wiley & Sons: Chichester, 2009.

(3)   Jones, T. E. *J. Phys. Chem. A* **2012**, *116* (16), 4233.

(4)   Blanco, M. A.; Martín Pendás, A.; Francisco, E. *J. Chem. Theory Comput.* **2005**, *1* (6), 1096.

(5)   Inostroza-Rivera, R.; Yahia-Ouahmed, M.; Tognetti, V.; Joubert, L.; Herrera, B.; Toro-Labbé, A. *Phys. Chem. Chem. Phys.* **2015**, 17797.

(6)   Cukrowski, I. *Comput. Theor. Chem.* **2015**, *1066*, 62.

(7)   Buyens, D. M.-J. S. Alkylation of adenine: A synthetic and computational study of the reaction mechanism, University of Pretoria, 2015.

(8)   Bach, R. D.; Coddens, B. A.; Wolber, G. J. *J. Org. Chem.* **1986**, *51* (7), 1030.

(9)   Bach, R. D.; Wolber, G. J. *J. Am. Chem. Soc.* **1985**, *107* (5), 1352.

(10)   Kost, D.; Aviram, K. *J. Am. Chem. Soc.* **1986**, *108* (8), 2006.

(11)   Kalendra, D. M.; Sickles, B. R. *J. Org. Chem.* **2003**, *68* (4), 1594.

(12)   Halvorsen, A.; Songstad, J. *J. Chem. Soc. Chem. Commun.* **1978**, No. 7, 327.

(13)   Lee, I.; Lee, H. W.; Yu, Y. *Bull. Chem. Soc.* **2003**, *24* (7), 993.

(14)   Ross, S. D.; Finkelstein, M.; Petersen, R. C. *J. Am. Chem. Soc.* **1968**, *90* (23), 6411.

(15)   Koh, H. J.; Han, K. L.; Lee, H. W.; Lee, I. *J. Org. Chem.* **2000**, *65* (15), 4706.

(16)   Fábián, A.; Ruff, F.; Farkas, Ö. *J. Phys. Org. Chem.* **2008**, *21* (11), 988.

(17)   Itoh, S.; Yoshimura, N.; Sato, M.; Yamataka, H. *J. Org. Chem.* **2011**, *76* (20), 8294.

(18)   Edwards, J. O.; Pearson, R. G. *J. Am. Chem. Soc.* **1962**, *84* (1), 16.

(19)   Lee, J. H.; Kim, M.; Kim, I. *J. Org. Chem.* **2014**, *79* (13), 6153.

(20)   Strassberger, Z.; Alberts, A. H.; Louwerse, M. J.; Tanase, S.; Rothenberg, G. *Green Chem.* **2013**, *15* (3), 768.

(21)   Hlaváč, J.; Hradil, P.; Mělnický, R.; Kvapil, L.; Šlézar, P.; Grepl--, M.; Hradil, P.; Lyčka, A.; Grepl, M. *J. Heterocycl. Chem.* **2008**, *45* (5), 1437.

(22)   M. J. Frisch, G. W. Trucks, H. B. Schlegel, G. E. Scuseria, M. A. Robb, J. R. Cheeseman, G. Scalmani, V. Barone, B. Mennucci, G. A. Petersson, H. Nakatsuji, M. Caricato, X. Li, H. P. Hratchian, A. F. Izmaylov, J. Bloino, G. Zheng, J. L. Sonnenberg, M. Had, J. C. Gaussian, Inc.: Wallingford, CT 2009,.

(23)   Paizs, C.; Toşa, M.; Majdik, C.; Bódai, V.; Novák, L.; Irimie, F.-D.; Poppe, L. *J. Chem. Soc., Perkin Trans. 1* **2002**, No. 21, 2400.

(24)   Bento, A. P.; Solà, M.; Bickelhaupt, F. M. *J. Comput. Chem.* **2005**, *26* (14), 1497.

(25)   Bento, A. P.; Solà, M.; Bickelhaupt, F. M. *J. Chem. Theory Comput.* **2008**, *4* (6), 929.

(26) Parthiban, S.; de Oliveira, G.; Martin, J. M. L. *J. Phys. Chem. A* **2001**, *105* (5), 895.

(27) Gonzales, J. M.; Cox, R. S.; Brown, S. T.; Allen, W. D.; Schaefer, H. F. *J. Phys. Chem. A* **2001**, *105* (50), 11327.

(28) Keith, T. A. TK Grismill Software: Overland Parks KS, USA 2013, aim.tkgristmill.com.

(29) Harder, S.; Streitwieser, A.; Petty, J. T.; von Schleyer, P. *J. Am. Chem. Soc.* **1995**, *117* (11), 3253.

(30) Jiang, Q.; Sheng, W.; Guo, C. *Green Chem.* **2013**, *15* (8), 2175.

(31) Goodall, M.; Kelly, P. M.; Parker, D.; Gloe, K.; Stephan, H. *J. Chem. Soc. Perkin Trans. 2* **1997**, No. 1, 59.

(32) Note that for the RC, representing the initial state, the nucleophile is in close proximity of **α-BrAcPh** with **PhO⁻** and **AcO⁻** only having net charges of -0.88 and -0.94 respectively. Because the molecules are in close proximity to each other at the initial state, the nucleophile has already donated some electron density to **α-BrAcPh**. The same statement can be made for the charge of Br. The net charge of Br for the PC for the reaction of **PhO⁻** and **AcO⁻** are -0.94 *e* and -0.96 *e,* respectively.

Chapter 4

Elucidating competition reaction of α-haloketones with methoxide: A DFT study

4.1. Introduction and aim

As discussed in Chapter 1, the reaction mechanism of α-haloketones (**α-BrAcPh** is used to represent the functional group) with methoxide (**MeO⁻**) has been challenged in recent studies to suggest that the alternative alcohol product, **7**, that is formed follows an epoxidation reaction route which is separate from the S_N2 reaction pathway (**Scheme 1.7**, *vide supra*). Previous computational studies[1] have suggested the possibility of a bifurcation reaction mechanism; preference of the nucleophile to undergo carbonyl addition (CA) rather than the nucleophilic substitution on the α-*C*, in the presence of a strong EWG on the phenyl ring. Further investigation was therefore prompted via kinetic studies.[2,3] However, the utilisation of Hammett plots (**Figure 1.5**, *vide supra*) showed that bifurcation is not present and the two-competing reactions, S_N2 and epoxidation, do not share a common TS, with either an EWG or EDG present on the phenyl ring.

Furthermore, it was shown that the addition of an EWG/EDG has a significant influence on the reaction rate and yield of the S_N2 ether product, **4**, and the epoxide alcohol product, **7** – **Scheme 1.7**. The formation of the alcohol, **4**, is favoured when an EDG is present. If no groups are present, the selectivity is shifted to the epoxide route, increasing the yield of **7**. Whereas the presence of an EWG influences the selectivity for the epoxidate reaction route even more. It was also shown that there is a significant increase in the reaction rate when considering a scale of EDGs to EWGs.

Investigation into these noteworthy experimental observations using computational modelling is encouraged. The aim of the work discussed in this chapter is therefore to (i) model the reaction mechanism of the two reaction routes, (ii) understand why the presence of an EDG/EWG results in a decrease/increase in reaction rate and (iii) understand why selectivity shifts between the two routes due to the substituents on the phenyl-ring of **α-BrAcPh**.

4.2 Computational Background

All structure optimisations were done using Gaussian 09, rev. D.01[4] with B3LYP/6-311++G(d,p) level of theory using the Integral Equation Formalism for Polarisable Continuum model (IEFPCM) for simulating Methanol as the solvent for all calculations. Frequency calculations were done at 25°C. These conditions follow the published procedures for the kinetic studies of sodium methoxide with the α-haloketones in question.[2,3]

TS structures were obtained using Berny or QST3 optimisation. Frequency calculations were performed to confirm that a true TS was obtained with a single negative vibrational frequency.

Thereafter intrinsic reaction path (IRC) calculations were used to obtain the lowest energy pathway to the reactant- and product-complex. To model the rotational barriers of the epoxide reaction pathway dihedral scans of 5° rotation per step was performed. To model the formation of the RC, the RC structure was taken and scans with steps of 0.05Å were used separating the α-haloketone and the nucleophile, **MeO⁻**.

IQA calculations were done in the same manner as mentioned in chapter 3 using AIMAll Studios[5] (ver. 16.05.18). Comparison of the electronic energy for the molecular systems, *E*, and the recovered IQA additive atomic energies, *E*(IQA), is shown in Appendix B.

4.3   Results and Discussion

4.3.1 PES for S$_N$2 reaction of MeO⁻ with α-BrAcPh.

The TS structure for **α-BrAcPh** undergoing nucleophilic substitution with **MeO⁻** was obtained through Berny optimisation. The single negative vibrational frequency showed an interesting difference from what is predicted for an S$_N$2 TS. Typically, the TS of a S$_N$2 reaction has the central atom vibrating between the leaving group (LG) and the attacking nucleophile, while there is minor to no movement of the LG and nucleophile. In the case of **MeO⁻** reacting with **α-BrAcPh**, although the central α-*C* atom moves as expected, the nucleophile clearly swings between the α-*C* (C6) and carbonyl-*C* (C9) - **Figure 4.1**, which is unexpected as the negative vibrational frequency of **PhO⁻** and **AcO⁻** reacting with **α-BrAcPh** did not have significant movement of the nucleophile - **Figure 3.2**, *vide supra*. The difference in the vibrational frequency would suggest that the reaction mechanism of **MeO⁻** does not follow the same pathway as **PhO⁻** and **AcO⁻**, and the carbonyl group has a significant role in the reaction mechanism.
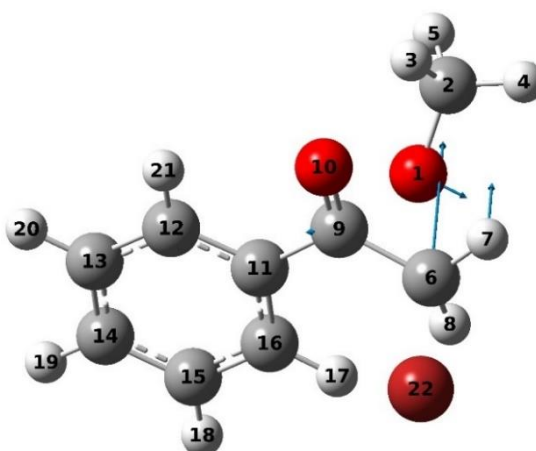
Figure 4.1: S$_N$2 TS structure of **MeO⁻** reacting with **α-BrAcPh**, with vectors showing the negative vibrational frequency that is present. Gaussian numbering of the atoms is included on each atom.

As the TS structure of the S_N2 reaction were obtained, IRC calculations were done to obtain the steepest pathway down the PES to the energy minima on either side of the TS, representing the RC and PC. The IRC calculations showed the PES for the reaction did not follow the typical reaction route - **Figure 4.2**. The nucleophile is shown to be highly attracted to the carbonyl-*C* (C9) prior to attacking the α-*C* (C6) and undergoing the nucleophilic substitution. The activation energy for the reaction is 3.97 kcal/mol suggesting that the reaction is highly reactive. Previous reports[2,3] confirm the presence of a small energy barrier as the reactions are done at room temperature. Furthermore, it should be emphasised that the results obtained from the IRC contradict the suggested mechanism of Yamataka and co-workers,[2,3] which suggested that no CA occurs prior to the S_N2 reaction.
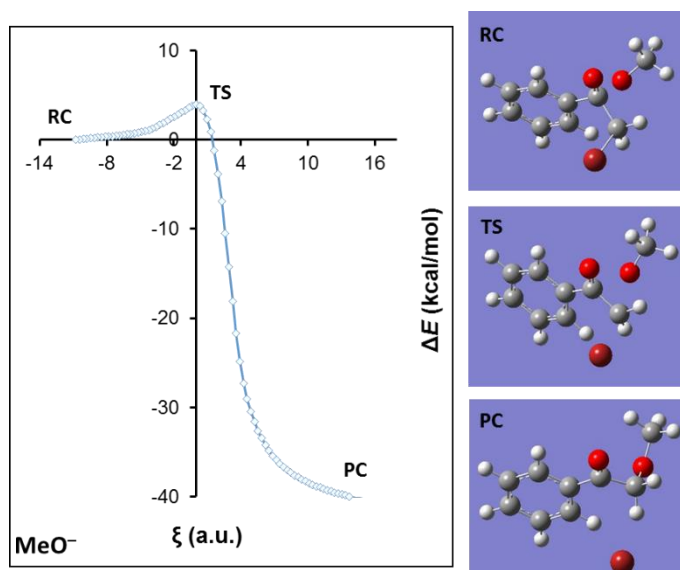
Figure 4.2: PES generated from IRC calculation for the S_N2 reaction of **MeO⁻** reacting with **α-BrAcPh**. Molecular graphs associated with each critical point is given on the right.

Due to the movement of the **MeO⁻** nucleophile, compared to other nucleophiles in typical S_N2 reactions, employing distance as a geometric parameter to describe the PES of this particular reaction is misleading; in **Figure 4.3**, where the only significant difference in distances is observed when the attacking-*O* (O1) and α-*C* (C6) nears the TS. Therefore, to describe the PES of the reaction based on distance would provide a misrepresentation of the PES. In contrast to chapter 3, where the horizontal axis is based on the distance between the attacking-*O* and the α-*C*, all the figures in this chapter which consider changes in energy, are based on the IRCs internal coordinates (ξ) generated.
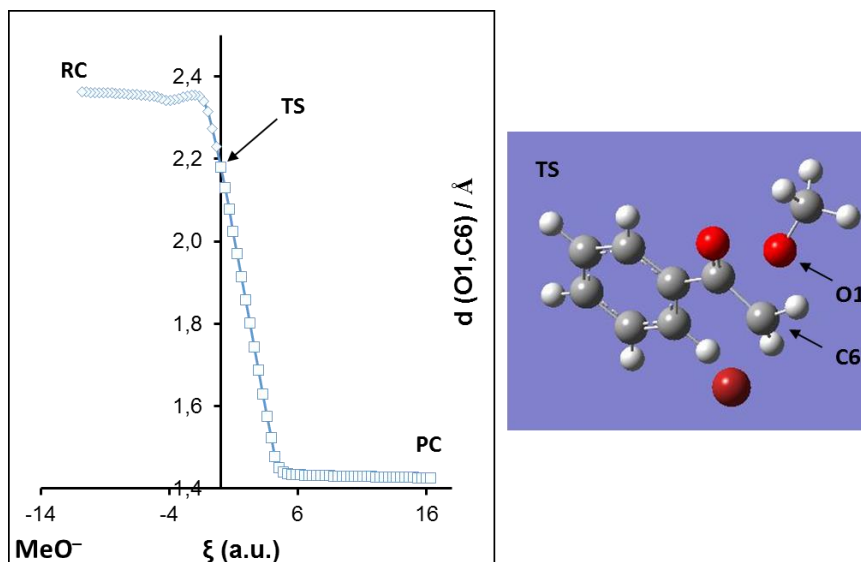
Figure 4.3: Distance between attacking-*O* (O1) and α-*C* (C6) during the IRC for the S_N2 reaction of **MeO⁻** reacting with **α-BrAcPh**. Molecular graph on the right shows the TS structure with O1 and C6 labelled.

The IRC of the S_N2 reaction between **MeO⁻** and **α-BrAcPh** shows that the RC structure is the result of CA; it is therefore necessary to also model the CA process to gain an informative representation of what the PES is. Thus, a scan was done to model the binding of **MeO⁻** to **α-BrAcPh** by increasing the distance between the nucleophile and carbonyl-*C* (O1 and C9) in increments of 0.05 Å - **Figure 4.4**.

The results generated portray the reality of the process but in the reverse order, whereby by the removal of **MeO⁻** from **α-BrAcPh** a nearly linear increase in electronic energy is noted with no energy barrier. This suggests that **MeO⁻** undergoes CA spontaneously, with no activation energy present. This result is in strong contrast to the results obtained for the CA of **PhO⁻** and **AcO⁻** with **α-BrAcPh** where an exponential increase in energy was noted as the distance between the nucleophiles and the carbonyl group decreases.
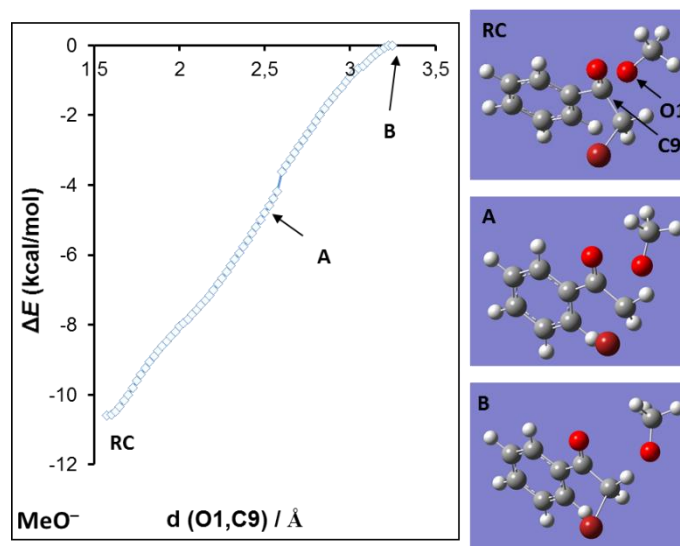
Figure 4.4: Change in energy with an increase in coordinate distance between attacking-*O* (O1) and carbonyl-*C* (C9) from the RC of the S$_N$2 reaction between **MeO⁻** and **α-BrAcPh**. Selected molecular graphs are given on the right.

An informative picture of how the S$_N$2 reaction mechanism of **MeO⁻** with **α-BrAcPh** differs from that of **PhO⁻** and **AcO⁻**, is illustrated in **Figure 4.2** and **Figure 4.4**. If the S$_N$2 reaction mechanism of **MeO⁻** is considered from the start, the nucleophile undergoes spontaneous CA to form a stable RC (-11.81 kcal/mol more stable than the separate reactants, R). Following the formation of the RC, the nucleophile detaches from the carbonyl-*C* (C9) and undergoes the nucleophilic substitution by attacking the α-*C* (C6) which displaces the LG (Br) with a small energy barrier of 3.97 kcal/mol.

4.3.2 PES for Epoxidation reaction of MeO⁻ with α-BrAcPh.

Previous computational studies have shown that CA occurs prior to the epoxidation reaction – (**Scheme 1.7**, *vide supra*),[1] thus the S$_N$2 and epoxidation reaction share a common intermediate as CA occurs for the S$_N$2 reaction as well. To obtain a TS structure for the epoxidation reaction, the LG (Br) should be orientation *trans* to the carbonyl-*O*. To obtain this orientation, the α-group is required to rotate approximately 120° to form RC-*trans*. The lowest rotational barrier of the α-group was obtained by studying the different possible orientations of the nucleophile. In **Figure 4.5**, the lowest rotational barrier of 4.6 kcal/mol was observed with the **MeO⁻** orientated away from the α-group (ori2). While if **MeO⁻** is orientated towards the α-group, ori1, a higher rotational barrier of 5.77 kcal/mol is exhibited. Interestingly these rotational barriers are larger than the activation energy noted for the S$_N$2 reaction. Since the energy barriers for the rotation of the α-group are of the same magnitude as the activation energy of the S$_N$2 reaction (3.97 kcal/mol, **Figure 4.2**), these rotations

68

also need to be considered when the activation energies of the S_N2 and epoxidation reactions are compared.

Furthermore, a small energy barrier of less than 2 kcal/mol was found, when the dihedral rotation of nucleophile (**MeO⁻**) from ori1 to ori2 were considered (Appendix B). Due to this negligible contribution to the PES of the epoxidation reaction, the discussion of the dihedral rotation of **MeO⁻** is not included in this chapter.
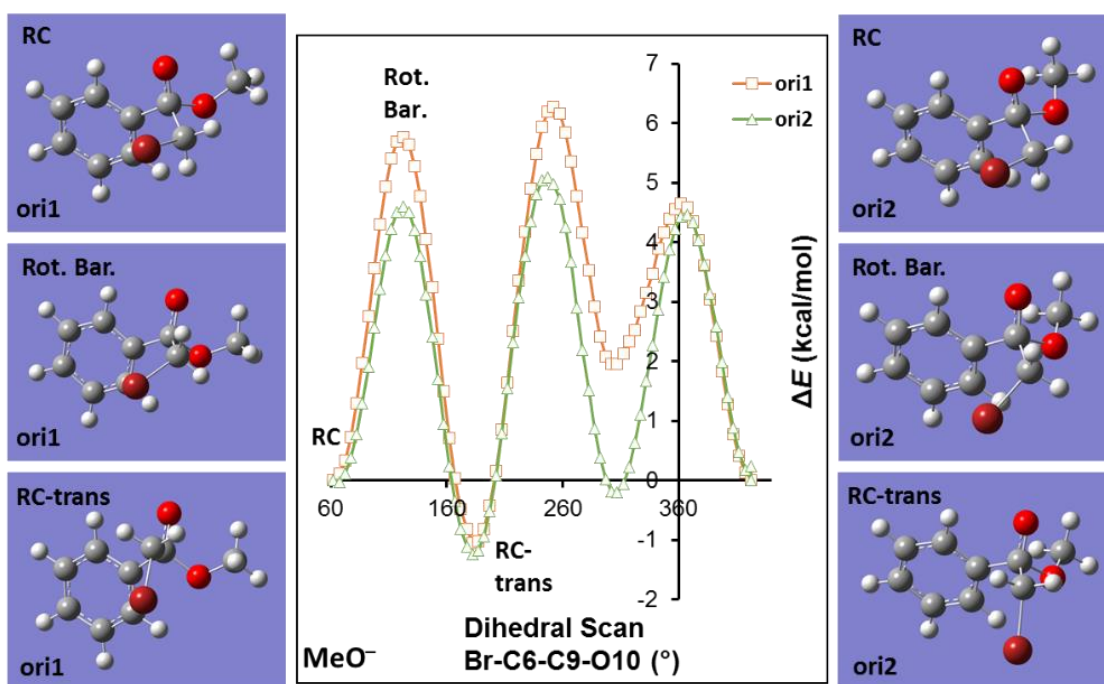
Figure 4.5: Change in energy during the dihedral scan of the α-group for RC structure of **MeO⁻** reacting with **α-BrAcPh**. Two dihedral scans of **MeO⁻** with different orientations are shown. Selected molecular graphs are shown for ori1 (left) and ori2 (right).

Figure 4.5 shows a stable intermediate, RC-*trans*, with an orientation of Br *trans* to the carbonyl-*O* (O10). This would suggest that **α-BrAcPh** might also have a relatively stable conformation with Br *trans* to the carbonyl-*O*. If that is so, it can be argued that CA and epoxidation can occur without having to consider the rotational barrier of the α-group. However, the dihedral scan of the α-group for the isolated reactant **α-BrAcPh** shows that only structures **C** and **D** are stable - **Figure 4.6**. Note that structure **E**, where Br is *trans* to the carbonyl-*O*, is at an energy maximum orientation, which is the opposite from what is observed in the RC-*trans* structure. Because Br is in the *trans* position for structure **E**, the α-group must move out of plane of the phenyl-group to prevent Br clashing with the ortho-hydrogen, resulting in the higher energy. It is therefore clear that an energy minimum structure is present when the Br is in the *trans* position only if **MeO⁻** is already bound to the carbonyl group. With **MeO⁻** bound to the carbonyl-*C* it results in the α-*C* not being in

the same plane as the phenyl ring of **α-BrAcPh**. This allows the Br to be in the *trans* position which is a stable conformation.
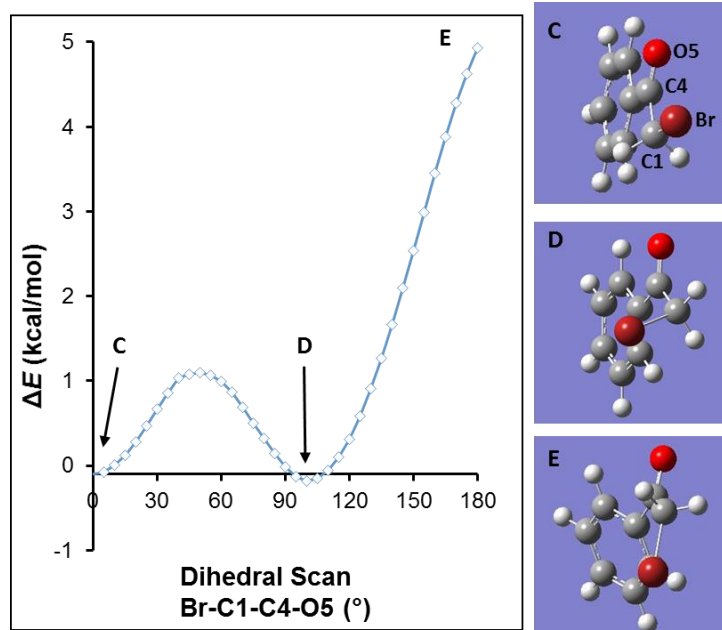
Figure 4.6: Change in electronic energy for a dihedral scan of α-group for **α-BrAcPh**. Selected molecular graph are given on the right.

From the RC-*trans* structure, the TS for the epoxidation reaction was obtained, followed by the IRC calculations needed to obtain the PES for the epoxidation reaction. Two orientations of **MeO⁻** bonded to the carbonyl-*C* were considered - **Figure 4.7**.

A difference in energy of 0.2 kcal/mol between the two TS orientations was found (with the lowest energy being of ori1, where the nucleophile is orientated towards the LG). This shows that the orientation of the nucleophile does not play a significant role as the difference in the energies of the TS are not substantial. (Note for the QFARP analysis on the epoxidation reaction, *vide infra*, ori1 was used.)

The activation energy of the epoxidation reaction is found to be 3.79 kcal/mol in **Figure 4.7**. This is directly comparable to the activation energy of the S_N2 reaction which was 3.97 kcal/mol - **Figure 4.2**. Thus, with the activation energies being so similar, it corresponds excellently with the experimental findings that the products of both reactions are formed in comparable yields.
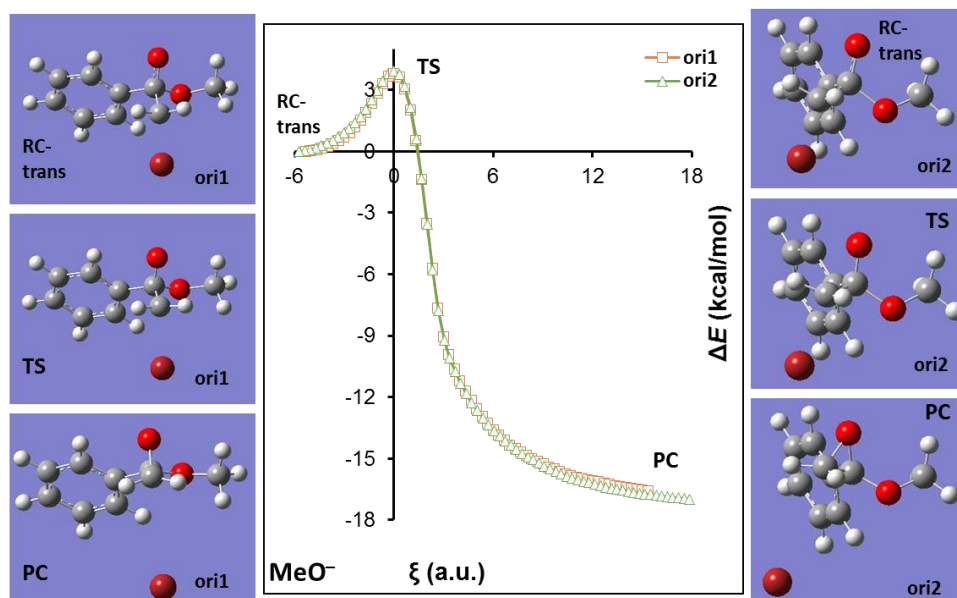
Figure 4.7: PES generated from IRC calculations for the epoxidation reaction of **MeO⁻** reacting with **α-BrAcPh**. Molecular graphs associated with each critical point are given. Ori1 and ori2 represent different orientations of **MeO⁻** which is bound to the carbonyl-*C*.

The displacement vectors for the TS structure of the epoxidation reaction, **Figure 4.8**, predict the bond formation between the carbonyl-*O* (O10) and the α-*C* (C6). The vector of C6 has the largest magnitude and is in the direction of the O10, with the adjacent hydrogens (H7, H8) showing similar vectors towards O10. This contrasts with the displacement vectors for the TS structure of the S_N2 reaction, **Figure 4.1**, predicts the bond formation between the α-*C* (C6) and the attacking-*O* (O1).
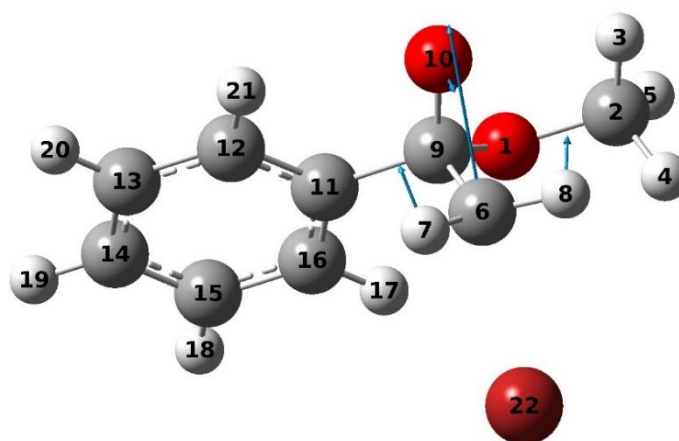
Figure 4.8: Epoxidation TS structure of **MeO⁻** reacting with **α-BrAcPh**, with vectors of the negative vibrational frequency shown. Gaussian numbering of the atoms is included for each atom.

4.3.3 Comparison of S_N2 and Epoxidation reaction of MeO⁻ with α-BrAcPh.

Having modelled PES for the S_N2 and epoxidation reaction involving **MeO⁻** with **α-BrAcPh**, electronic and Gibbs free energies are compared - **Figure 4.9**. The results clearly show that both reaction routes are possible with similar activation energy barriers in both cases. The PES related to electronic energy and Gibbs free energy, however, have some significant differences. One important difference being of the critical points between R and P which are negative for the electronic energy but positive for the Gibbs free energy. This is not surprising as the Gibbs free energy includes the entropic energy term which is not accounted for in the electronic energy.

As discussed in the introduction, the Gibbs free energy barrier for a reaction determines the reaction rate and selectivity for a reaction. The energy barrier for the TS of the S_N2 reaction has been found to be $\Delta G^{\#} = 4.9$ kcal/mol - **Figure 4.9**(b). The TS has an energy barrier of 5.1 kcal/mol for the epoxidation reaction, which is noticeably lower than the energy of the Rot. Bar. (rotational barrier) structure with an energy barrier of 7.8 kcal/mol. The activation energy of the α-group's rotations is shown to be higher than that of the epoxidation TS's energy. Thus, unexpectedly the rotation of the α-group is the rate limiting step for the epoxidation reaction. The S_N2 reaction has an energy barrier $\Delta G^{\#} = 7.8 – 4.9 = 2.9$ kcal/mol lower than the epoxidation reaction for **α-BrAcPh**. Showing that while both reactions occur, the epoxidation reaction is favoured, contradicting the experimental findings.

Furthermore, comparing the final energies of the separated products, P, for the two reactions shows the S_N2 product is significantly more stable than the epoxide product. It is expected the epoxide product will have increased reactivity to finally produce the alcohol product, **7** by the opening of the three-membered ring. Modelling of the reaction whereby the epoxide reacts further to form the alcohol product, **7**, has not been investigated computationally, due to the likelihood of the rate-determining step being involved in the formation of the epoxide, rather than the formation of the alcohol.

Figure 4.9: PES related to (a) electronic energy and (b) Gibbs free energy generated for the S_N2 and epoxidation reaction of **MeO⁻** reacting with **α-BrAcPh**.

From these findings, it is evident that both reactions have low energy barriers which are analogous. The modelling of the S_N2 reactions showed that **MeO⁻** undergoes CA to form the RC. The nucleophile then detaches from the carbonyl-*C* to form a bond with the neighbouring α-*C*, displacing the leaving group, Br. While for the competing epoxidation reaction, the same intermediate structure RC is shared. The α-group rotates around to allow Br to be *trans* to the carbonyl-*O*, RC-*trans*. The carbonyl-*O* then attaches the α-*C*, displacing the LG, to produce the epoxide. The reaction mechanism does not support what has been reported previously (**Scheme 1.7**, vide supra) and thus a new reaction mechanism is proposed - **Scheme 4.1**.
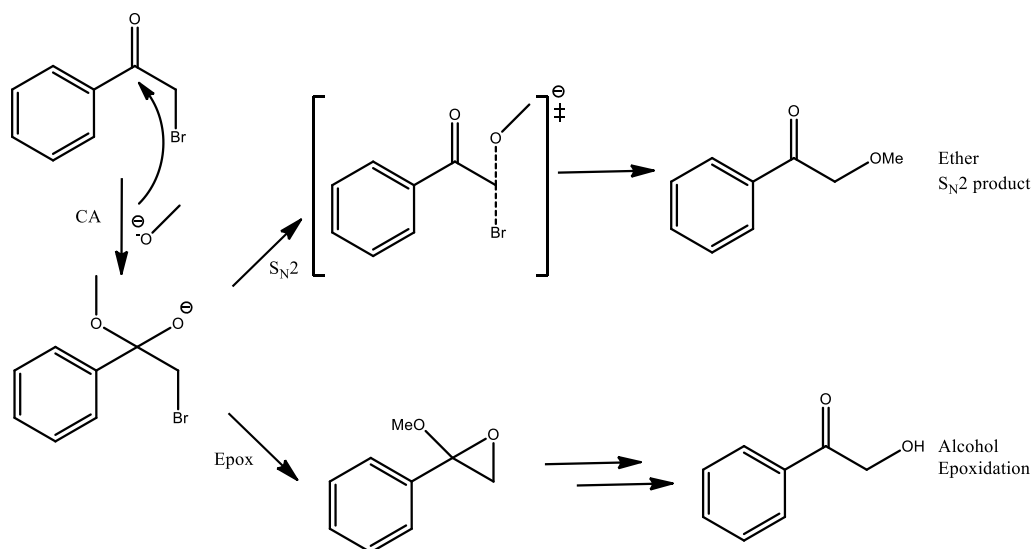
Scheme 4.1: Proposed reaction mechanism for the shared RC intermediate, via carbonyl addition, for the S_N2 and epoxidation reaction of **MeO⁻** reacting with **α-BrAcPh**.

73

4.3.4 Effect of substituents on the PES of S_N2 and Epoxidation reaction

The effects of substituents on the para-position of the phenyl ring on the yield of the two different products were investigated. For this computational study, only the strongest EDG and EWG that were used in the previous kinetic studies[2,3] were explored (**Scheme 4.2**). A methoxy attached on the *para* position of the phenyl ring of **α-BrAcPh**, 2-bromo-4′-methoxyacetophenone (**p-OMe**) represented an EDG, while the effects an EWG were investigated by placing a nitro-group on the *para* position, 2-bromo-4′-nitroacetophenone (**p-NO₂**).

p-OMe
Favours S_N2

p-NO₂
Favours Epoxidation
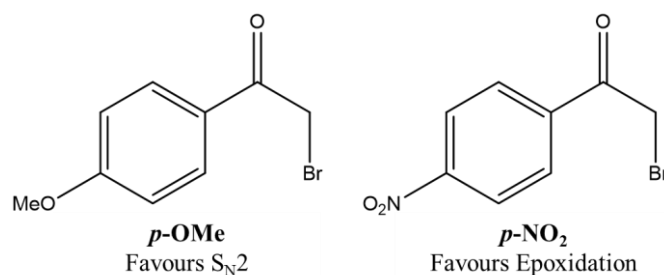
Scheme 4.2: Line structures of 2-bromo-4′-methoxyacetophenone (**p-OMe**) and 2-bromo-4′-nitroacetophenone (**p-NO₂**) which favour the S_N2 and epoxidation reaction with **MeO⁻**, respectively.

The PES of the competing reaction for **p-OMe** (**Figure 4.10**) and **p-NO₂** (**Figure 4.11**) was obtained in the same manner as was done for the reactions between **α-BrAcPh** and **MeO⁻**.

By comparing the three modelled systems (**α-BrAcPh**, **p-OMe** and **p-NO₂**) undergoing the S_N2 and epoxidation reactions, a clearer picture is gained when considering the PES of all the reactions. Experimentally, it was found that the **p-OMe** favoured the S_N2 over the epoxidation reaction. When the Gibbs free energy of **p-OMe** is considered (**Figure 4.10**), it is noted that the energy barrier of the S_N2 reaction is $\Delta G^{\#} = 6.4$ kcal/mol, while the epoxidation reactions highest barrier is of the Rot. Bar., which is $\Delta G^{\#} = 10.1$ kcal/mol. The difference in activation energy of 3.7 kcal/mol for the reaction shows the S_N2 reaction is more favoured. Note that for **α-BrAcPh**, the difference in the activation energies between the two routes was found to be 2.9 kcal/mol. This supports the experimental findings that an EDG increases the selectivity towards the S_N2 product.

When considering the PES of **p-NO₂** (**Figure 4.11**), the energy of the Rot. Bar. is 8.0 kcal/mol lower than that of the PES of **p-OMe** reactions, while the activation energy of the TS structure of the S_N2 and epoxidation reaction have decreased by 4.6 and 6.3 kcal/mol, respectively. From these results, two important observations are made. The first one being that the energy barrier of the S_N2 and epoxidation reaction are now nearly equivalent for **p-NO₂**, though experimentally it has been shown that the epoxidation route is significantly more favoured over the S_N2 reaction for **p-NO₂** with **MeO⁻**, thereby predicting a selectivity *trend*. Secondly, a decrease in activation energy of both

74

reactions (S$_N$2 and epoxidation), from EDG to EWG. The reaction rate for both reactions increase, which was confirmed from previously reported kinetic studies and these results correctly predicted the trend. However, the magnitude of the energy barriers should be interpreted with caution.

(a) (b)
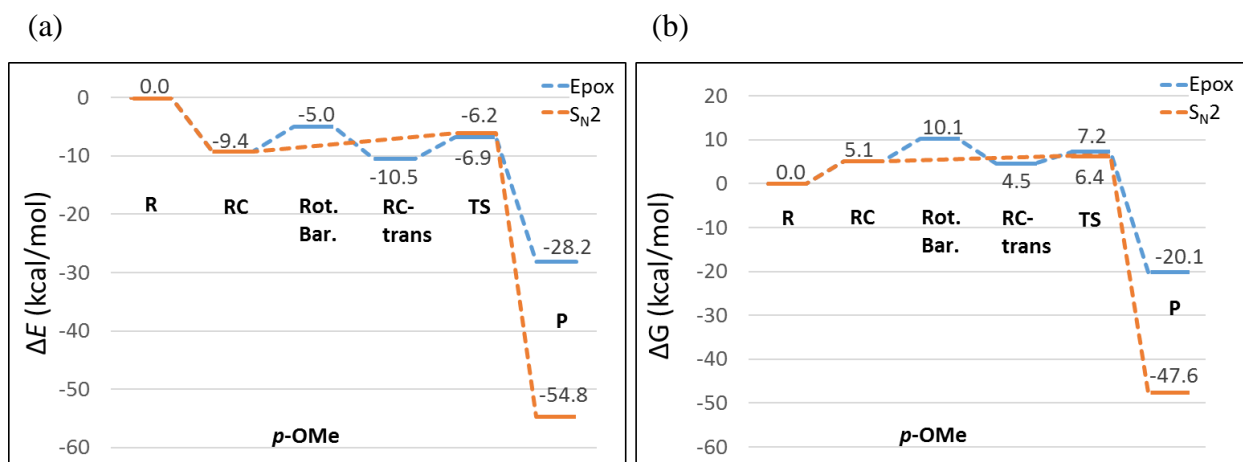
Figure 4.10: PES related to (a) electronic energy and (b) Gibbs free energy generated by the S$_N$2 and epoxidation reaction of **MeO$^-$** reacting with **p-OMe**.

(a) (b)
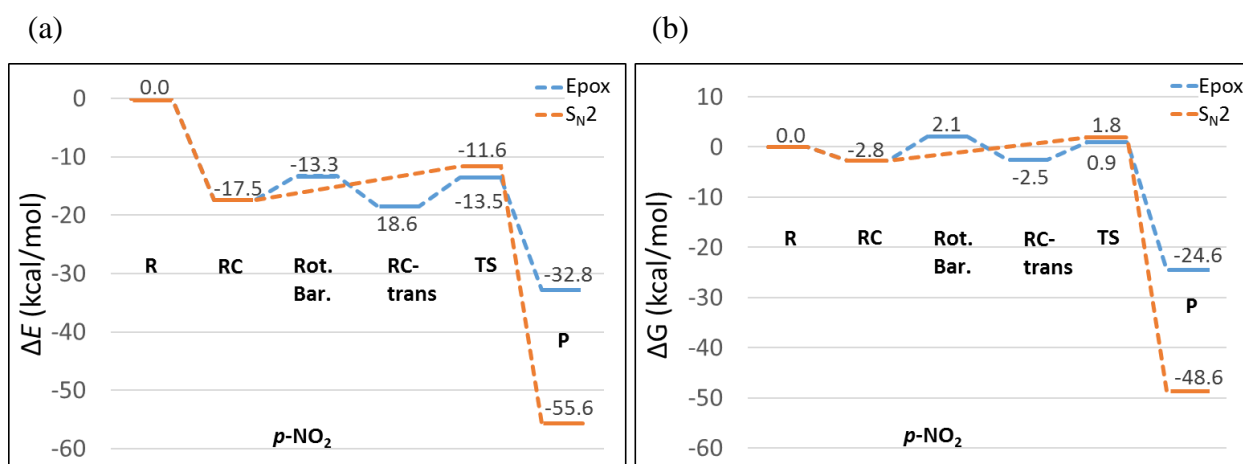
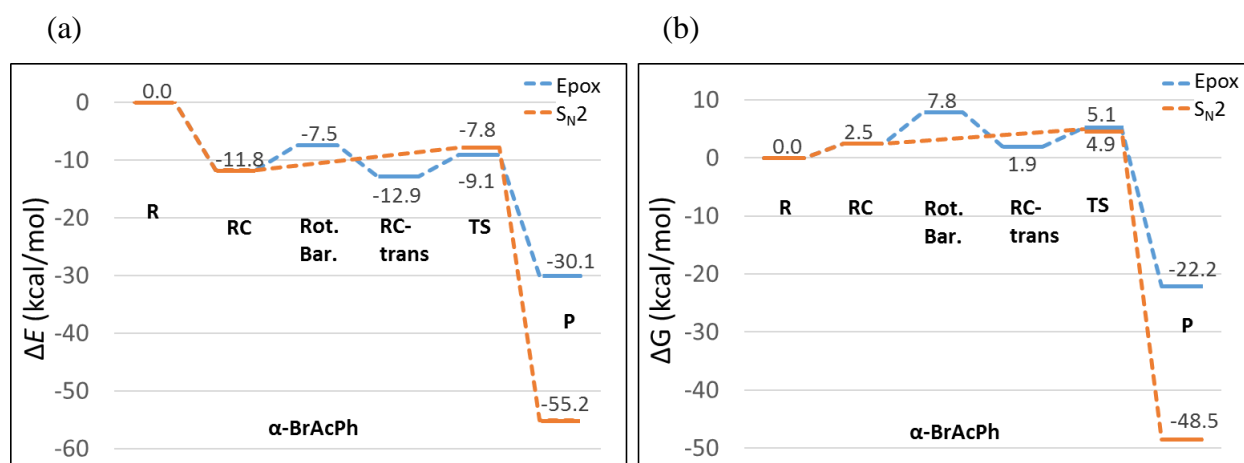**Figure 4.11**: PES related to (a) electronic energy and (b) Gibbs free energy generated by the S$_N$2 and epoxidation reaction of **MeO$^-$** reacting with **p-NO$_2$**.

4.3.5 Charge of fragments during S$_N$2 and Epoxidation reactions

To further elucidate each reaction, IQA/QFARP was utilised. Interactions between fragments and atoms were considered to explain the substituent effect on reactivity on a fundamental level. (Note: IQA decomposes the electronic energy and not the Gibbs free energy.) The molecular graphs of the RC, TS and PC for the two reactions are shown in **Table 4.1**, where some interesting interaction lines have been noted. (Molecular graphs of all structures are shown in Appendix B.)

For the S$_N$2 reaction, **Table 4.1** (a), the only interaction line between **MeO$^-$** and **α-BrAcPh** at the RC was that of O1–C9, d(O1,C9) = 1.58 Å. For the TS structure, this interaction line is still present, though significantly weaker, d(O1,C9) = 2.10 Å. It is only well after the TS that the

75

interaction line shifted to C6. For the PC structure, interaction lines between H8–H17 and H8–Br are noted, similar to what was noted for the reactions of **PhO⁻** and **AcO⁻** with **α-BrAcPh** in chapter 3. Interestingly, attractive interaction of $E_{\text{int}}^{\text{H8,Br}}$ is shown be -7.10 kcal/mol at the PC, while $E_{\text{int}}^{\text{H8,H17}}$ is -2.04 kcal/mol, even though both hydrogens have a partial positive charge. [At the PC, q(H8) = 0.05, q(H17) = 0.04, q(Br) = -0.97 e.] The same interaction lines which have been discussed are observed for the S_N2 reaction of *p*-**OMe** and *p*-**NO₂** with **MeO⁻**.

For the epoxidation reaction, **Table 4.1** (ii, a), the RC-*trans* structure is shown to have d(C6,Br) = 2.05 Å. Interestingly for the RC structure of the S_N2 reaction d(C6,Br) = 2.01 Å. Thus, rotation of the α-group results in some lengthening of the C6–Br bond. Furthermore, $E_{\text{int}}^{\text{C6,Br}}$ for the RC and RC-*trans* structures of the S_N2 and epoxidation reactions are shown to be -131 kcal/mol and -123 kcal/mol, respectively. This shows the interaction of C6–Br weakens when Br is trans to the carbonyl-*O* (O10), this weakening of the halogen bond would only assist the epoxidation reaction.

At the TS of the epoxidation reaction, the α-group and carbonyl-*O* move towards one another [d(C6,O10) = 1.98 Å], and away from Br [d(C6,Br) = 2.45 Å]. An interaction line between C6–O10 is not established yet (similarly an interaction line between O1–C6 was not present at the TS for the S_N2 reaction either), and it is only after the TS that this interaction line is noted. By the end of the reaction, the PC structure d(C6,O10) = 1.45 Å, while some interaction lines of Br with H4, C6 and C16 are observed.

Grouping of fragments for QFARP analysis was done in the same manner as chapter 3 – **Table 4.2**. The same fragmentation was used for the analysis of the S_N2 and epoxidation reactions, graphical representation of the fragments for the epoxidation reaction are shown in Appendix B.

Table 4.1: Molecular graphs of (a) reactant-complex, (b) TS and (c) product-complex generated from IRC-calculations for the (i) S_N2 and (ii) Epoxidation reaction of **α-BrAcPh** with **MeO⁻**, numbering of each atom shown on the right.

(i) S_N2	(ii) Epoxidation
(a)	(a)
(b)	(b)
(c)	(c)

77
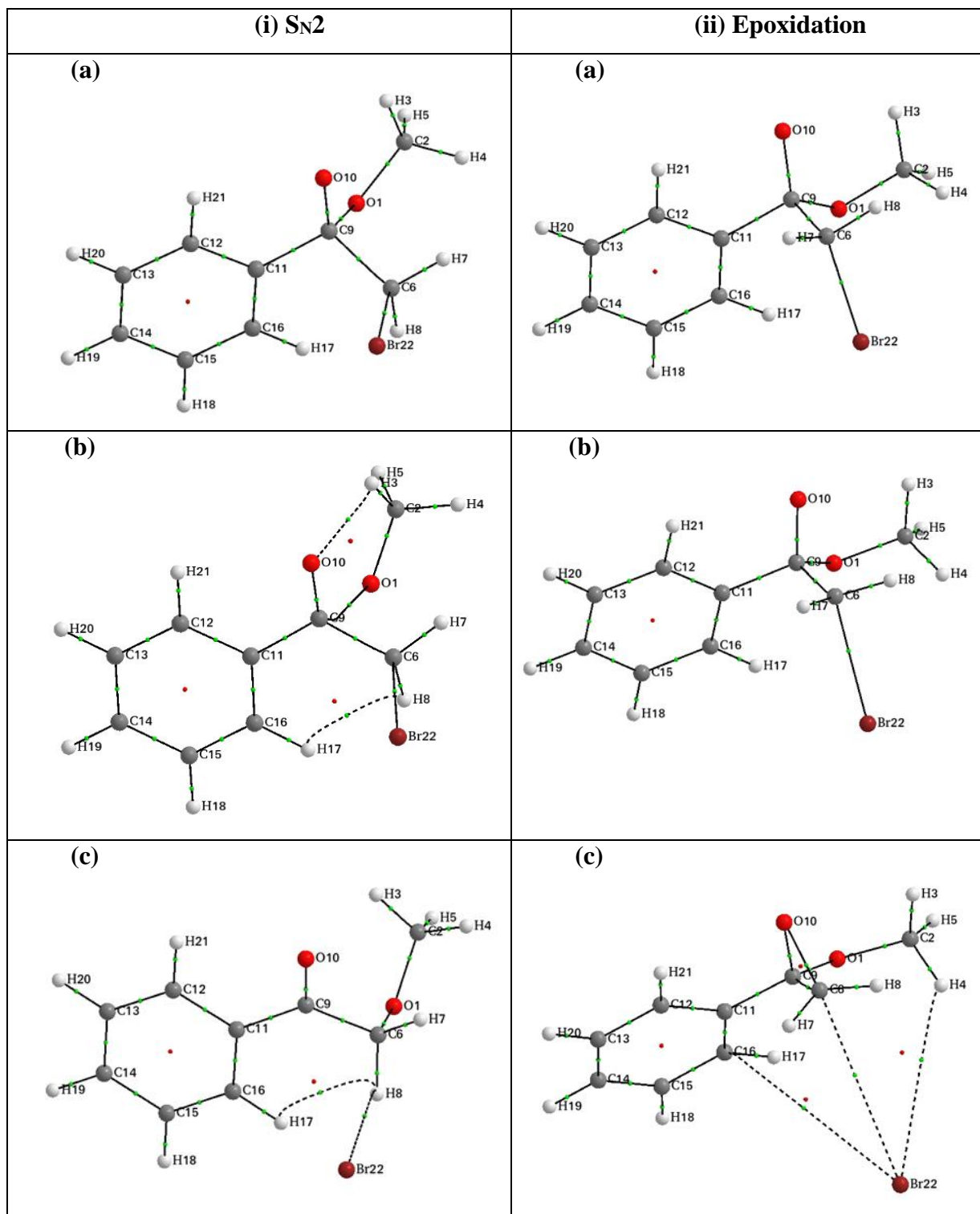
Table 4.2: Molecular graphs for the of the RC for the S_N2 reaction of **MeO⁻** reacting with **α-BrAcPh**, **p-OMe** and **p-NO₂**. Fragments which are used in QFARP analysis are represented graphically in dashed lines with each atom having its numbering shown on the right.
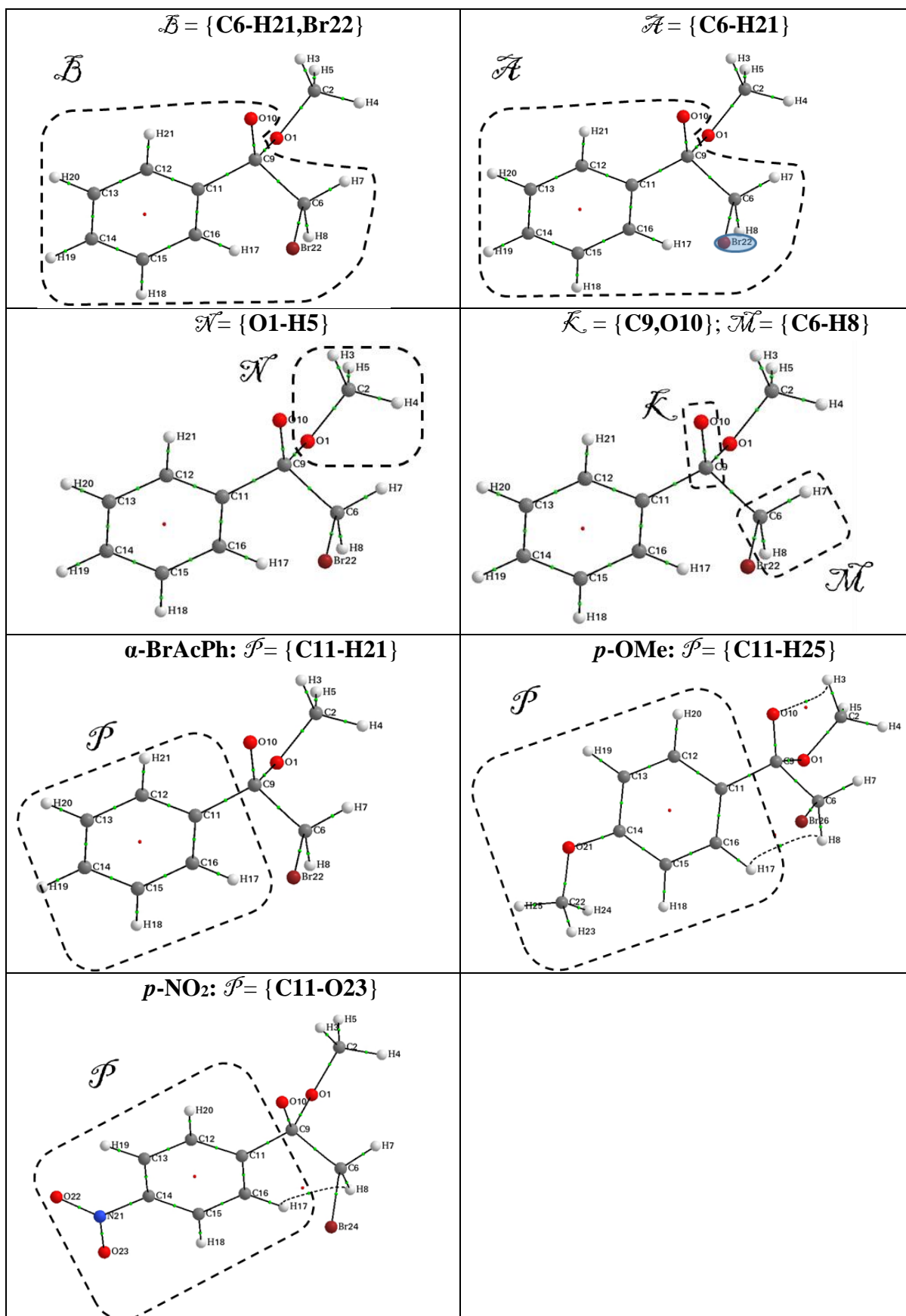
With the molecular system fragmented, the net charge of fragments can be used to gain insight into how the electron density changes throughout the system during the two reactions - **Figure 4.12**. For the S_N2 reaction shown on the left, the change in charge is similar to that observed for the **PhO⁻** and **AcO⁻** reaction - **Figure 3.16**, *vide supra*. The LG, Br, progressively increases its electron population to finally have a charge of approximately from -0.27 to -1 *e*. Fragment $\mathcal{K}$ is found to have a charge of -0.2 *e* which varies slightly during the reaction. $\mathcal{M}$ also shares the same trend as observed for the **PhO⁻** and **AcO⁻** reactions, where the α-group gradually becomes more positive as the charge changes from 0.09 to 0.56 *e*, due to the replacement of Br, with a more electronegative O (O1). Fragments $\mathcal{P}$ and $\mathcal{N}$ however, are shown to differ significantly from the previously studied S_N2 reactions. $\mathcal{P}$ gradually takes on a positive charge from -0.09 to 0.10 *e*, this is unexpected as this change was not noted for the early studied S_N2 reactions where fragment $\mathcal{P}$ has a charge of 0.1 *e* throughout the reaction. Thus, the CA of **MeO⁻** and **α-BrAcPh** which occurs prior to the S_N2 reaction, results in $\mathcal{P}$ having a negative charge of -0.09 *e*. When **MeO⁻** shifts from C9 to C6, during the S_N2 reaction, $\mathcal{P}$ gains its partial positive charge again. Interestingly, $\mathcal{N}$ begins with a charge of -0.52 *e*, which is also the result of the CA that occurred earlier, as opposed to a charge of -1 *e* which the nucleophile would have had prior to the CA. Significant variation in charge is noted for $\mathcal{N}$ during the S_N2 reaction, with the final charge being -0.50 *e*, this is expected as significant electron rearrangement would be expected during the nucleophilic substitution.

For the epoxidation reaction - **Figure 4.12**(b), the significant similarities with the S_N2 reaction are noted. The initial charges for the structure of the epoxidation reaction, RC-*trans*, is like that of the S_N2 reaction with $\mathcal{M}$, $\mathcal{P}$ and $\mathcal{N}$ having initial charges of 0.09, -0.09 and -0.54 *e*, respectively. No significant changes during the reaction are noted for $\mathcal{N}$, as the nucleophile, **MeO⁻**, does not play a direct involvement in the epoxidation. Br gradually becomes more negative to have a charge final charge of -0.98 *e*. Like for the S_N2 reaction, $\mathcal{P}$ progressively becomes positive during the epoxidation reaction, along with $\mathcal{K}$ which decreases in charge from -0.14 to -0.03 *e*.
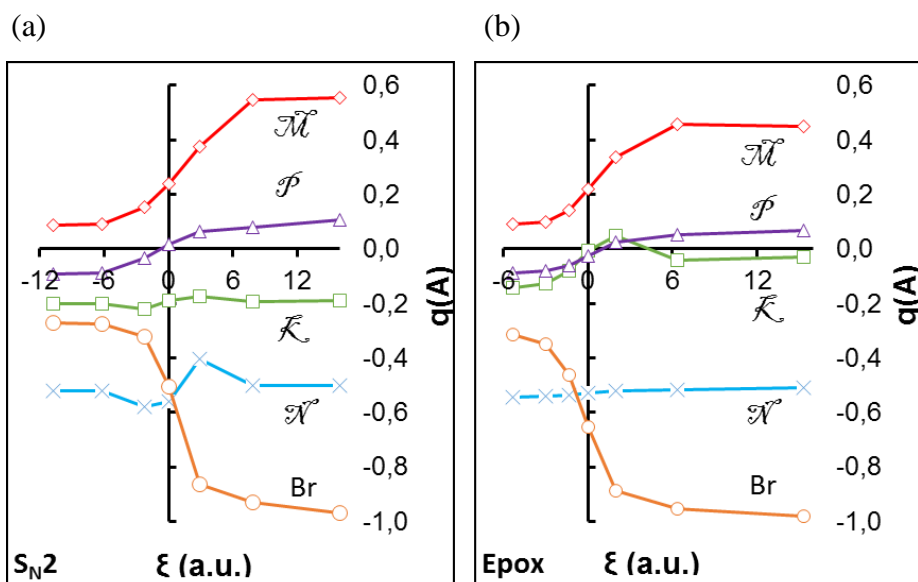
Figure 4.12: Charge of fragments shown in **Table 4.1** along the (a) S_N2 and (b) epoxidation reactions of **MeO⁻** reacting with **α-BrAcPh**.

4.3.6 QFARP analysis of S_N2 reaction

The analysis of the S_N2 and epoxidation reactions, by means of QFARP are done separately, to identify and explain the difference in selectivity observed with varying substituents on the aromatic ring. For the analysis of these reaction, only structures that were generated from the IRC calculations were used, thus other processes along the PES such as CA and rotation of the α-group were not considered.

For the S_N2 reaction, the additive energy of the fragments were first considered to identify fragments which contribute significantly to the (de)stabilisation - **Figure 4.13** and **Figure 4.14**. Interestingly, significant changes in additive energy were noted for all fragments, whereas for the reactions studied in chapter 3 $\mathscr{P}$ and $\mathscr{K}$ did not change substantially. For the S_N2 reactions of **α-BrAcPh**, **p-OMe** and **p-NO₂**, $\mathscr{K}$ and Br provided stabilisation, while $\mathscr{P}$ and $\mathscr{M}$ are destabilised with the removal of electron density. For all three reactions, the same trend was observed while the magnitude of the energy change varies. When the **p-NO₂** reaction is compared with the other two reactions which favour the S_N2 reaction experimentally: (i) Br provides the most stabilisation while (ii) $\mathscr{P}$ and $\mathscr{M}$ provide the most destabilisation.

The stabilising and destabilising energies of the fragments largely cancel one another out when comparing the differences for the three systems **α-BrAcPh**, **p-OMe** and **p-NO₂**. For example, at the TS, the additive energy of Br for the **p-NO₂** reaction is noted to be -4.2 kcal/mol more stabilising than for the **p-OMe** reaction. However, when the destabilisation at the TS from fragment $\mathscr{M}$ is

80

considered, the additive energy of $\mathcal{M}$ for the **p-NO₂** reaction is 4.6 kcal/mol more destabilising than for **p-OMe**. These energy differences therefore contribute insignificantly towards the electronic energy of the molecular system.

The additive energy of $\mathcal{N}$ shows a similar trend which was noted in chapter 3. The nucleophile contributes to the (i) destabilisation of the activation energy by approximately 11 kcal/mol but also (ii) contributes significantly to the stabilisation to the final products energy. Note that **p-OMe** has the greatest stabilising effect to the TS and the products.
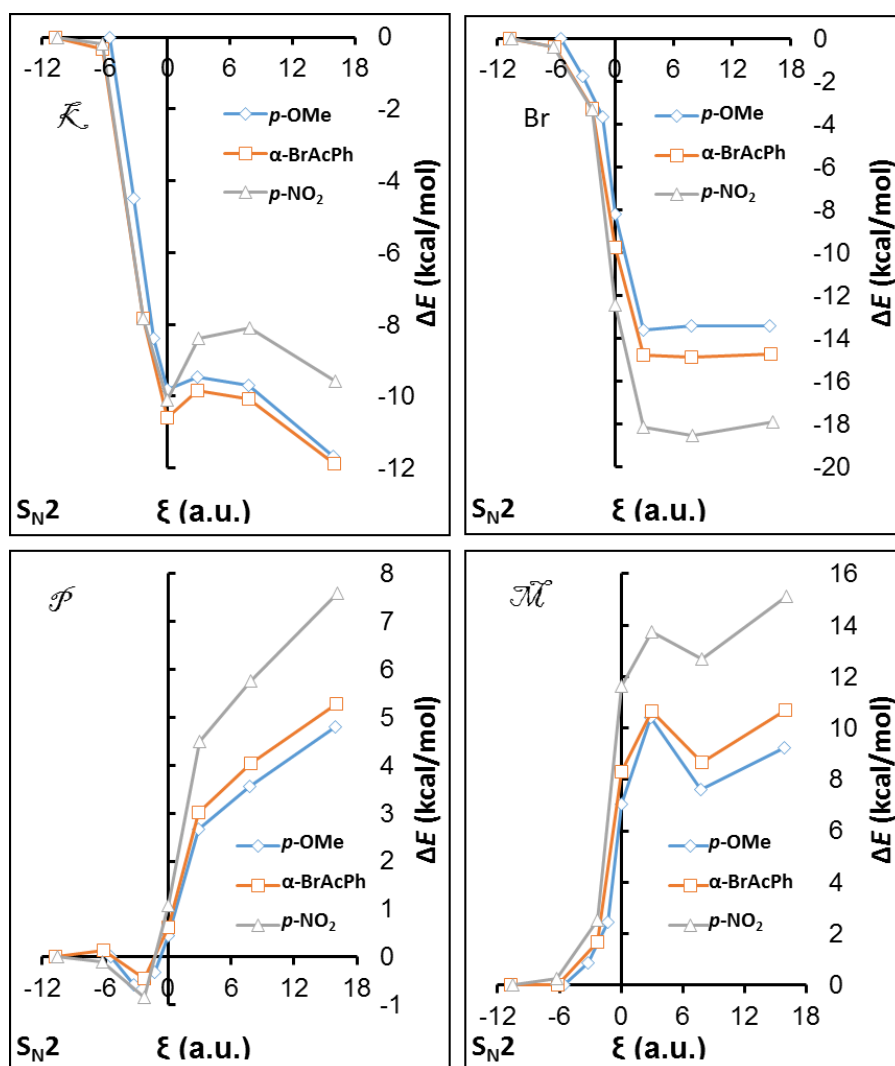
Figure 4.13: Change in the additive energy of fragments $\mathcal{K}$, $\mathcal{P}$, $\mathcal{M}$ and Br (**Table 4.1**) along the S_N2 reaction pathway of **MeO⁻** reacting with **α-BrAcPh**, **p-OMe** and **p-NO₂**.

81
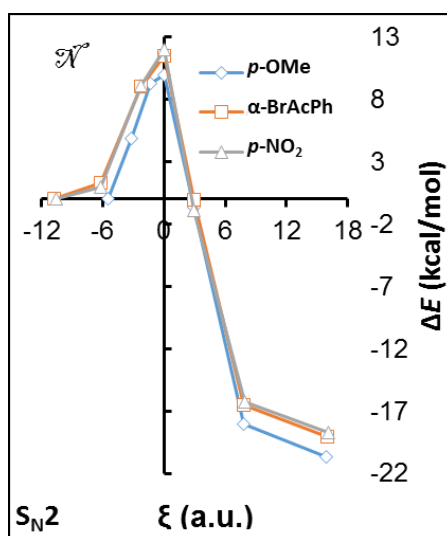
Figure 4.14: Change in the additive energy of fragment $\mathscr{N}$ (**Table 4.1**) along the S_N2 reaction pathway of **MeO⁻** reacting with **α-BrAcPh**, **p-OMe** and **p-NO₂**.

For the S_N2 reaction, the nucleophile detaches itself from the carbonyl group first to undergo the nucleophilic substitution on the neighbouring α-*C*. Thus, it is important to consider the interaction energies of the bonds that are formed (O1-C6) and broken (O1-C9) during the reaction, as well as the fragment interactions - **Figure 4.15**. At the beginning of the reaction for **α-BrAcPh**, $E_{int}^{O1,C9}$ is shown to be -332 kcal/mol while $E_{int}^{O1,C6}$ is only -13 kcal/mol. By the end of the reaction however, $E_{int}^{O1,C9}$ and $E_{int}^{O1,C6}$ are -128 kcal/mol and -341 kcal/mol, respectively. This shows the establishment of new stronger interactions (O1-C6) as the reaction proceeds. When fragments interactions of $\mathscr{N}$ with $\mathscr{M}$ and $\mathscr{K}$ are considered, the same trends are noted. In the case of $E_{int}^{\mathscr{K},\mathscr{N}}$, the interaction at the beginning of the reaction is -183 kcal/mol, which is 149 kcal/mol lower than that of $E_{int}^{O1,C9}$. This energy difference is due to the repulsive interaction of $E_{int}^{O1,O10}$ and $E_{int}^{C2,C9}$ which are included in the fragment analysis. An interesting observation is made when the interaction energies at the TS are compared. At the TS, $E_{int}^{O1,C9}$ and $E_{int}^{O1,C6}$ differ by 135 kcal/mol, while $E_{int}^{\mathscr{K},\mathscr{N}}$ and $E_{int}^{\mathscr{M},\mathscr{N}}$ only differs by 0.6 kcal/mol for the reaction of **α-BrAcPh**. Therefore, because fragments were considered, the repulsive interactions were also included and shows that the repulsive interactions play an important role to allow the nucleophile to experience the same amount of interaction with $\mathscr{K}$ and $\mathscr{M}$ at the TS.

82
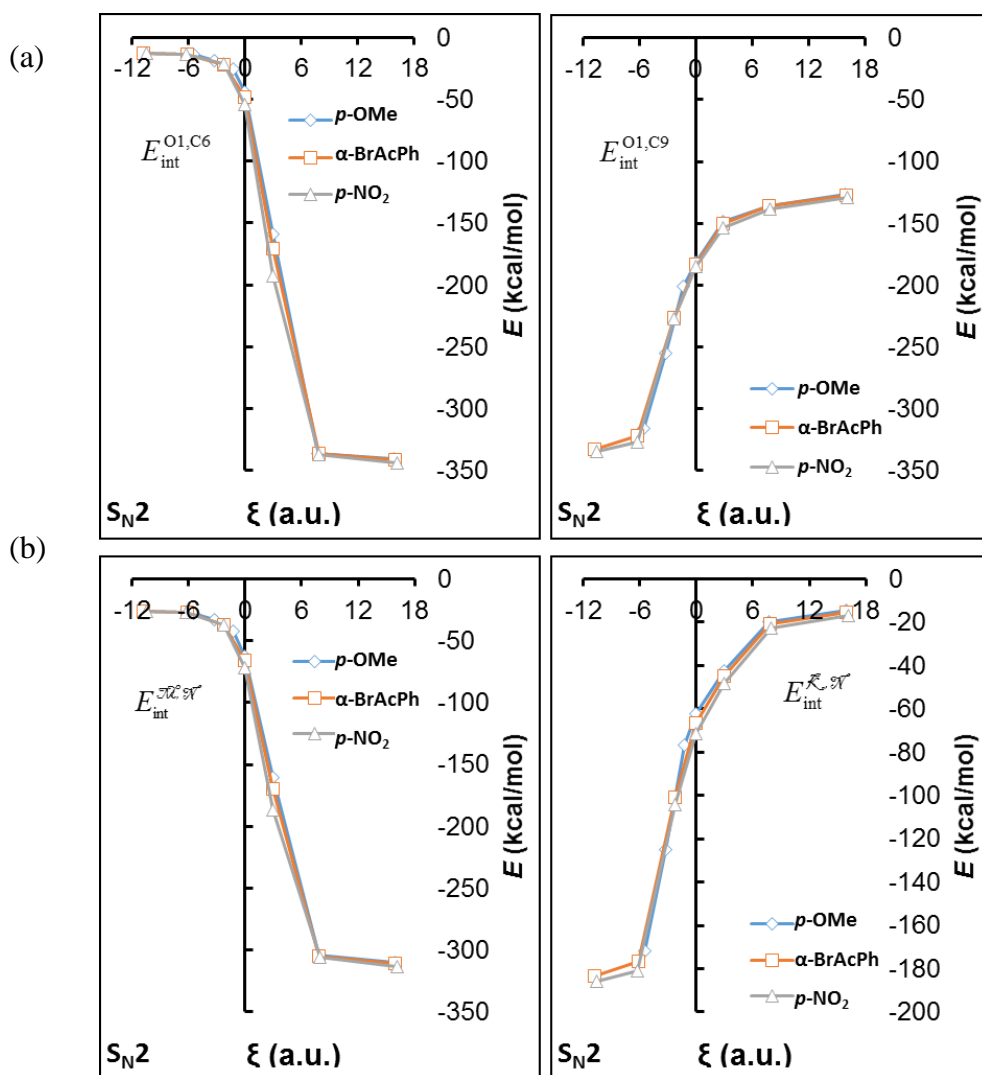
Figure 4.15: Interaction energies for the bonds (a) formed (O1C6) and broken (O1C9), and (b) the interactions of fragments $\mathscr{N}$ with $\mathscr{M}$ and $\mathscr{K}$ along the S_N2 reaction pathway of **MeO⁻** reacting with **α-BrAcPh**, *p*-**OMe** and *p*-**NO2**.

To understand the interactions on a larger scale, the interactions of $\mathscr{N}$ with the α-haloketone system, $\mathscr{B}$, were considered - **Figure 4.16**. The attraction between **α-BrAcPh** and the nucleophile, $E_{int}^{\mathscr{B},\mathscr{N}}$, shows a significant decrease from -220 kcal/mol to -132 kcal/mol at the TS, as **MeO⁻** detaches itself from the carbonyl group. This attractive interaction increases significantly after the TS to form the new product with an interaction energy of -304 kcal/mol. Interestingly, $E_{int}^{\mathscr{B},\mathscr{N}}$ for the reactions *p*-**OMe** and *p*-**NO₂** at the TS are -125 kcal/mol and -148 kcal/mol, respectively.

While the attractive interaction $E_{int}^{\mathscr{B},\mathscr{N}}$ at the TS is weakest for the *p*-**OMe** reaction, the energy difference when compared with *p*-**NO₂** and **α-BrAcPh** are minimal when one considers how large the overall changes in the interaction energy are during the reaction.

83

Comparing $E_{\text{int}}^{\mathcal{B},\mathcal{N}}$ at the beginning and end of the reaction shows a significant increase in attraction of -94 kcal/mol for *p*-OMe - **Figure 4.16**, while **α-BrAcPh** and *p*-NO₂ have increases of -84 kcal/mol in attraction. This suggests that the presence of an EDG enhances the additional attraction gained from the nucleophile being bound to the α-*C*. However, an analysis based only on this interaction, $E_{\text{int}}^{\mathcal{B},\mathcal{N}}$, is not sufficient to explain the difference in reactivity.

Note that in chapter 3, the same interaction analysis of $E_{\text{int}}^{\mathcal{B},\mathcal{N}}$ was done – **Figure 3.5**, *vide supra*. Interestingly because **PhO⁻** and **AcO⁻** did not detach from the carbonyl group, $E_{\text{int}}^{\mathcal{B},\mathcal{N}}$ gradually becomes more attractive with no energy barrier as compared to **Figure 4.16**, where for the S$_N$2 reaction of **MeO⁻** a significant barrier is noted.
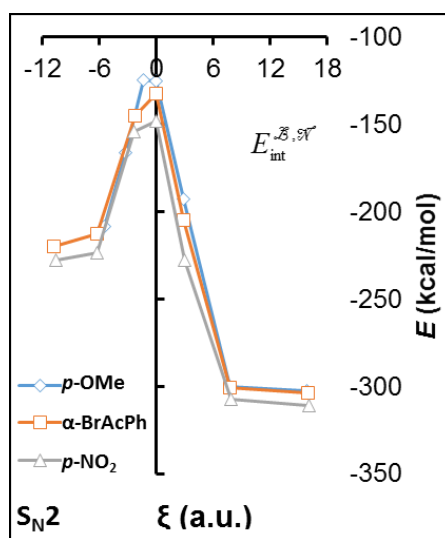
Figure 4.16: Interaction energy between fragment $\mathcal{B}$ and $\mathcal{N}$ along the S$_N$2 reaction pathway of **MeO⁻** reacting with **α-BrAcPh**, *p*-OMe and *p*-NO₂.

While the interaction energy between fragments has been considered, the intra-fragment interactions, such as of $\mathcal{N}$, has not been discussed thus far. In chapter 3, it was shown that significant weakening of interaction between the attacking-*O* and the nucleophiles adjacent-*C* occurs during the reaction, which contributes to the activation energy of the reaction - **Figure 3.12**, *vide supra*. The same analysis was done for **MeO⁻** reacting with **α-BrAcPh**, *p*-OMe and *p*-NO₂ - **Figure 4.17**. $E_{\text{int}}^{\text{O1,C2}}$ shows that up until the TS there is a significant increase in the attraction. After the TS, however, this interaction strength decreases significantly again.

The fluctuation in the interaction strength of $E_{\text{int}}^{\text{O1,C2}}$ can be explained by considering the bonding environment of the attacking-*O* (O1) during the reaction: From the beginning of the reaction until

the TS, the interaction between the attacking-*O* (O1) and carbonyl-*C* (C9) weakens significantly. Consequently, the attacking-*O* begins to strengthen its interaction with the adjacent-*C* (C2) to which it is bound. While after the TS, the attacking-*O* now begins to increase its interactions with the α-*C*, while weakening the O1–C2 interaction. The energy difference of $E_{int}^{O1,C2}$ between the RC and PC structures is shown to be 5.4 kcal/mol for the **α-BrAcPh** reaction. While this diatomic interaction is slightly weakened, it is negligible compared to the attractive interaction energy gained for $E_{int}^{\mathcal{B},\mathcal{N}}$.
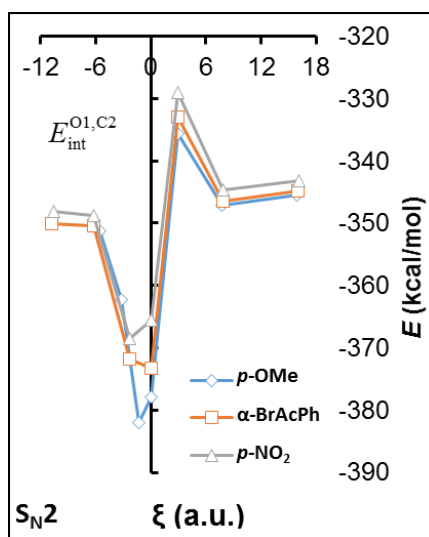
Figure 4.17: Interaction energy between O1 and C2, along the S$_N$2 reaction pathway of **MeO⁻** reacting with **α-BrAcPh**, ***p*-OMe** and ***p*-NO₂**.

The last group of interactions to consider for the S$_N$2 reactions is of the LG, Br - **Figure 4.18**. As expected, at the initial stages of the reaction, Br has a strong attractive interaction with the rest of the molecular system, $E_{int}^{Br,\mathcal{H}}$ = -137 kcal/mol for the reaction of **α-BrAcPh**. With the attraction between Br and $\mathcal{M}$, $E_{int}^{Br,\mathcal{M}}$, contributing largely to $E_{int}^{Br,\mathcal{H}}$. As the reaction progresses the attractive interactions which Br experiences weakens significantly. At the TS, $E_{int}^{Br,\mathcal{M}}$ is found to be -104 kcal/mol for **α-BrAcPh**. This significant weakening of interaction energy for Br comes from the covalent bond (C6-Br) breaking, as well as the repulsion noted between the LG and the nucleophile, $\mathcal{N}$.

85
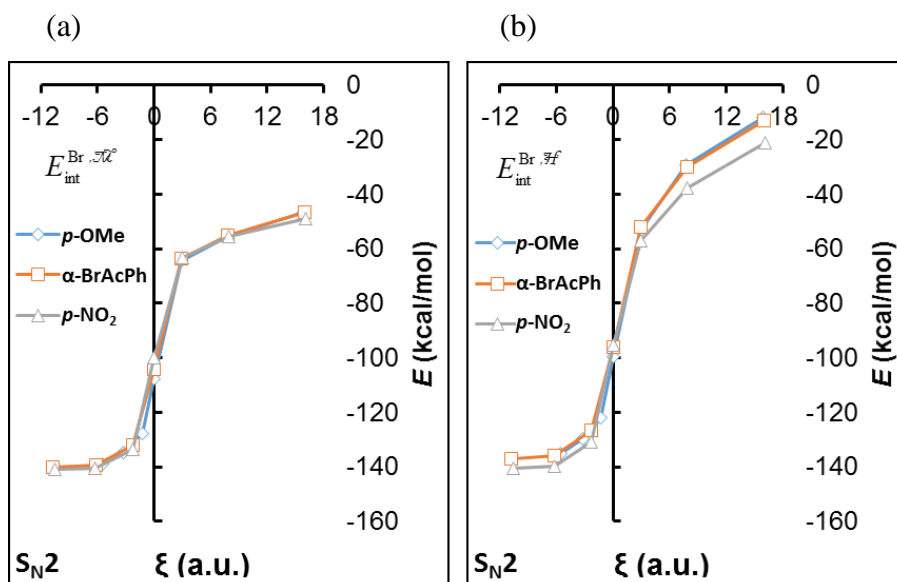
Figure 4.18: Interaction energy between Br and fragments (a) $\mathcal{M}$ and (b) $\mathcal{H}$, along the S_N2 reaction pathway of **MeO⁻** reacting with **α-BrAcPh**, ***p*-OMe** and ***p*-NO₂**.

4.3.7 QFARP analysis of Epoxidation reaction

QFARP analysis on the epoxidation reaction was performed to gain further insight into the reaction. Change in the additive energy of the fragments during the epoxidation reaction were considered first - **Figure 4.19** and **Figure 4.20**. While there are, significant similarities noted in the additive energy of the fragments and effect of the substituents when compared with that of the S_N2 reaction (**Figure 4.13** and **Figure 4.14**), there are also some differences to note.

Beginning with the similarities of the epoxidation reaction to the S_N2 reaction: Br, $\mathcal{P}$ and $\mathcal{M}$ contribute in a stabilising manner to the reaction, with approximately the same variation in magnitude being noted with the addition of the different substituents. Fragment $\mathcal{K}$ on the other hand has a destabilisation effect which peaks at the TS, while for the S_N2 reaction (**Figure 4.13**) $\mathcal{K}$ provides a stabilisation effect. It is also clear that the EWG of ***p*-NO₂** results in an increased destabilising contribution for $\mathcal{K}$, $\mathcal{P}$ and $\mathcal{M}$. While it is also found that the reaction of ***p*-NO₂** has an increased stabilisation for Br relative to **α-BrAcPh** and **MeO⁻** of -3 kcal/mol at the TS. However, the additional stabilisation energy for the ***p*-NO₂** reaction is not larger than the destabilisation noted for the other fragments.

These findings are surprising as the additive energy of the fragments suggests that the reaction of ***p*-NO₂** is the least reactive of the three systems, which contradicts experimental findings. This means that IQA was not able to recover trends in the electronic energy when comparing the three systems (**α-BrAcPh**, ***p*-NO₂** and ***p*-NO₂**). While the IQA energy trends that are noted can be

86

considered valid, the actual energy values that are recovered for the different systems can be misleading and should be compared with caution.

Furthermore, $\mathscr{N}$ provides a stabilising effect which only increases over the course of the reaction. This contrasts with the S_N2 reactions studied thus far where $\mathscr{N}$ resulted in a destabilisation contribution at the TS followed by a significant stabilising effect afterwards. Note also that substituents do not have any effect on the additive energy of $\mathscr{N}$, which has not been noted for any other fragment.
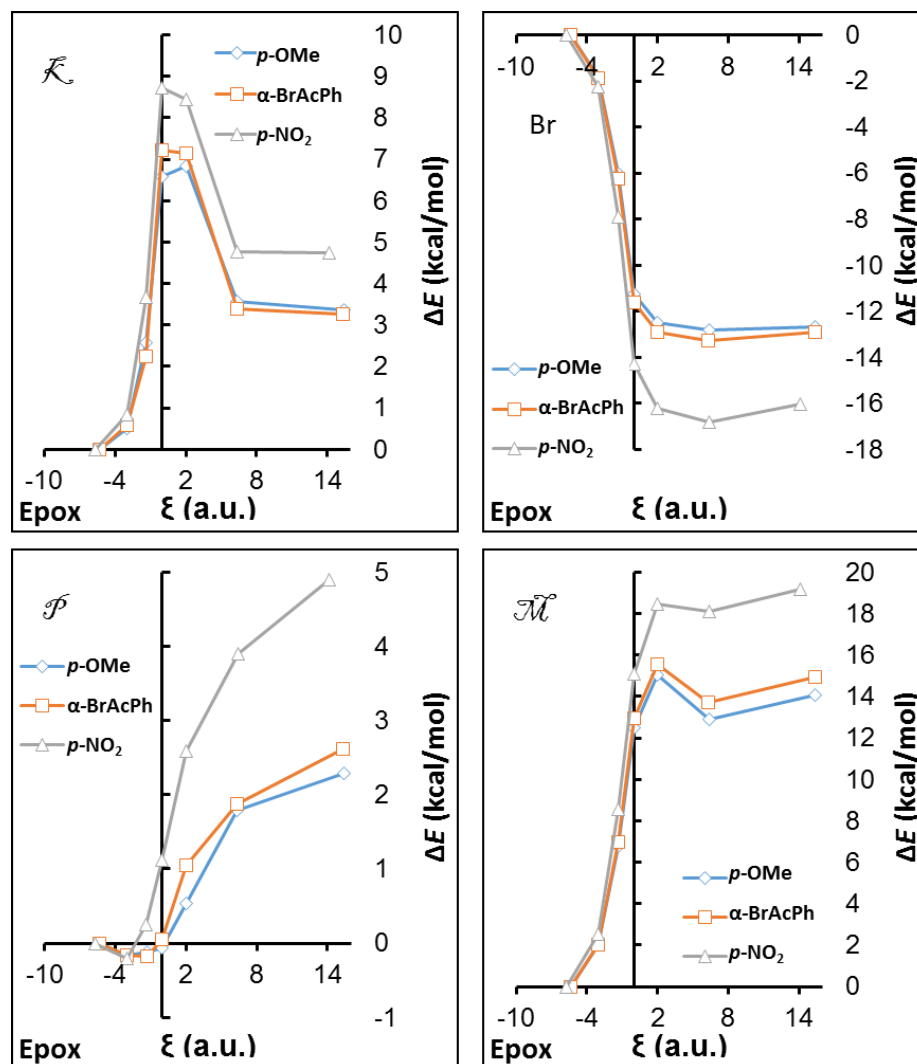
Figure 4.19: Change in additive energy of fragments $\mathscr{K}$, $\mathscr{P}$, $\mathscr{M}$ and Br (**Table 4.1**) along the epoxidation reaction pathway of **MeO⁻** reacting with **α-BrAcPh**, **p-OMe** and **p-NO₂**.

87
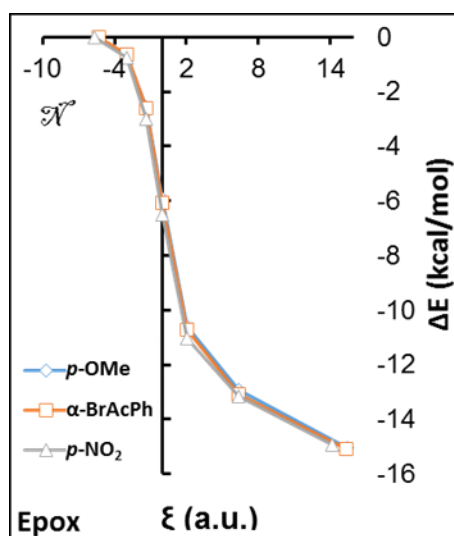
Figure 4.20: Change in the additive energy of fragment $\mathcal{N}$ (**Table 4.1**) along the epoxidation reaction pathway of **MeO⁻** reacting with **α-BrAcPh**, **p-OMe** and **p-NO₂**.

The additive energy of the fragments provides an uncertain picture on the understanding of the reactivity, therefore significant changes in interaction energies were considered next. The interaction energies for the bonds that are formed (C6-O10) and broken (C6-Br) were investigated - **Figure 4.21** (a). Initially, $E_{\text{int}}^{\text{C6,O10}}$ has a weak interaction of -21 kcal/mol at the RC, while by the end of the reaction the PC has a value of -286 kcal/mol. As expected, the opposite trend is noted for $E_{\text{int}}^{\text{C6,Br}}$ where interaction energies of -123 kcal/mol and -23 kcal/mol are found for the RC and PC structures, respectively. Note that the final interacting energy $E_{\text{int}}^{\text{C6,O10}}$ is far more attractive than the initial value of $E_{\text{int}}^{\text{C6,Br}}$. The trend is consistent for the other studied S$_N$2 reaction where the new covalent bond has a larger attraction than the previous bond which had to be broken during the process of the reaction. When the interactions of fragment $\mathcal{M}$ with $\mathcal{K}$ and Br are considered, the same trend is observed. $E_{\text{int}}^{\mathcal{M},\mathcal{K}}$ is however substantially greater than $E_{\text{int}}^{\text{C6,O10}}$ which is due to the presence of the additional interaction energy provided by the C6–C9 covalent bond that remains consistent throughout the reaction.

Interestingly, similar to what was noted from the S$_N$2 reactions (**Figure 4.15**), the presence of different substituents did not have any significant effect on the interaction energies of the bonds formed or broken during the reaction - **Figure 4.21**.
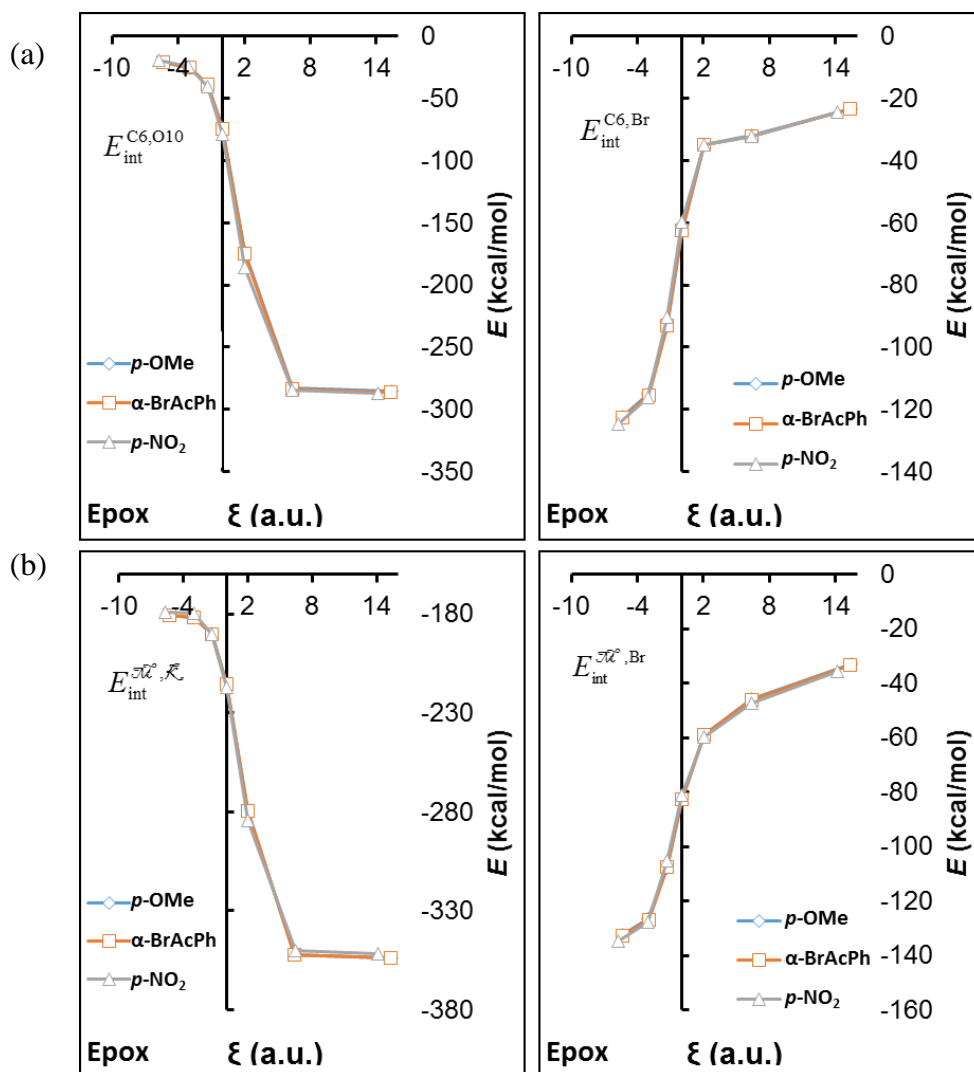
Figure 4.21: Interaction energies for the bonds (a) formed (C6O10) and broken (C6Br), and (b) the interactions of fragments $\mathcal{M}$ with $\mathcal{K}$ and Br along the epoxidation reaction pathway of **MeO⁻** reacting with **α-BrAcPh**, **p-OMe** and **p-NO₂**.

The last interaction to consider is that of fragment $\mathcal{N}$, to understand how the epoxidation reaction affected the bonding of the nucleophile to the carbonyl group - **Figure 4.22**. From the interaction energy, $E_{\text{int}}^{\mathcal{K},\mathcal{N}}$ is shown to increase by -74 kcal/mol, with an initial interaction of -229 kcal/mol for **α-BrAcPh**. The same trend is noted for $E_{\text{int}}^{\mathcal{B},\mathcal{N}}$ where the initial interaction is -263 kcal/mol and increases in strength by -89 kcal/mol by the end of the epoxidation reaction.

This shows that the bonding which the nucleophile is involved, increases significantly even though it is not directly involved in the epoxidation reaction. This increased attraction which $\mathcal{N}$ experiences for the epoxidation reaction supports the results of the additive energy of $\mathcal{N}$ shown in **Figure 4.20**.

Furthermore, for the p-**NO₂** reaction $\mathscr{N}$ experiences a greater attraction to $\mathscr{B}$ of approximately -10 kcal/mol throughout the reaction than for the reactions of **α-BrAcPh** and p-**OMe**. While this additional attraction would be beneficial for the p-**NO₂** reaction it cannot solely be used to explain the enhanced reactivity that is noted experimentally.
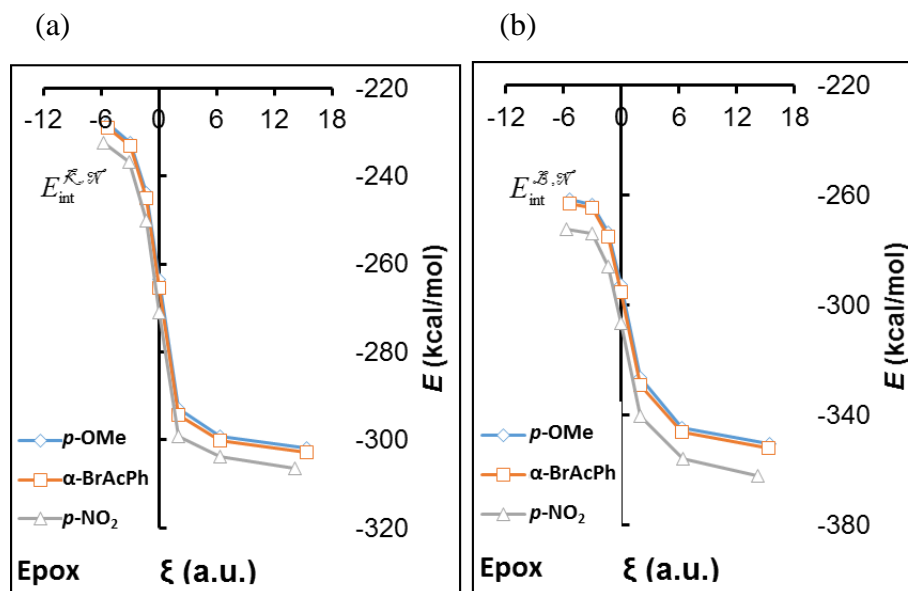
Figure 4.22: Interaction energy of fragment $\mathscr{N}$ with (a) $\mathscr{K}$ and (b) $\mathscr{B}$ along the epoxidation reaction pathway of **MeO⁻** reacting with **α-BrAcPh**, p-**OMe** and p-**NO₂**.

4.4 Conclusion

A computational study on the reaction of between **MeO⁻** with **α-BrAcPh** was embarked on, to understand the formation of products that are reported from experimental studies. Previous studies suggested that two competing reactions, S_N2 and epoxidation, are occurring.

Unexpectedly, modelling the S_N2 reaction of **MeO⁻** with **α-BrAcPh** shows CA occurs first, forming a stable intermediate, RC. The nucleophile then detaches from the carbonyl-C and attacks the neighbouring α-C. The negative vibrational frequency of the TS also shows the unexpected movement of the nucleophile between the carbonyl-C and α-C. The stable intermediate which is noted for the S_N2 reaction is also an intermediate of the epoxidation reaction. The α-group is required to rotate around to allow Br to be *trans* to the carbonyl-O, RC-*trans*. The epoxidation reaction then proceeds with the carbonyl-O attacking the α-C, resulting in the displacement of the LG, Br. The activation energy of the epoxidation TS was unpredictability lower than that of the rotation of the α-group. Following analysis of the PES for the two reactions shows that the energy barriers are of the same magnitude.

90

Consideration of the PES for the ***p*-OMe** reaction shows that the presence of an EDG increases the activation energy of the TS for both reactions as well as the rotational barrier of the epoxidation reaction, with the latter being the most affected. These computational findings are supported by the experimental studies which have found that there is a decrease in the two reaction rates and increased selectivity towards the S_N2 product.

On the other hand, ***p*-NO₂** illustrates the presence of an EWG, which decreases all the energy barriers, especially the rotational barrier. Experimentally it is shown that the presence of EWG increases the reaction rate while also increasing the favourability towards the epoxidation reaction route, which also supports the computational findings further.

IQA/QFARP analysis on the S_N2 and epoxidation reactions for **α-BrAcPh**, ***p*-OMe** and ***p*-NO₂** was performed with some differences between the reactions being noted:

i) The carbonyl group, fragment $\mathcal{K}$, provides a destabilising effect for the epoxidation reaction, while a stabilising effect is noted for the S_N2 reaction.

ii) The nucleophile, fragment $\mathcal{N}$, provides a noticeable stabilising effect throughout the epoxidation reaction. However, for the S_N2 reaction the fragment contributes to the destabilisation of the TS, resulting in a large activation energy, but the TS begins to provide stability for the final PC structure.

While IQA/QFARP provided insight into the competing reactions, differences in reactivity could not be explained. With several fragment and diatomic interactions being considered, the analysis did not provide a sufficient conclusion to explain what causes the increase/decrease in the activation energies with the presences of an EDG/EWG on the phenyl-ring of **α-BrAcPh**.

The QFARP analysis did not consider the CA reaction which both reaction routes share and the rotation of the α-group which has been shown to be affected significantly when comparing the PES of the three molecular systems. Thus, for future work it is recommended that further studies of the CA and specifically the rotation of the α-group using QFARP be done to obtain a further understanding about these important steps for the two competing reaction routes.

4.5   References

(1)   Itoh, S.; Yoshimura, N.; Sato, M.; Yamataka, H. *J. Org. Chem.* **2011**, *76* (20), 8294.

(2)   Katayama, M.; Sasagawa, K.; Yamataka, H. *J. Phys. Org. Chem.* **2012**, *25* (8), 680.

(3)   Tagawa, K.; Sasagawa, K.; Wakisaka, K.; Monjiyama, S.; Katayama, M.; Yamataka, H. *Bull. Chem. Soc. Jpn.* **2014**, *87* (1), 119.

(4)   M. J. Frisch, G. W. Trucks, H. B. Schlegel, G. E. Scuseria, M. A. Robb, J. R. Cheeseman, G. Scalmani, V. Barone, B. Mennucci, G. A. Petersson, H. Nakatsuji, M. Caricato, X. Li, H. P. Hratchian, A. F. Izmaylov, J. Bloino, G. Zheng, J. L. Sonnenberg, M. Had, J. C. Gaussian, Inc.: Wallingford, CT 2009,.

(5)   Keith, T. A. TK Grismill Software: Overland Parks KS, USA 2013, aim.tkgristmill.com.

Chapter 5

Conclusions

5.1 Conclusions

While S$_N$2 reactions have been studied for decades using numerous techniques, the knowledge that has been gained thus far is still not adequate to explain certain obscure experimental observations. One such observation is that the nucleophilic substitution of methoxide (**MeO⁻**) with α-haloketones such as α-bromoacetophenone (**α-BrAcPh**), can afford the formation of compounds other than the ether product, **4** – **Scheme 1.7**. While some experimental[1,2] and computational[3] studies have been done on the matter, the results have not been conclusive. Thus, the aim of this project was to study S$_N$2 reactions of **α-BrAcPh** with particular consideration of **MeO⁻** as the nucleophile.

The reactions of **α-BrAcPh** with phenolate (**PhO⁻**) and acetate (**AcO⁻**) which show no by-product formation were initially studied, in order to form a basis to which the **MeO⁻** reaction could be compared. Reported experimental results[4] showed **PhO⁻** is slightly more reactive than **AcO⁻**, in the presence of a base, polar solvent and elevated temperatures.

The reactions of **PhO⁻** and **AcO⁻** were modelled and it was found the activation energy, ΔG$^{\#}$, was 11.2 and 16.6 kcal/mol, respectively and the ΔG between reactants (R) and products (P) showed that the **PhO⁻** reaction is -11.6 kcal/mol more exothermic than the **AcO⁻** reaction – **Figure 3.3**, *vide supra*. These findings, the activation energy and exothermic effect, support the experimental observations regarding the reactivity of **PhO⁻** and **AcO⁻**.

Analysis of the reactions was performed with Quantum fragments along reaction pathway (QFARP), which is an energy decomposition scheme, to gain a fundamental insight into which interactions drive the reactions forward and how these interactions change during the reaction. The molecular systems were fragmented primarily based on functional groups and atoms which are directly involved in the reaction. Analysis of the fragments was performed to identify which inter-fragment interactions contribute in a stabilising or destabilising manner to the reaction. QFARP analysis for the reaction of **PhO⁻** and **AcO⁻** showed:

(i) The additive energy of the leaving group (Br) was shown to provide the most stabilisation throughout the reaction. This is due to the stabilisation gain from the self-energy being significantly larger than the loss in attractive interaction energy.

(ii) The α-group, $\mathcal{\widetilde{M}}$, is the most destabilised during the reaction due to the withdrawn electron density as Br is replaced by a more electronegative-O (nucleophile).

(iii) Interestingly, when comparing the additive energy of the fragments for the **PhO⁻** and **AcO⁻** reactions, it is noted that the increased activation energy for the **AcO⁻** reaction

94

is the result of fragment $\mathscr{M}$ being more destabilised than that of the **PhO⁻** reaction. This means that the nucleophile **AcO⁻** destabilises $\mathscr{M}$ more than **PhO⁻** does, which causes the reaction to be less reactive.

(iv) The nucleophile is shown to contribute to the destabilisation of the energy barrier but also to the stabilisation of the product after the TS. The destabilisation is due to a significant weakening of the intramolecular interaction of the attacking-*O* and its adjacent-*C*, while the stabilisation contribution is due to the formation of the new bond between the attacking-*O* and the α-*C*.

(v) Further investigation of diatomic interactions showed that there are very strong attractive interactions between the carbonyl ($\mathscr{K}$) and nucleophile ($\mathscr{N}$). These attractive interactions are complimented by repulsive interactions between the fragments which largely cancel one another out, resulting in the nucleophile having a greater attraction to the α-group, $\mathscr{M}$, than the carbonyl group, $\mathscr{K}$. Scans of the nucleophile moving towards the carbonyl-*C* results in an exponential increase in the electronic energy, thereby suggesting that the nucleophiles will not undergo Carbonyl Addition (CA).

(vi) Finally, the attractive interaction between the nucleophile, $\mathscr{N}$, and **α-BrAcPh**, $\mathscr{B}$, increases exponentially, with the initial attraction largely being contributed from the interaction between the nucleophile and the hydrogens of the α-group.

The findings above are very insightful, and it is believed that most of these observations would not have been noted if other analysis approaches had been used.

The nucleophile substitution of **α-BrAcPh** with **MeO⁻** was subsequently modelled and it was found that CA occurs initially to form a stable intermediate, RC. The nucleophile detaches itself from the carbonyl-*C* and binds to the adjacent α-*C*, with detachment of the leaving group. For the TS structure, it was noted the attacking-*O* was in closer proximity to the carbonyl-*C* than the α-*C*. Interestingly, the negative vibrational frequency showed the α-group moving between Br and the attacking-*O*, while the nucleophile was noted to swing between the carbonyl-*C* and α-*C* (which has not been observed in other S$_N$2 reactions). It is also worth noting that speculations several decades ago have been reported regarding the occurrence of CA prior to the nucleophilic substitution.[5] However prior to this study there has been little evidence to suggest this mechanism.

In the case of the epoxidation reaction that was modelled between **α-BrAcPh** and **MeO⁻**, CA also occurs first forming the RC, followed by rotation of the α-group to allow Br to be *trans* to the

carbonyl-*O*, RC-*trans*. The epoxidation reaction is followed with the negative vibrational frequency of the TS structure having the α-group and carbonyl-*O* moving towards one another.

The PES for the S_N2 and epoxidation reaction were compared, with the $\Delta G^{\#}$ energy for the TS structure of the reactions being 4.9 and 5.1 kcal/mol higher than R, respectively. These energy differences are negligible; however, it was further found the rotational barrier of the α-group is shown to be 7.8 kcal/mol, and thus plays an important role in the reaction rate of the epoxidation.

The kinetic studies performed between **α-BrAcPh** and **MeO⁻** were completed at 25°C. This mild reaction temperature complements the activation energy found for the S_N2 and epoxidation reactions. This contrasts the activation energies for the reaction with **PhO⁻** and **AcO⁻** where the activation energies are significantly higher and reaction conditions are harsher with refluxing of the solutions required.

Experimental results[1,2] for the reaction between **α-BrAcPh** and **MeO⁻** show that the product originating from the S_N2 reaction, **4**, is favoured over that of the epoxidation reaction. Moreover, if an EDG is present on the phenyl-ring (such as a methoxy in the para-position, *p*-**OMe**) of **α-BrAcPh** then both reaction rates decrease and the S_N2 reaction is more favoured. However, if an EDG is present on the phenyl-ring (such as a nitro in the para-position, *p*-**NO₂**) then both reaction rate increase and the epoxidation reaction becomes favoured.

These observations are supported by the trends that are observed from the modelling when the PES of these reactions are considered. For the *p*-**OMe** system, $\Delta G^{\#}$ energy barrier of the TS increases by approximately 1.5 kcal/mol and 2.1 kcal/mol for S_N2 and epoxidation reactions, respectively. Interestingly, the rotational barrier of the α-group for the epoxidation reaction is shown to increase by 2.3 kcal/mol. For the *p*-**NO₂** system, the opposite effect on the PES is noted. Relative to **α-BrAcPh**, $\Delta G^{\#}$ energy barrier is shown to decrease by -3.1 kcal/mol and -4.2 kcal/mol for the S_N2 and epoxidation reaction, respectively. Notably, the rotational barrier also decreases significantly by -5.7 kcal/mol. These results support the experimental trends for the change in reaction rates for *p*-**OMe** and *p*-**NO₂**, as well as a shift in selectivity between the two reaction routes.

Analysis utilising QFARP for the S_N2 and epoxidation reactions was done to gain further insight. Noticeably, the new bonds that are formed from the reaction were significantly stronger than the bonds that were broken. It was also found that the nucleophile, $\mathscr{N}$, gained a significant attraction to the rest of the molecular system, even for the epoxidation reaction where $\mathscr{N}$ is not directly involved in the reaction.

Furthermore, some differences between the S_N2 and epoxidation reaction routes were found. Firstly, the carbonyl group, $\mathcal{K}$, provides a stabilising effect for the S_N2 reaction while a destabilising effect is noted for the epoxidation reaction. Secondly, $\mathcal{N}$ provides a considerable stabilising effect for the epoxidation reaction. However, for the S_N2 reaction $\mathcal{N}$ provides destabilisation to the TS while also significant stabilisation for the product structure, which had also been noted for the S_N2 analysis of **PhO⁻** and **AcO⁻** with **α-BrAcPh**.

While QFARP analysis that was performed could not explain the change in reaction rate with the presence of different substituents or why one reaction route would be favoured over the other, the analysis still provided valuable insight into the reaction mechanism which would not have been gained with other computational approaches.

5.2 Future Work

With the proposed new reaction mechanism, further modelling should be done to determine whether other nucleophiles also share this reaction mechanism. Other nucleophiles such as ethanol, ethanethiol and the addition of EDG/EWG on nucleophiles would provide greater insight into what affects the mechanism and what can further influence the competition between the S_N2 and epoxidation reaction routes. Also, using QFARP and changing the leaving group to other stronger/weaker leaving group should provide further insight into what makes certain leaving groups better than others.

While Yamataka and co-workers have done kinetic studies of **MeO⁻** at various concentrations,[1,2] the studies did not consider the affect that temperature has on the reaction rates. If these studies are repeated, experimental activation energies could be obtained, which can then be compared with the modelled activation energies to gauge how accurate the modelling is and to decide if higher levels of theory are required.

Additionally, molecular dynamic studies would also be insightful to understand if the solvent plays a significant role in these reactions. Other computational methods, such as the Activation Strain Model (ASM)[6] have been used to study other S_N2 reactions and could be applied to the S_N2 and epoxidation reactions studied in an effort to gain a deeper understanding of the strain- and interaction-energies. It is plausible that using other approaches will gain further insight into these reactions which cannot be obtained utilising QFARP alone.

The QFARP analysis for the reaction of **MeO⁻** is not complete. The analysis should be expanded to the CA and rotation of the α-group to understand how the substituents have a significant effect on PES.

Currently, generation on the QFARP interaction terms is not automated, thus the development of a data analysis program would increase the rate which the interaction terms are generated and allow for faster analysis of results.

This work has shown that QFARP is a powerful analysis approach which provides valuable insights into the S_N2 and epoxidation reaction. QFARP can be applied to other organic reactions to gain a deeper fundamental understanding of what drives the particular reaction forward.

Finally, it is important to recall that all studies were performed at relatively low level of theory that, in addition, does not account for dispersion. This might be a reason why some trends obtained from the QFARP studies were inconclusive. It is then recommended to incorporate the Grimme's empirical dispersion correction, by use of Gaussian's keyword 'empiricaldispersion=GD3' in future computational studies as well as aug-cc-pVDZ basis set, which is known to be slightly better than the one used in this studies, namely 6-311++(G(d,p). Furthermore, to verify the integrity of the computational and, in particular, IQA data, it would be advantageous to optimise selected and most important B3LYP-generated structures at higher level of theory (at least MP2(FC), preferably CCSD) and run IQA using improved integration. The added value of this recommendation would be a possibility of comparative studies at different levels of theory from which one would learn whether B3LYP/aug-cc-pVDZ/GD3 is good enough to explain relatively small differences in reactivity, driving forces, etc. Unfortunately, CCSD/aug-cc-pVDZ is computationally expensive in both terms, i.e., in optimisation of electronic structures as well as in IQA calculations; this is why it was not implemented in this pilot exploratory studies.

5.3 References

(1) Katayama, M.; Sasagawa, K.; Yamataka, H. *J. Phys. Org. Chem.* **2012**, *25* (8), 680.

(2) Tagawa, K.; Sasagawa, K.; Wakisaka, K.; Monjiyama, S.; Katayama, M.; Yamataka, H. *Bull. Chem. Soc. Jpn.* **2014**, *87* (1), 119.

(3) Itoh, S.; Yoshimura, N.; Sato, M.; Yamataka, H. *J. Org. Chem.* **2011**, *76* (20), 8294.

(4) Edwards, J. O.; Pearson, R. G. *J. Am. Chem. Soc.* **1962**, *84* (1), 16.

(5) Bunton, C. A. *Nucleophilic Substitution at a Saturated Carbon Atom*; Elsevier: London, 1963.

(6) Bento, A. P.; Bickelhaupt, F. M. *J. Org. Chem.* **2008**, *73* (18), 7290.

Appendix A

Supplementary Information for Chapter 3

Videos of vibration of the negative frequency for the TS of the S$_N$2 reaction of **PhO⁻** and **AcO⁻** with **α-BrAcPh** are included on attached CD.

Table A.1: Electronic (*E*) and recover energy of the molecular system from IQA (*E*$_{IQA}$) for structures of separate reactants, products and structure generated from IRC calculations of **PhO⁻** reacting with **α-BrAcPh**.

		IRC Coord	d (C1,O17) / Å	*E* (au)	Δ*E* (kcal/mol)	*E*_IQA (au)	Δ*E*_IQA (kcal/mol)	ΔΔ*E* (kcal/mol)
Separate Reagents	**α-BrAcPh**			-2958.547464		-2958.538356		5.715
	PhO⁻			-307.082231		-306.988582		58.766
	α-BrAcPh + PhO⁻		∞	-3265.629695	1.1	-3265.526938	12.7	64.481
		-4.109	2.673	-3265.631428	0.0	-3265.547191	0.0	52.860
		-2.394	2.53	-3265.630643	0.5	-3265.547383	-0.1	52.246
		-1.032	2.315	-3265.627137	2.7	-3265.546351	0.5	50.694
		(TS) 0	2.141	-3265.624964	4.1	-3265.543566	2.3	51.078
		1.72	1.836	-3265.635189	-2.4	-3265.546426	0.5	55.699
		3.096	1.587	-3265.655226	-14.9	-3265.559392	-7.7	60.137
		5.8339	1.4478	-3265.668089	-23.0	-3265.566975	-12.4	63.450
IRC		8.584	1.448	-3265.671022	-24.8	-3265.567029	-12.4	65.257
	Prod + Br⁻		∞	-3265.681503	-31.4			
Separate Products	**Prod**			-691.344579				
	Br⁻			-2574.336924				

Table A.2: Electronic (E) and recover energy of the molecular system from IQA (E_{IQA}) for structures of separate reactants, products and structure generated from IRC calculations of **AcO⁻** reacting with **α-BrAcPh**.

		IRC Coord	d (C1,O17) / Å	E (au)	ΔE (kcal/mol)	E_IQA (au)	ΔE_IQA (kcal/mol)	$\Delta\Delta E$ (kcal/mol)
	α-BrAcPh			-2958.546321		-2958.538864		4.680
	AcO⁻			-228.693050		-228.599168		58.912
Separate Reagents	**α-BrAcPh +AcO⁻**		∞	-3187.239372		-3187.138032		63.592
		-7.81134	2.90	-3187.243660	0.0	-3187.167181	0.0	47.991
		-5.09096	2.76	-3187.243143	0.3	-3187.167427	-0.2	47.513
		-2.38083	2.51	-3187.241026	1.7	-3187.167338	-0.1	46.240
		-1.02108	2.29	-3187.235840	4.9	-3187.163368	2.4	45.477
		(TS) 0	2.11	-3187.233407	6.4	-3187.160788	4.0	45.569
		1.02112	1.93	-3187.236923	4.2	-3187.161239	3.7	47.492
		2.38261	1.68	-3187.252287	-5.4	-3187.170148	-1.9	51.543
		5.09078	1.46	-3187.269159	-16.0	-3187.179381	-7.7	56.336
IRC		13.5984	1.45	-3187.274501	-19.4	-3187.179431	-7.7	59.658
	Prod + Br-		∞	-3187.280658		-3187.177706	-6.6	64.603
Separate Products	**Prod**			-612.952802		-612.941094		7.347
	Br-			-2574.327856		-2574.236612		57.256

Figure A.1 shows that there is a small variation in the additive energy of fragment $\mathcal{K}$ and $\mathcal{P}$ during the S$_N$2 reaction of **PhO⁻** and **AcO⁻** with **α-BrAcPh**.
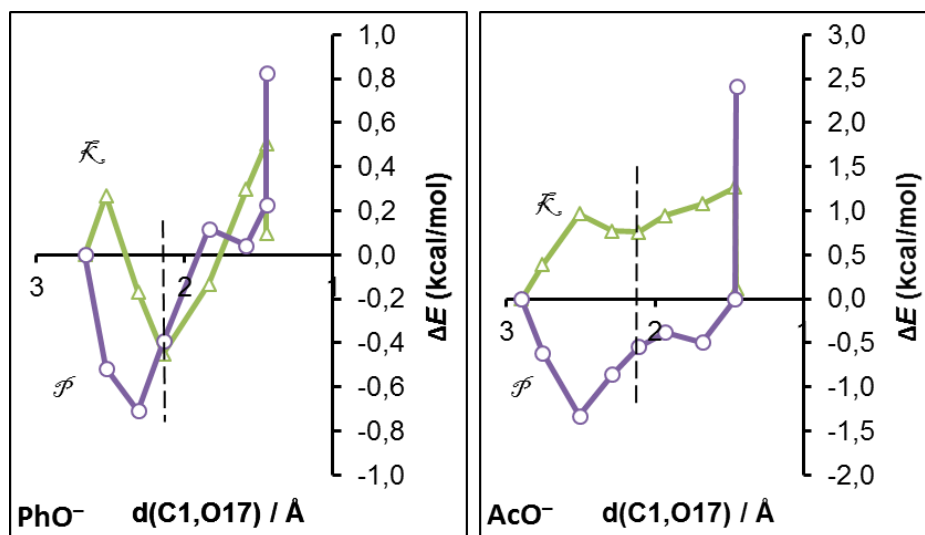
Figure A.1: Change in the additive energy of fragments $\mathcal{K}$ and $\mathcal{P}$ for S$_N$2 reaction of **PhO⁻** and **AcO⁻** with **α-BrAcPh**.

3

The interactions of the phenyl fragment, $\mathscr{P}$, with other fragments were also considered, **Figure A.2**, however, no important trends or significant changes in values were noted.
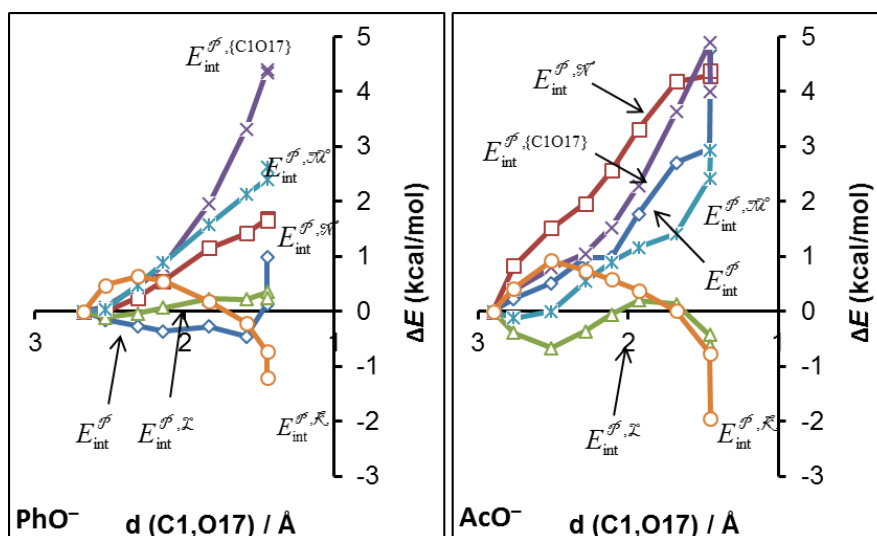
Figure A.2: Change in interaction energy of fragment $\mathscr{P}$ with other selected fragments for S$_N$2 reaction of **PhO⁻** and **AcO⁻** with **α-BrAcPh**.

Figure A.3 shows that the stabilisation provided by the nucleophile during the S$_N$2 reaction with **α-BrAcPh** is due to the additive energy of O17, ΔE_{add}^{O17}. While at the TS for the reactions, the nucleophile provides a destabilising effect, which is due nucleophile fragment $\mathscr{R}$ which excludes the attacking-O (O17). It is only after the TS when $\Delta E_{add}^{O17} > \Delta E_{add}^{\mathscr{R}}$.
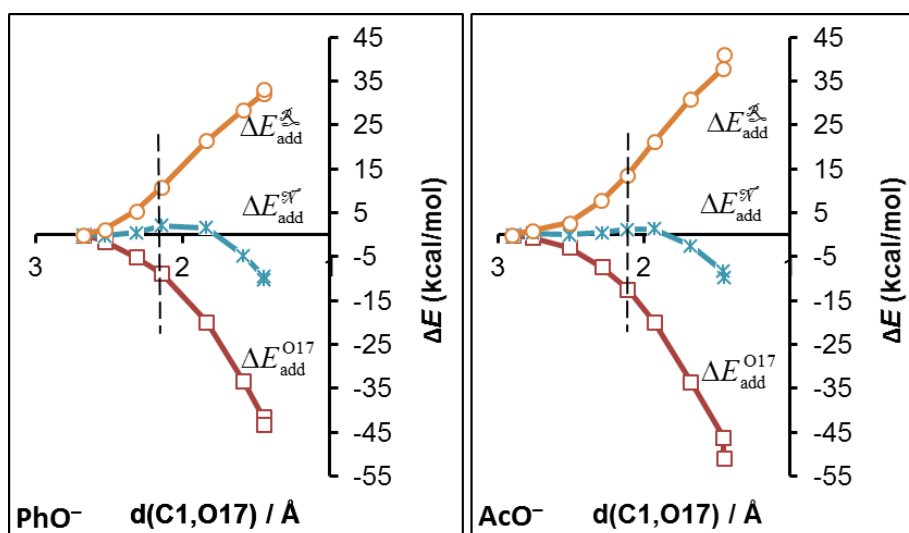
Figure A.3: Change in the additive energy of atom O17 and fragments $\mathscr{N}$ and $\mathscr{R}$ for S$_N$2 reaction of **PhO⁻** and **AcO⁻** with **α-BrAcPh**.

4
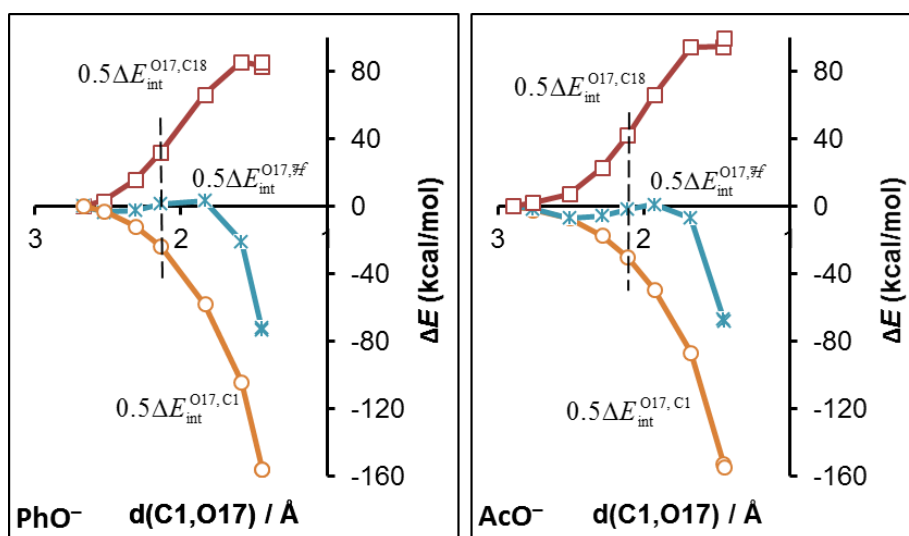
Figure A.4: Change in interaction energy of O17 with C1, C18 and the molecular system, $\mathscr{H}$, for the S_N2 reaction of **PhO⁻** and **AcO⁻** with **α-BrAcPh**.

Modelling carbonyl addition (CA) of **α-BrAcPh** with **PhO⁻** and **AcO⁻** was done by decreasing the distance between the carbonyl-*C* (C4) and attacking-*O* (O17) and monitor the change in electronic energy – **Figure A.5**. Results show an exponential increase in energy as CA occurs, suggesting that CA will not occur for these two systems.
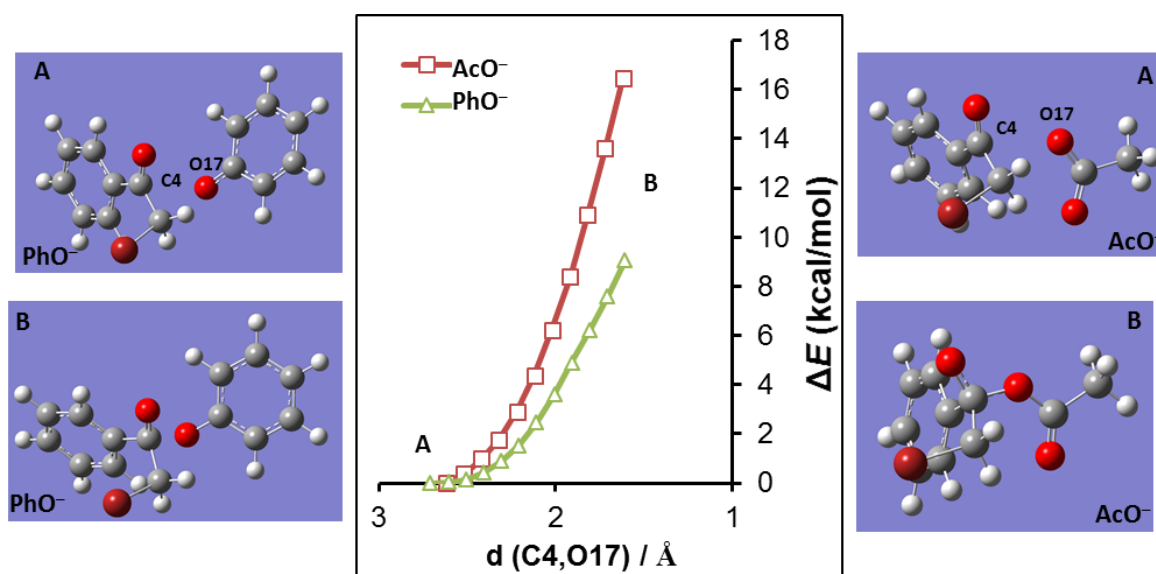
Figure A.5: Change in electronic energy for **PhO⁻** and **AcO⁻** undergoing carbonyl addition with **α-BrAcPh**.

Table A.3: Charge of individual atoms (*e*) during the S_N2 reaction of **PhO⁻** and **α-BrAcPh**.

IRC Coordinate	-4.11	-2.39	-1.03	0.00	1.72	3.10	5.83	8.58
d (C1,O17) / Å	2.67	2.53	2.32	2.14	1.84	1.59	1.45	1.45
C1	0.003	0.014	0.048	0.078	0.160	0.297	0.442	0.444
H2	0.090	0.089	0.098	0.104	0.099	0.075	0.051	0.052
H3	0.084	0.084	0.094	0.100	0.094	0.071	0.050	0.050
C4	0.992	0.993	0.995	0.997	0.995	0.978	0.964	0.962
O5	-1.143	-1.148	-1.148	-1.146	-1.143	-1.146	-1.142	-1.136
C6	-0.016	-0.017	-0.017	-0.017	-0.020	-0.024	-0.030	-0.031
C7	-0.018	-0.019	-0.019	-0.018	-0.017	-0.018	-0.017	-0.016
C8	-0.021	-0.022	-0.022	-0.022	-0.021	-0.021	-0.020	-0.019
C9	-0.024	-0.025	-0.025	-0.024	-0.023	-0.023	-0.022	-0.021
C10	-0.020	-0.021	-0.021	-0.020	-0.019	-0.020	-0.019	-0.017
C11	-0.016	-0.017	-0.017	-0.016	-0.015	-0.015	-0.016	-0.016
H12	0.057	0.056	0.056	0.056	0.057	0.056	0.055	0.056
H13	0.034	0.033	0.033	0.034	0.035	0.035	0.036	0.037
H14	0.036	0.036	0.036	0.036	0.037	0.037	0.038	0.039
H15	0.035	0.034	0.034	0.035	0.036	0.036	0.037	0.038
H16	0.034	0.034	0.034	0.035	0.037	0.038	0.040	0.040
O17	-1.225	-1.209	-1.163	-1.108	-1.010	-0.997	-1.064	-1.059
C18	0.736	0.729	0.699	0.659	0.566	0.496	0.474	0.469
C19	-0.098	-0.095	-0.085	-0.072	-0.048	-0.032	-0.026	-0.025
C20	-0.054	-0.052	-0.047	-0.041	-0.031	-0.025	-0.021	-0.020
C21	-0.074	-0.072	-0.063	-0.054	-0.040	-0.032	-0.029	-0.028
C22	-0.054	-0.053	-0.048	-0.042	-0.032	-0.026	-0.023	-0.022
C23	-0.091	-0.085	-0.074	-0.063	-0.041	-0.026	-0.016	-0.016
H24	-0.007	-0.005	0.003	0.011	0.025	0.035	0.042	0.043
H25	-0.001	0.001	0.006	0.013	0.023	0.030	0.033	0.034
H26	-0.005	-0.004	0.002	0.009	0.021	0.028	0.029	0.030
H27	-0.001	0.000	0.006	0.012	0.024	0.030	0.033	0.033
H28	-0.005	-0.002	0.006	0.015	0.030	0.039	0.044	0.045
Br29	-0.231	-0.257	-0.402	-0.549	-0.777	-0.876	-0.922	-0.943
Total	-1.001	-0.999	-1.000	-1.001	-1.001	-1.000	-1.000	-0.998

6

Table A.4: Charge of individual atoms (*e*) during the S_N2 reaction of **PhO⁻** and **α-BrAcPh**.

IRC Coordinate	-4.11	-2.39	-1.03	0.00	1.72	3.10	5.83	8.58
d (C1,O17) / Å	2.67	2.53	2.32	2.14	1.84	1.59	1.45	1.45
C1	0.003	0.014	0.048	0.078	0.160	0.297	0.442	0.444
H2	0.090	0.089	0.098	0.104	0.099	0.075	0.051	0.052
H3	0.084	0.084	0.094	0.100	0.094	0.071	0.050	0.050
C4	0.992	0.993	0.995	0.997	0.995	0.978	0.964	0.962
O5	-1.143	-1.148	-1.148	-1.146	-1.143	-1.146	-1.142	-1.136
C6	-0.016	-0.017	-0.017	-0.017	-0.020	-0.024	-0.030	-0.031
C7	-0.018	-0.019	-0.019	-0.018	-0.017	-0.018	-0.017	-0.016
C8	-0.021	-0.022	-0.022	-0.022	-0.021	-0.021	-0.020	-0.019
C9	-0.024	-0.025	-0.025	-0.024	-0.023	-0.023	-0.022	-0.021
C10	-0.020	-0.021	-0.021	-0.020	-0.019	-0.020	-0.019	-0.017
C11	-0.016	-0.017	-0.017	-0.016	-0.015	-0.015	-0.016	-0.016
H12	0.057	0.056	0.056	0.056	0.057	0.056	0.055	0.056
H13	0.034	0.033	0.033	0.034	0.035	0.035	0.036	0.037
H14	0.036	0.036	0.036	0.036	0.037	0.037	0.038	0.039
H15	0.035	0.034	0.034	0.035	0.036	0.036	0.037	0.038
H16	0.034	0.034	0.034	0.035	0.037	0.038	0.040	0.040
O17	-1.225	-1.209	-1.163	-1.108	-1.010	-0.997	-1.064	-1.059
C18	0.736	0.729	0.699	0.659	0.566	0.496	0.474	0.469
C19	-0.098	-0.095	-0.085	-0.072	-0.048	-0.032	-0.026	-0.025
C20	-0.054	-0.052	-0.047	-0.041	-0.031	-0.025	-0.021	-0.020
C21	-0.074	-0.072	-0.063	-0.054	-0.040	-0.032	-0.029	-0.028
C22	-0.054	-0.053	-0.048	-0.042	-0.032	-0.026	-0.023	-0.022
C23	-0.091	-0.085	-0.074	-0.063	-0.041	-0.026	-0.016	-0.016
H24	-0.007	-0.005	0.003	0.011	0.025	0.035	0.042	0.043
H25	-0.001	0.001	0.006	0.013	0.023	0.030	0.033	0.034
H26	-0.005	-0.004	0.002	0.009	0.021	0.028	0.029	0.030
H27	-0.001	0.000	0.006	0.012	0.024	0.030	0.033	0.033
H28	-0.005	-0.002	0.006	0.015	0.030	0.039	0.044	0.045
Br29	-0.231	-0.257	-0.402	-0.549	-0.777	-0.876	-0.922	-0.943
Total	-1.001	-0.999	-1.000	-1.001	-1.001	-1.000	-1.000	-0.998

7

Table A.5: Molecular graphs of the structures generated from IRC-calculations for the S_N2 reaction of **PhO⁻** with **α-BrAcPh**. The numbering of each atom is shown above.

d(C1,O17) = 2.67 Å	d(C1,O17) = 2,53 Å	d(C1,O17) = 2,31 Å
d(C1,O17) = 2,14 Å (TS)	d(C1,O17) = 1,84 Å	d(C1,O17) = 1,59 Å
d(C1,O17) = 1,45 Å	d(C1,O17) = 1,44 Å	

8

Table A.6: Molecular graphs of the structures generated from IRC-calculations for the S_N2 reaction of **AcO⁻** with **α-BrAcPh**. The numbering of each atom is shown above.

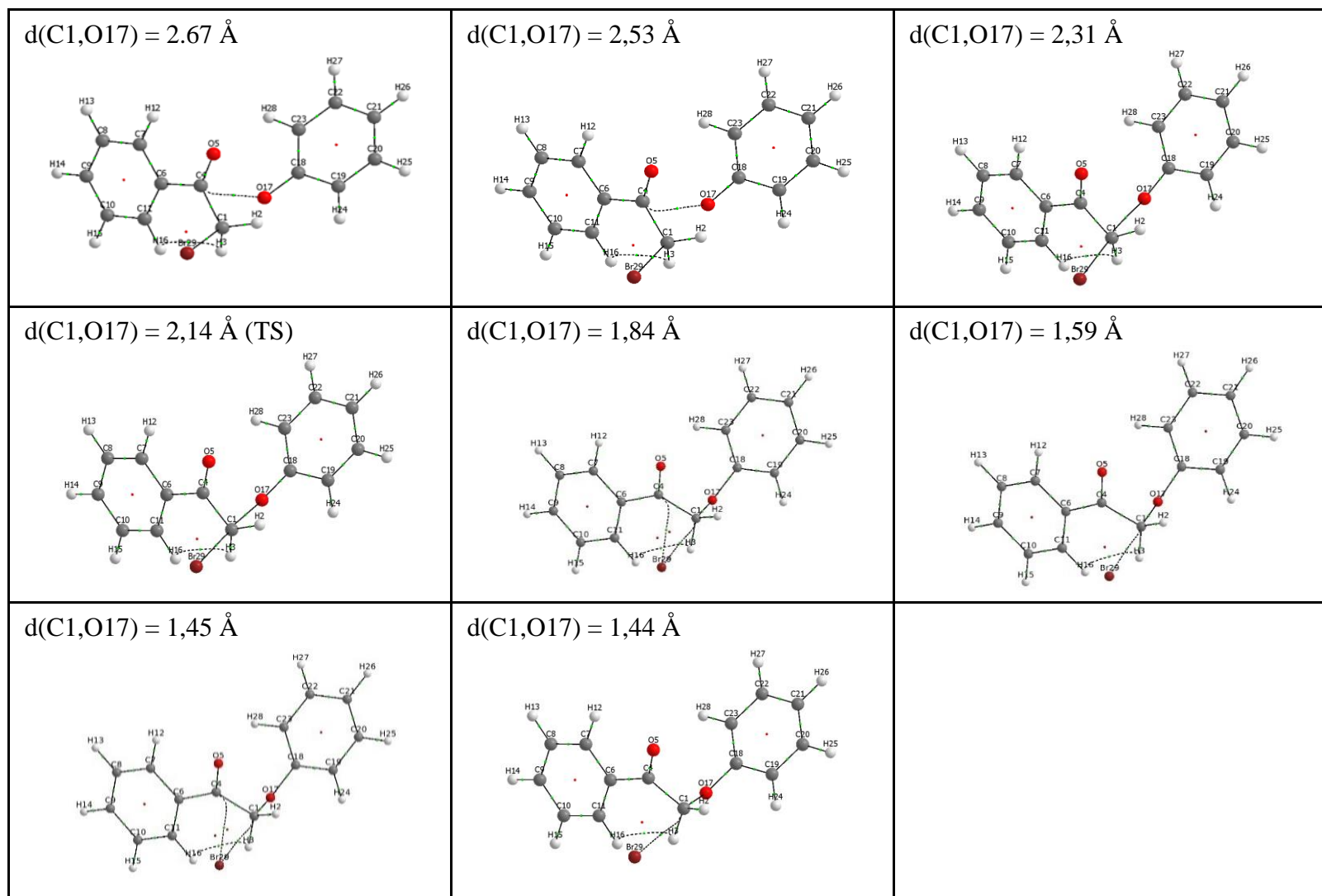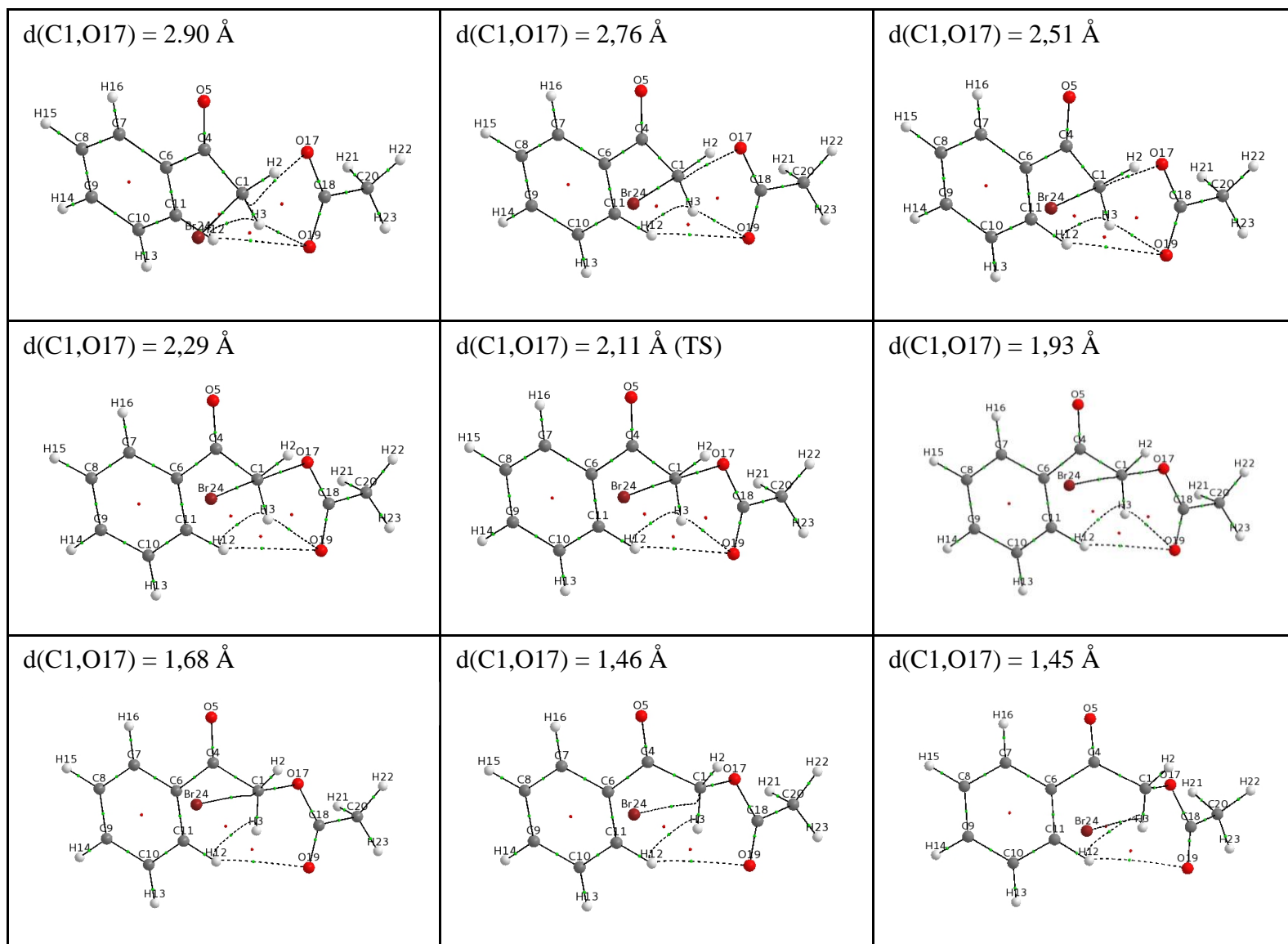d(C1,O17) = 2.90 Å

d(C1,O17) = 2,76 Å

d(C1,O17) = 2,51 Å

d(C1,O17) = 2,29 Å

d(C1,O17) = 2,11 Å (TS)

d(C1,O17) = 1,93 Å

d(C1,O17) = 1,68 Å

d(C1,O17) = 1,46 Å

d(C1,O17) = 1,45 Å

9

Appendix B

Supplementary Information for Chapter 4

B1

Videos of vibration of the negative frequency for the TS of the S$_N$2 and epoxidation reaction of **MeO⁻** with **α-BrAcPh,** *p*-**OMe** and *p*-**NO₂** are included on attached CD.

Table B.1 show the electronic energy, *E*, and the recovered IQA additive energy, E_{IQA}, for selected IRC generated structures for the S$_N$2 reaction of **MeO⁻** with **α-BrAcPh**, *p*-**OMe** and *p*-**NO₂**. **Table B.2** presents the same information for the epoxidation reaction.

Table B.1: Electronic (*E*) and recover energy of the molecular system from IQA (E_{IQA}) for structures of separate reactants, products and structure generated from IRC calculations for the S$_N$2 reaction of **MeO⁻** reacting with **α-BrAcPh**.

Substituents	IRC Coord	d(O1,C6) / Å	*E* (au)	Δ*E* (kcal/mol)	E_{IQA} (au)	ΔE_{IQA} (kcal/mol)	ΔΔ*E* (kcal/mol)
p-OMe	-5.50	2.35381	-3188.38170	0.00	-3188.28736	0.00	59.20
	-3.24	2.35417	-3188.38032	0.87	-3188.28916	-1.13	57.20
	-1.29	2.35498	-3188.37857	1.96	-3188.28842	-0.66	56.57
	(TS) 0	2.21496	-3188.37758	2.59	-3188.28836	-0.63	55.99
	2.92	1.72401	-3188.40448	-14.29	-3188.30432	-10.64	62.85
	7.78	1.43139	-3188.44372	-38.92	-3188.33525	-30.05	68.07
	15.89	1.42659	-3188.45056	-43.21	-3188.33792	-31.73	70.68
H (α-BrAcPh)	-10.76	2.36243	-3073.82471	0.00	-3073.73383	0.00	57.03
	-6.19	2.35493	-3073.82393	0.49	-3073.73270	0.71	57.24
	-2.28	2.35441	-3073.82110	2.26	-3073.73536	-0.96	53.80
	(TS) 0	2.17968	-3073.81860	3.83	-3073.73370	0.08	53.28
	2.94	1.6866	-3073.84755	-14.34	-3073.75129	-10.96	60.41
	7.83	1.43088	-3073.88329	-36.76	-3073.77967	-28.76	65.02
	15.99	1.4255	-3073.88939	-40.59	-3073.78107	-29.64	67.98
p-NO₂	-10.53	2.35381	-3278.39675	0.00	-3278.31614	0.00	50.58
	-6.24	2.35417	-3278.39595	0.51	-3278.31531	0.52	50.60
	-2.30	2.35498	-3278.39244	2.71	-3278.31680	-0.41	47.46
	(TS) 0	2.21496	-3278.38839	5.25	-3278.31271	2.15	47.49
	2.96	1.72401	-3278.41981	-14.47	-3278.33074	-9.16	55.89
	7.90	1.43139	-3278.44979	-33.28	-3278.35511	-24.45	59.41
	16.13	1.42659	-3278.45472	-36.38	-3278.35362	-23.52	63.44

$\Delta\Delta E = \Delta E_{IQA} - \Delta E$

B2

Table B.2: Electronic (E) and recover energy of the molecular system from IQA (E_{IQA}) for structures of separate reactants, products and structure generated from IRC calculations for the epoxidation reaction of **MeO⁻** reacting with **α-BrAcPh**.

Substituents	IRC Coordinate	d(O10,C6) / Å	E (au)	ΔE (kcal/mol)	E_{IQA} (au)	ΔE_{IQA} (kcal/mol)	$\Delta\Delta E$ (kcal/mol)
p-OMe	-5.35	2.2706	-3188.38442	0.00	-3188.29298	0.00	57.38
	-3.01	2.2417	-3188.38331	0.69	-3188.29327	-0.19	56.50
	-1.34	2.1646	-3188.38089	2.22	-3188.29195	0.64	55.81
	(TS) 0	1.9841	-3188.37872	3.57	-3188.29008	1.82	55.62
	2.01	1.6543	-3188.37872	3.57	-3188.29400	-0.64	53.16
	6.36	1.4603	-3188.40706	-14.21	-3188.30498	-7.53	64.05
	15.40	1.4550	-3188.41147	-16.98	-3188.30572	-7.99	66.36
H (α-BrAcPh)	-5.33	2.2716	-3073.82654	0.00	-3073.73877	0.00	55.07
	-3.00	2.2427	-3073.82546	0.67	-3073.73883	-0.03	54.37
	-1.33	2.1625	-3073.82290	2.28	-3073.73844	0.21	53.00
	(TS) 0	1.9789	-3073.82054	3.76	-3073.73473	2.54	53.85
	2.00	1.6497	-3073.83222	-3.57	-3073.73857	0.13	58.77
	6.34	1.4596	-3073.84856	-13.82	-3073.75049	-7.35	61.54
	15.35	1.4545	-3073.85302	-16.62	-3073.75025	-7.20	64.49
p-NO₂	-5.72	2.2706	-3278.39926	0.00	-3278.32131	0.00	48.92
	-3.03	2.2417	-3278.39755	1.07	-3278.32110	0.13	47.97
	-1.35	2.1646	-3278.39420	3.18	-3278.31883	1.55	47.29
	(TS) 0	1.9841	-3278.39141	4.93	-3278.31468	4.16	48.15
	2.02	1.6543	-3278.40367	-2.76	-3278.31772	2.25	53.93
	6.40	1.4603	-3278.41810	-11.82	-3278.32642	-3.21	57.53
	14.16	1.4550	-3278.42146	-13.93	-3278.32472	-2.14	60.70

$\Delta\Delta E = \Delta E_{IQA} - \Delta E$

Dihedral scans of the nucleophile, **MeO⁻**, for the RC and RC-*trans* structure was performed – **Figure B.1**. Results show that the nucleophile can rotate between ori1 and ori2 with small energy barriers of less than 2 kcal/mol. The orientation of the α-group is shown to have insignificant influence of the energy barrier for rotational between ori1 and ori2.
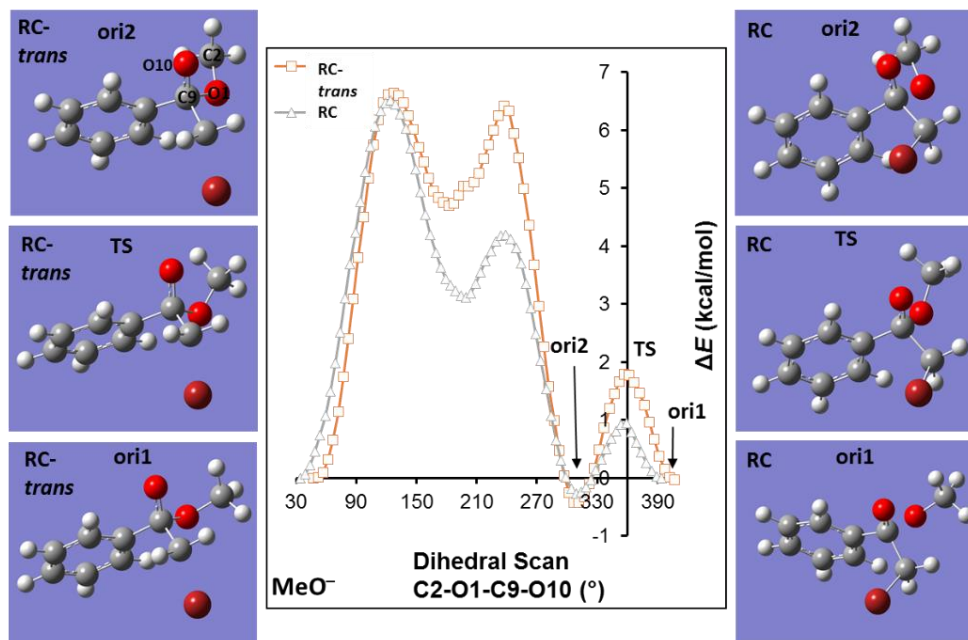

Figure B.1: Change in the electronic energy of dihedral scan for rotation of **MeO⁻** for structures RC and RC-*trans*.
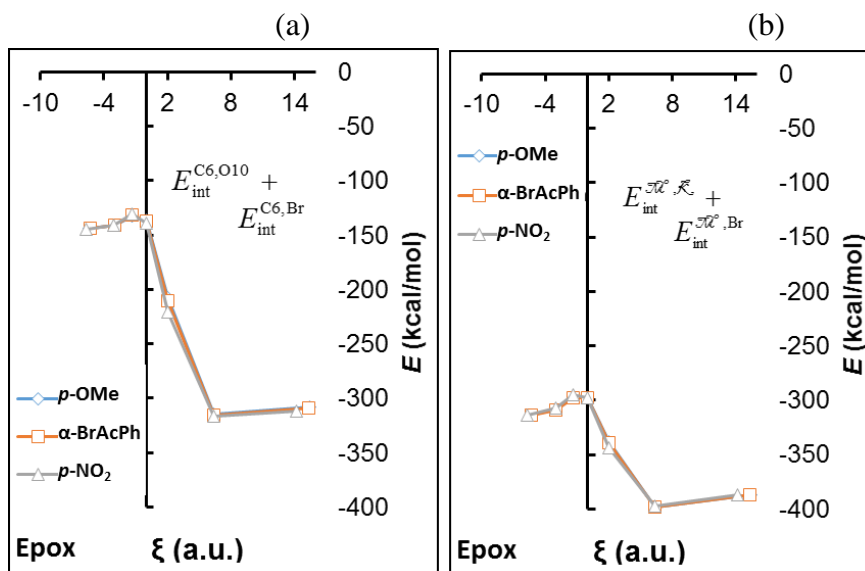

Figure B.2: Sum of the interaction energies for the bonds (a) formed (C6O10) and broken (C6Br), and (b) the interactions of fragments $\mathcal{M}$ with $\mathcal{K}$ and Br along the S_N2 reaction pathway of **MeO⁻** reacting with **α-BrAcPh**, **p-OMe** and **p-NO₂**.

B4

Table B.3: Molecular graphs for the of the RC for the epoxidation reaction of **MeO⁻** reacting with **α-BrAcPh**, **p-OMe** and **p-NO₂**. Fragments which are used in QFARP analysis are represented graphically in dashed lines with each atom having its numbering shown on the right.
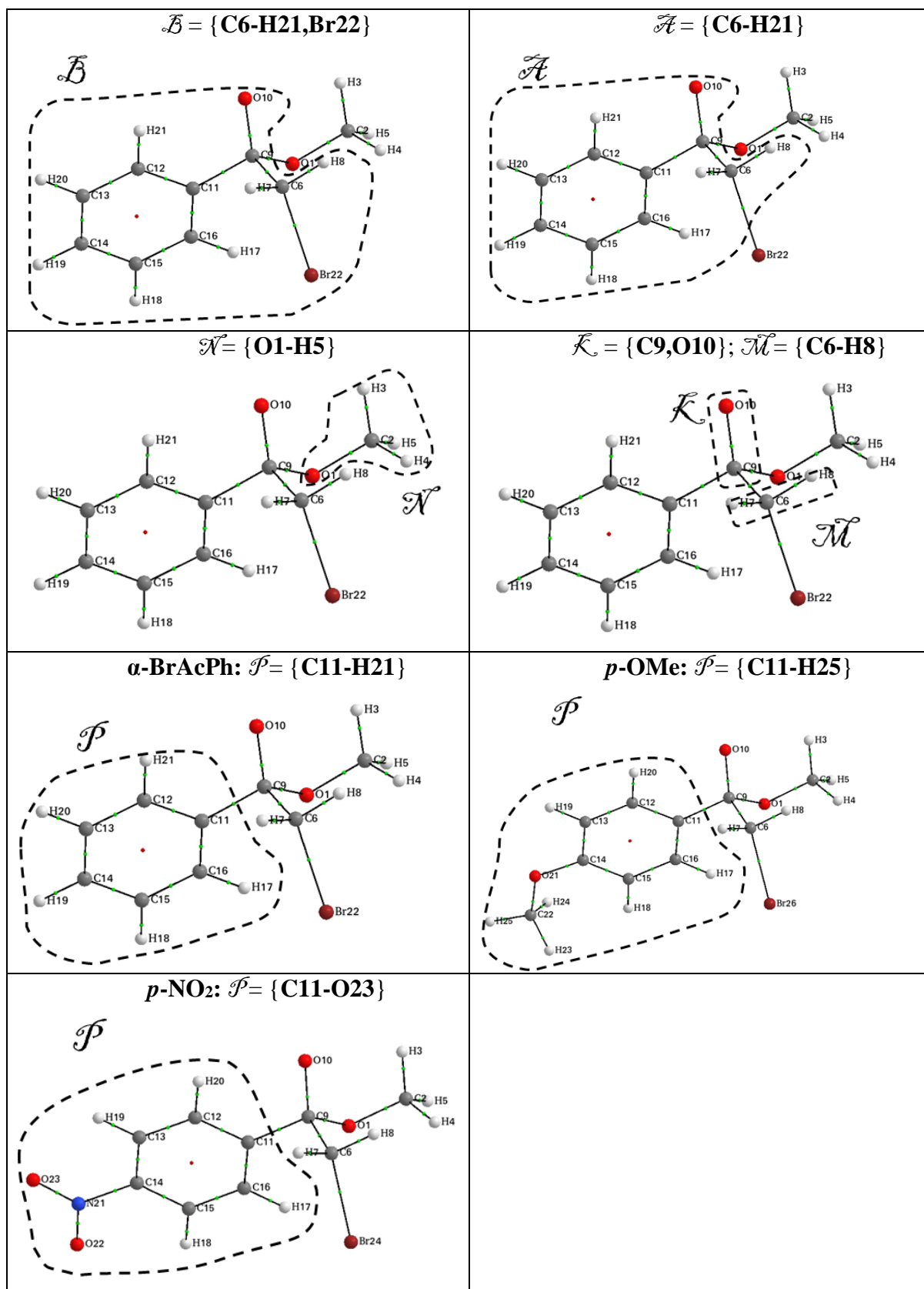

$\mathcal{B} = \{C6\text{-}H21, Br22\}$

$\mathcal{A} = \{C6\text{-}H21\}$

$\mathcal{N} = \{O1\text{-}H5\}$

$\mathcal{K} = \{C9, O10\}$; $\mathcal{M} = \{C6\text{-}H8\}$

α-BrAcPh: $\mathcal{P} = \{C11\text{-}H21\}$

p-OMe: $\mathcal{P} = \{C11\text{-}H25\}$

p-NO₂: $\mathcal{P} = \{C11\text{-}O23\}$

B5

Table B.4: Molecular graphs of the structures generated from IRC-calculations for the S_N2 reaction of **MeO⁻** with **α-BrAcPh**. The numbering of each atom is shown on the right.

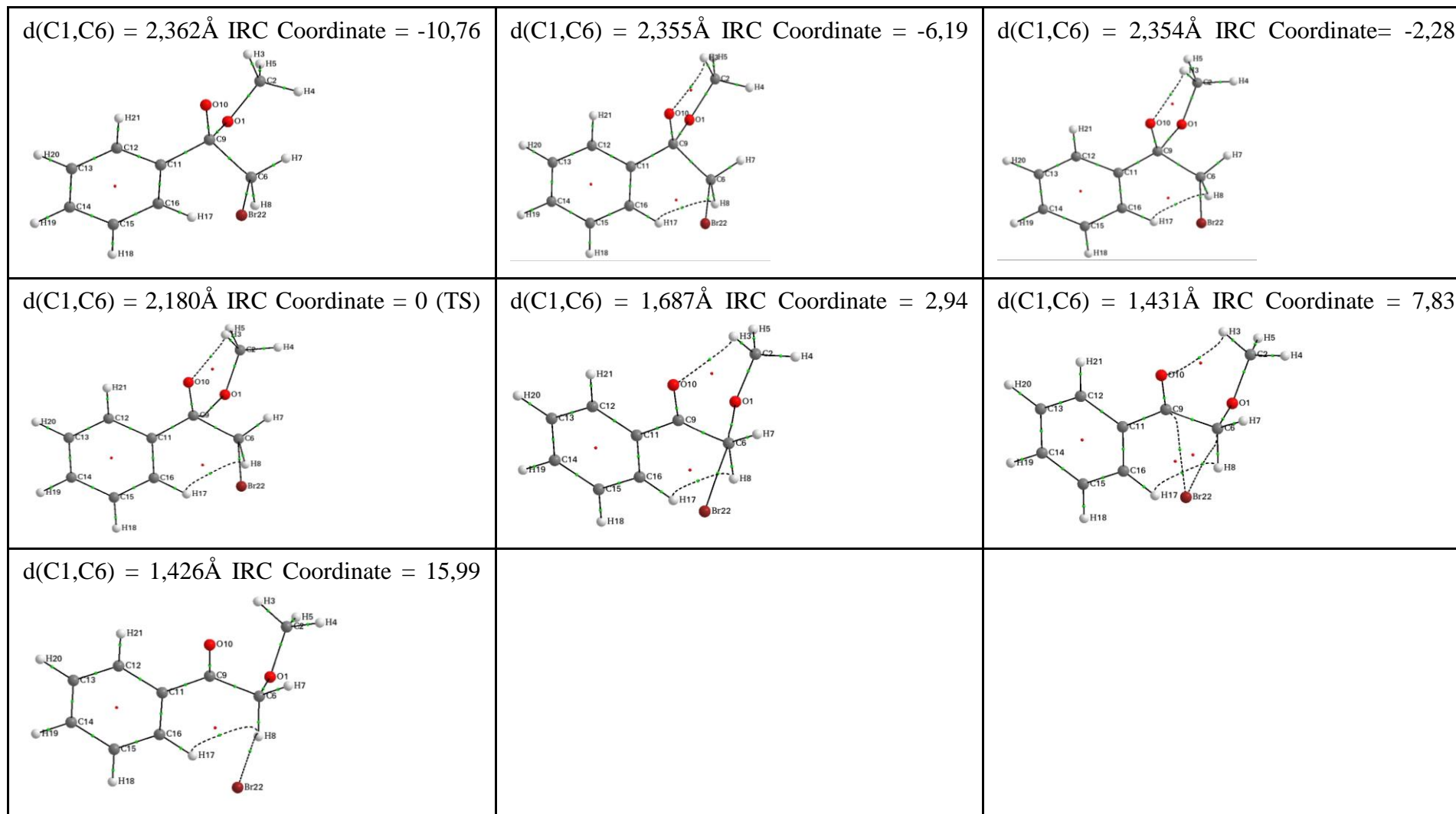|		
d(C1,C6) = 2,362Å IRC Coordinate = -10,76	d(C1,C6) = 2,355Å IRC Coordinate = -6,19	d(C1,C6) = 2,354Å IRC Coordinate= -2,28
d(C1,C6) = 2,180Å IRC Coordinate = 0 (TS)	d(C1,C6) = 1,687Å IRC Coordinate = 2,94	d(C1,C6) = 1,431Å IRC Coordinate = 7,83
d(C1,C6) = 1,426Å IRC Coordinate = 15,99		

Table B.5: Molecular graphs of the structures generated from IRC-calculations for the S_N2 reaction of **MeO⁻** with **p-OMe**. The numbering of each atom is shown on the right.
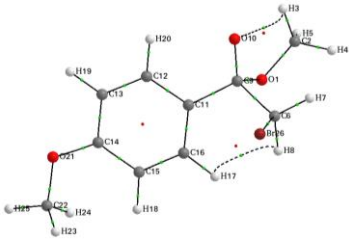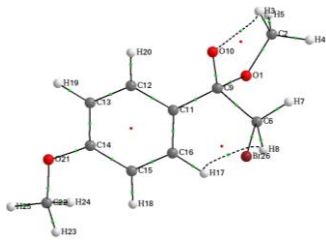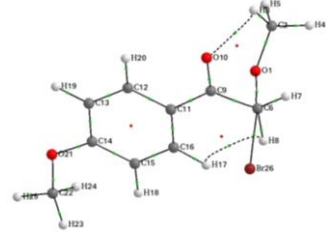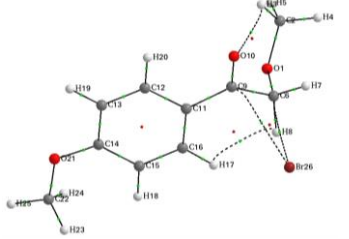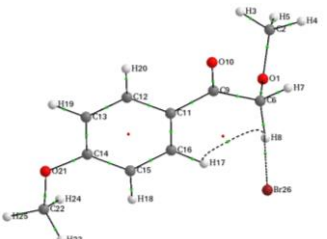
d(C1,C6) = 2,3538Å IRC Coordinate = -5,50	d(C1,C6) = 2,3541Å IRC Coordinate = -3,24	d(C1,C6) = 2,355Å IRC Coordinate = -1,29
d(C1,C6) = 2,215Å IRC Coordinate = 0 (TS)	d(C1,C6) = 1,724Å IRC Coordinate = 2,92	d(C1,C6) = 1,431Å IRC Coordinate = 7,78
d(C1,C6) = 1,427Å IRC Coordinate = 15,89		

B7

Table B.6: Molecular graphs of the structures generated from IRC-calculations for the S_N2 reaction of **MeO⁻** with **p-NO₂**. The numbering of each atom is shown on the right.
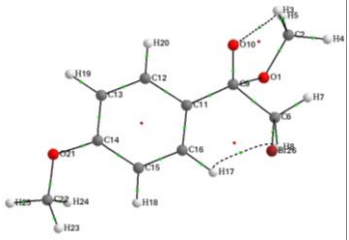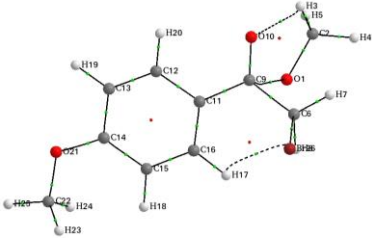
d(C1,C6) = 2,3538Å IRC Coordinate = -10,53	d(C1,C6) = 2,3542Å IRC Coordinate = -6,24	d(C1,C6) = 2,355Å IRC Coordinate = -2,30
d(C1,C6) = 2,215Å IRC Coordinate = 0 (TS)	d(C1,C6) = 1,724Å IRC Coordinate = 2,92	d(C1,C6) = 1,431Å IRC Coordinate = 7,90
d(C1,C6)= 1,427Å IRC Coordinate = 16,13		

B8

Table B.7: Molecular graphs of the structures generated from IRC-calculations for the epoxidation reaction of **MeO⁻** with **α-BrAcPh**. The numbering of each atom is shown on the right.

d(O10,C6) = 2,272Å IRC Coordinate = -5,33	d(O10,C6) = 2,243Å IRC Coordinate = -3,00	d(O10,C6) = 2,163Å IRC Coordinate = -1,33
d(O10,C6) = 1,979Å IRC Coordinate = 0 (TS)	d(O10,C6) = 1,650Å IRC Coordinate = 2,00	d(O10,C6) = 1,460Å IRC Coordinate = 6,34
d(O10,C6) = 1,4545Å IRC Coordinate= 15,35		

B9

Table B.8: Molecular graphs of the structures generated from IRC-calculations for the epoxidation reaction of **MeO⁻** with *p*-OMe. The numbering of each atom is shown on the right.
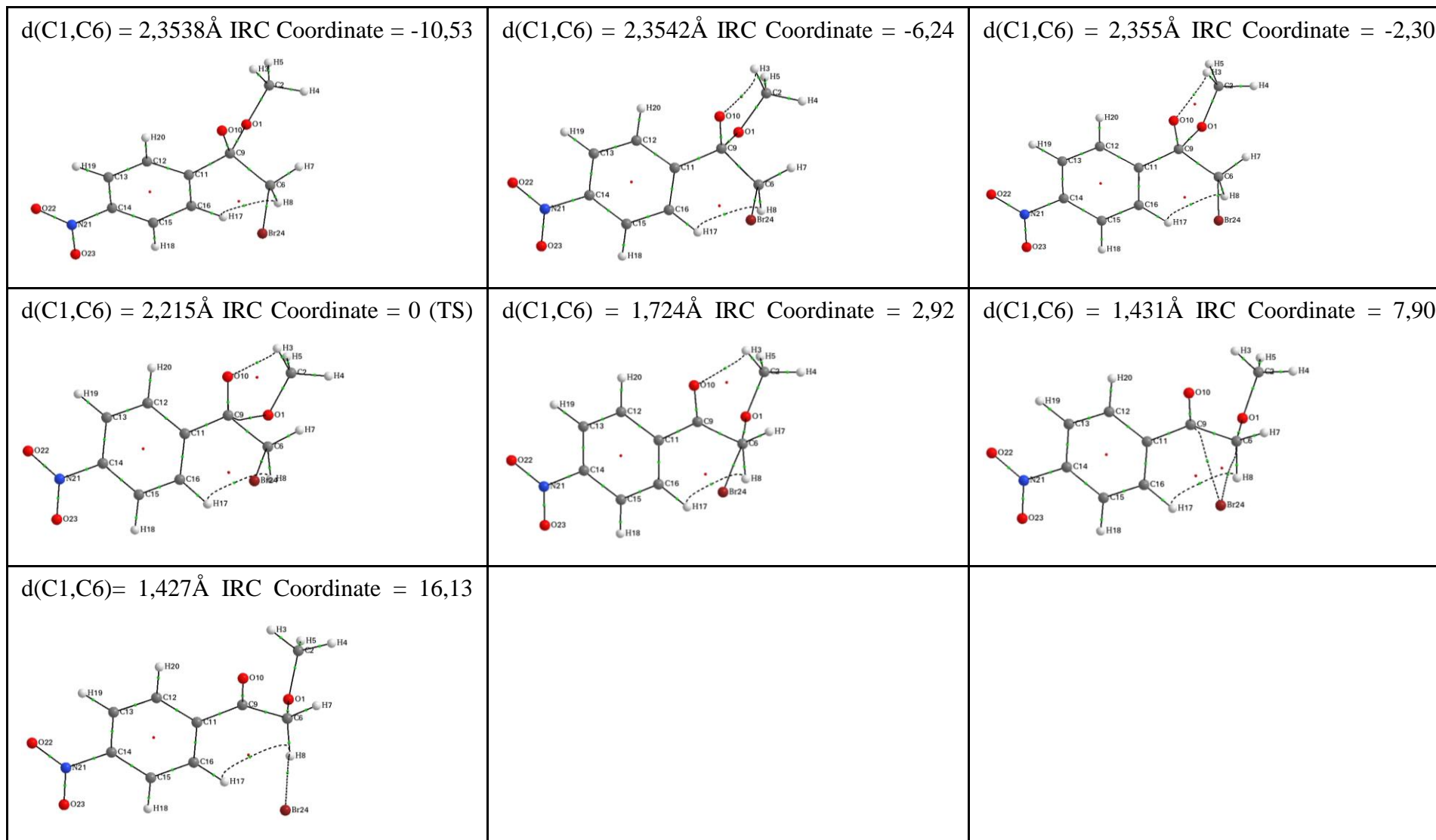
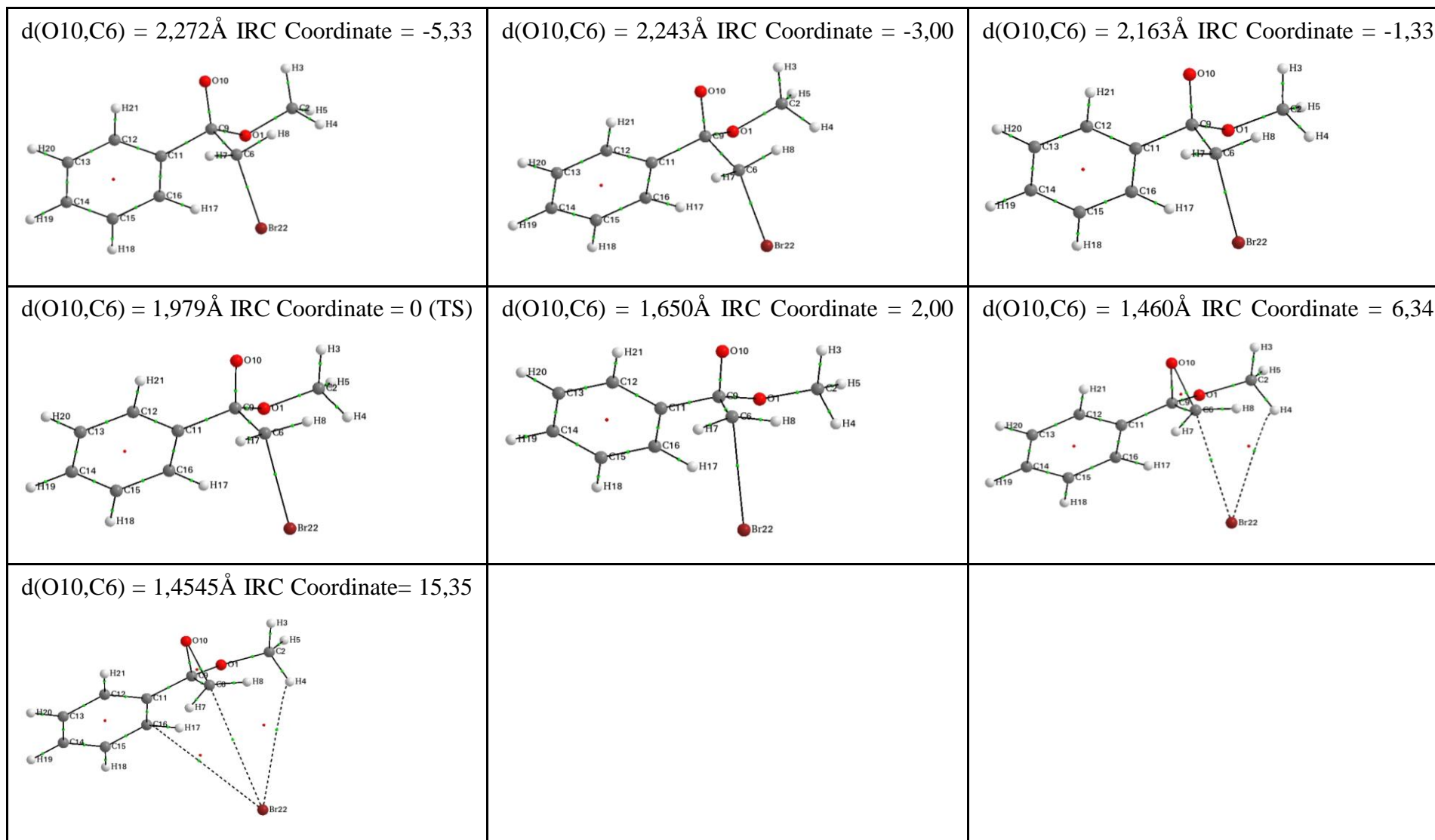|		
d(O10,C6) = 2,271Å IRC Coordinate = -5,35	d(O10,C6) = 2,242Å IRC Coordinate = -3,01	d(O10,C6) = 2,165Å IRC Coordinate = -1,34
d(O10,C6) = 1,984Å IRC Coordinate = 0 (TS)	d(O10,C6) = 1,654Å IRC Coordinate = 2,01	d(O10,C6) = 1,460Å IRC Coordinate = 6,36
d(O10,C6) = 1,455Å IRC Coordinate = 15,40		

Table B.9: Molecular graphs of the structures generated from IRC-calculations for the epoxidation reaction of **MeO⁻** with *p*-NO₂. The numbering of each atom is shown on the right.
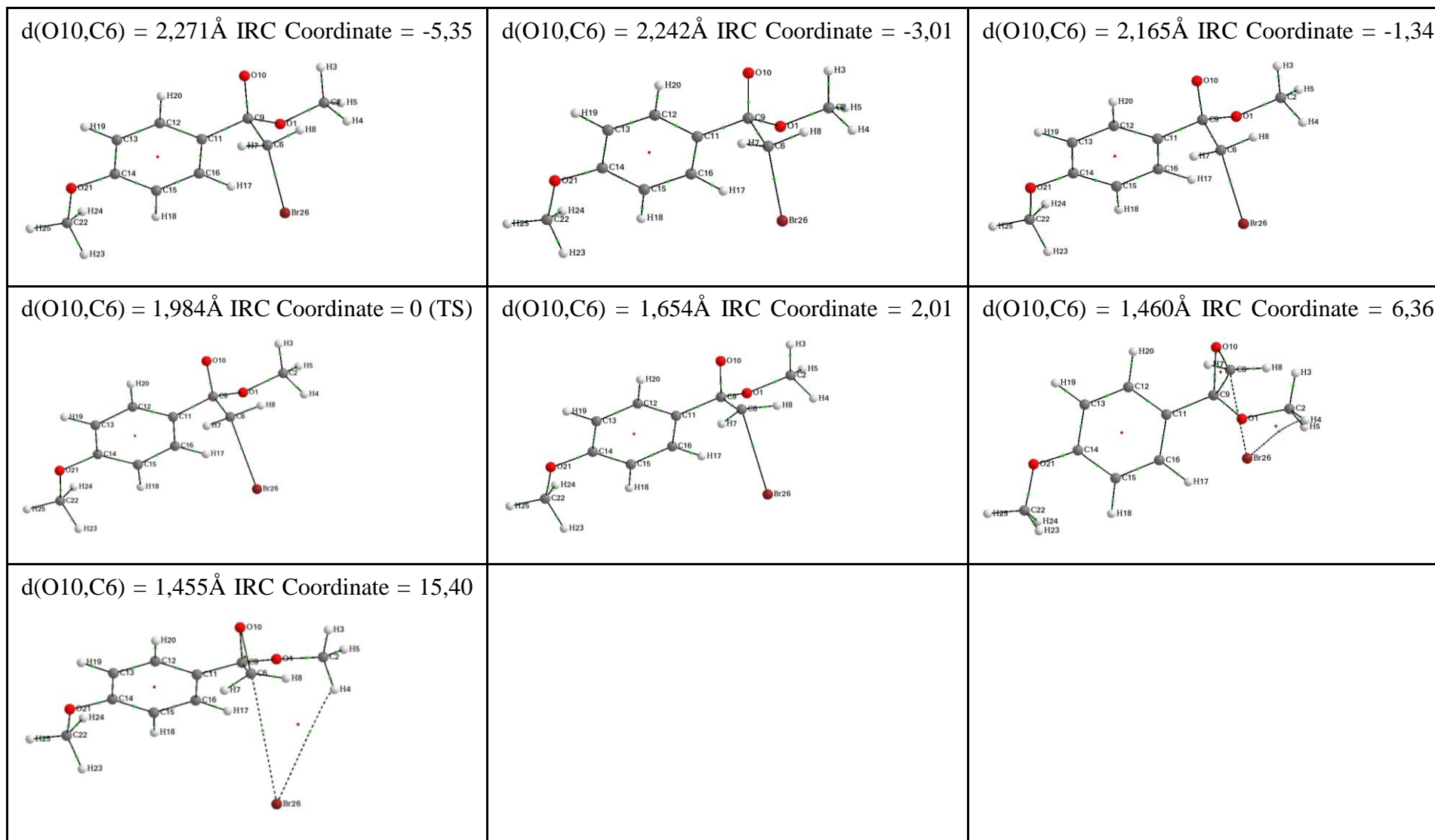
d(O10,C6) = 2,271Å IRC Coordinate = -5,72	d(O10,C6) = 2,242Å IRC Coordinate = -3,03	d(O10,C6) = 2,165Å IRC Coordinate = -1,35
d(O10,C6) = 1,984Å IRC Coordinate = 0 (TS)	d(O10,C6) = 1,654Å IRC Coordinate = 2,02	d(O10,C6) = 1,460Å IRC Coordinate = 6,40
d(O10,C6) = 1,455Å IRC Coordinate = 14,16		